DEVELOPMENT OF A NON-NEWTONIAN LATCHING DEVICE

by

BRIAN ANDERSON

B.S., Kansas State University, 2007

A THESIS

submitted in partial fulfillment of the requirements for the degree

MASTER OF SCIENCE

Department of Mechanical Engineering
College of Engineering

KANSAS STATE UNIVERSITY
Manhattan, Kansas

2010

Approved by:

Major Professor
Dr. B. Terry Beck

Abstract

The objective of this project was to first evaluate the feasibility of developing a viscous damping device that used a Non-Newtonian Shear Thickening Fluid (STF) and incorporating it as a door latch into an existing commercial dryer unit. The device would keep the door closed during sudden large magnitude impact loads while still allowing the door to open normally when force is applied gradually at the door handle.

The first phase of the project involved performing background research on the subject and performing preliminary analysis in order to determine if the concept was feasible enough to be worth constructing a physical prototype. This preliminary analysis consisted of a literature review of existing damping mechanisms and shear thickening fluids, rheometer testing of shear thickening suspensions to obtain viscosity data, and performing numerical simulations to determine if a damper that fit the size requirements could produce enough resistance force.

The focus for the second phase of the project was to demonstrate a proof of concept in the form of a working model prototype. This prototype did not need be of identical shape and proportions as the finalized design, but would be developed to facilitate experimental testing and evaluation of performance under the desired operating conditions. It was also necessary to design and construct the test setup for the dynamic testing of the dryer door opening so that the opening displacement as well as the force applied to the door could be recorded as a function of time.

The final phase of the project consisted of improving upon the original prototype in order to prove the validity of a viscous latch beyond the proof of concept phase in a form closer to what is desired for the commercial product. This required reducing the physical size of the new prototype latch so as to fit within the space available in a particular dryer, incorporate a one-way ratcheting device into the latch to allow unrestricted closing of the door, and increase the operational temperature range of the damper.

Table of Contents

List of Figures vii
List of Tables xiii
Acknowledgements xiv
CHAPTER 1 - Introduction 1
1.1 Motivation for Project 1
1.2 Design Objectives 2
CHAPTER 2 - Phase I: Background/Feasibility Study 5
2.1 Identification of All Relevant Latch Specifications 5
2.2 Literature Review 6
Review of Latch Damping Mechanisms 6
Viscous Damped Hinge 6
Viscous Coupling Unit 7
Fluid Damped Vehicle Door Latch 7
Shear Thickening Fluids 8
Suspensions 8
Surfactant Solutions 9
Ionomer Fluids 9
Desired Fluid Properties 10
2.3 Fluid Testing and Selection 12
Identification of Viable Shear Thickening Fluids 12
Viscosity Testing 12
2.4 Damper Design Process 13
Early Concepts 14
Cylinder 14
Disk 15
Paddle Wheel 15
Linear Latch 16
2.5 Prediction Model 16

Step 1: Conservation of Momentum for Door 17
Step 2: Correlation between Movement of Door and Latch Rotation 19
Step 3: Determine Resistance Force of Latch 21
Performance predictions 22
Worst Case Pressure Pulse 23
User Opening 24
2.6 Shielding Latch from Temperature Pulse 25
2.7 Thermal Expansion to Control Fluid Layer Thickness 26
2.8 Phase I Summary 28
CHAPTER 3 - Phase II: Proof of Concept 29
3.1 Initial Prototype Latch Design 29
Prototype Spindle 30
Spindle Engage Mechanism 31
Latch Support Structure 32
3.2 Dryer Door Test Setup 32
Dryer Door Support Structure 33
Instrumentation 34
Actuator 34
Force Measurement 34
Displacement Measurement 35
Data Acquisition 36
3.3 Test Results 36
Mechanical Latch Tests 37
Dynamic Testing Without Latch 38
Dynamic Testing With Viscous Latch 41
3.4 Static Testing 46
Room Temperature Static Testing 47
Non-Room Temperature Testing 48
3.5 Phase II Summary 50
CHAPTER 4 - Phase III: Transition to Commercial Product 51
4.1 Second Prototype Design 51

Size Reduction 51
Gap Ratio 52
Ratcheting Mechanism 53
Filling Damper 54
Temperature Range 55
4.2 Test Results 58
Viscous Damper Only 58
Opening 58
Extreme Case 63
Closing Test 65
Mechanical and Viscous Latches 68
Opening 69
Extreme Case 73
Latch Closing 74
Testing Obstacles 77
Self-Centering Effect 77
Catch Binding 77
Drying: 78
4.3 Phase III Summary 79
CHAPTER 5 - Summary and Future Work 80
5.1 Summary 80
5.2 Future Work 82
References 83
Appendix A - Simulation Programs 85
A.1 Dynamic Door Opening Model 85
MatLab Code 85
Dynamic Opening Model Results 88
Worst Case Pressure Pulse: 5.2 in. of H20 for 0.5 seconds 90
Maximum Opening Force: 15 lbf on handle 91
Minimum Opening Force: 6 lbf on handle 92
A.2 Temperature Pulse Analysis 93

Step 1: Steel Plate 93
Step 2: Insulation 95
Mathcad Worksheet 97
Appendix B - Viscosity Testing 102
B.1 Testing Equipment 102
Brookfield Engineering DV-III Rheometer with SC4-28 Spindle 102
Malvern Instruments: C-VOR Digital Rheometer 103
Brookfield R/S-CPS Rheometer 104
Appendix C - Dryer Door Test Setup 110
C.1 Component Specifications 110
Load Cell 110
LVDT 111
Voice Coil Linear Actuator 111
Servo Amplifier 112
Data Acquisition Card 113
C.2 LabVIEW Code 116
C.3 Reading Test Cell Data 118
C.4 Calibration 119
Load Cell 119
LVDT (Linear Variable Differential Transformer) 121
Voice Coil and Amplifier 122
C.4 Uncertainty 124
Load Cell 124
LVDT 124
DAQ 124
Appendix D - Prototype Drawings 125

List of Figures

Figure 1-1: Washer Door Latch Mechanism 1
Figure 1-2: Dryer Door Latch Mechanism 2
Figure 1-3: Dryer Door Latch Mechanism 2
Figure 1-4: Dryer Door Latch Space Limitations 3
Figure 1-5: Viscous Latch--Basic Mechanical Concept 4
Figure 2-1: Viscous Damped Hinge. Modified From Rude & Brokowski (2006) 6
Figure 2-2: Viscous Coupling Unit from Drew and Davis (2010) 7
Figure 2-3: Fluid Damped Vehicle Door Latch. Modified From: McFarland (1998) 8
Figure 2-4: Behavior of particles in suspensions, Modified from: (Egres, Netteshein, & Wagner, 2006) 9
Figure 2-5: Ideal Shear Thickening Fluid 10
Figure 2-6: Actual Shear Thickening Behavior 11
Figure 2-7: Simplified Model for a Real Shear Thickening Fluid 11
Figure 2-8: Rheometer Test Data 13
Figure 2-9: Couette Flow 14
Figure 2-10: Fluid Damped Cylinder 15
Figure 2-11: Fluid Damped Disks 15
Figure 2-12: Fluid Damped Paddlewheel 16
Figure 2-13: Linear Latch 16
Figure 2-14: Door Hinge Force-Moment Diagram 17
Figure 2-15: Damper Travel 19
Figure 2-16: Cam Motion 20
Figure 2-17: Latch Resistance 21
Figure 2-18: Door Resistance 22
Figure 2-19: Door Geometry for Dynamic Model 23
Figure 2-20: Damper Geometry for Dynamic Model 23
Figure 2-21: Door Displacement and Forces for Worst Case Pressure Pulse 24
Figure 2-22: Door Displacement and Forces for 15 Pound Opening Force 24

Figure 2-23: Door Displacement for 6 Pound Opening Force 25
Figure 2-24: Temperature Pulse Results 26
Figure 2-25: Estimated Shear Thickening Behavior 27
Figure 2-26: Effectiveness of Thermal Expansion 28
Figure 3-1: Damper Cut-Away 29
Figure 3-2: Viscous Latch 30
Figure 3-3: Exploded View of Damper Model 30
Figure 3-4: Catch Diagram 31
Figure 3-5: First Prototype Catch 31
Figure 3-6: First Prototype Mounting 32
Figure 3-7: Instrumentation 33
Figure 3-8: Support Structure 33
Figure 3-9: Voice Coil Linear Actuator 34
3-10: Mounted Load Cell and Actuator 35
3-11: LVDT Mounting 35
Figure 3-12: Door Testing Force Control Signals 36
Figure 3-13: 15 lb Mechanical Latch 37
Figure 3-14: 10 lb Mechanical Latch 37
Figure 3-15: 5lb Mechanical Latch 38
Figure 3-16: 15 lb No Latch 39
Figure 3-17: 10 lb No Latch 39
Figure 3-18: 5 lb No Latch 40
Figure 3-19: Inertia Test Displacement 40
Figure 3-20: Inertia Verification 41
Figure 3-21: 15 lb Viscous Latch 42
Figure 3-22: 10 lb Viscous Latch 42
Figure 3-23: 5 lb Viscous Latch 43
Figure 3-24: Viscous Damper LVDT Readings (Superimposed) 44
Figure 3-25: Experimental Opening Rates 45
Figure 3-26: Experimental and Calculated Opening Rate Comparison 46
Figure 3-27: Static Damper Test 47

Figure 3-28: Room Temperature Static Test Results 47
Figure 3-29: Temperature Control 48
Figure 3-30: Temperature Effects 49
Figure 3-31: Viscosity Curves at Elevated Temperatures 49
Figure 4-1: Latch Mounting 52
Figure 4-2: Gap Ratio 53
Figure 4-3: Clasp and One-Way Bearing 54
Figure 4-4: Filling Commercial Prototype 54
Figure 4-5: Viscosity vs. Temperature Curve 55
Figure 4-6: Viscosity vs. Shear Rate for Various Temperatures 56
Figure 4-7: Critical Shear Rate vs. Temperature 57
Figure 4-8: Critical Shear Rate vs. Solvent Viscosity 57
Figure 4-9: Door Pivoting 59
Figure 4-10: 5 lb Load Cell Readings 60
Figure 4-11: 5 lb LVDT Readings 60
Figure 4-12: 10 lb Load Cell Readings 61
Figure 4-13: 10 lb LVDT Readings 61
Figure 4-14: 20 lb Load Cell Readings 62
Figure 4-15: 20 lb LVDT Readings 62
Figure 4-16: Opening Rate Comparison 63
Figure 4-17: 40 lb Load Cell Readings 64
Figure 4-18: 40 lb LVDT Readings 64
Figure 4-19: 7 lb Closing Load Cell 65
Figure 4-20: 7 lb Closing LVDT 66
Figure 4-21: 15 lb Closing Load Cell 66
Figure 4-22: 15 lb Closing LVDT 67
Figure 4-23: Original Mechanical Latch 68
Figure 4-24: Mechanical Latches 68
Figure 4-25: Weak Latch 69
Figure 4-26: 10 lb Dual Latch Load Cell 69
Figure 4-27: 10 lb Dual Latch LVDT 70

Figure 4-28: 15 lb Dual Latch Load Cell 71
Figure 4-29: 15 lb Dual Latch LVDT 71
Figure 4-30: 20 lb Dual Latch Load Cell 72
Figure 4-31: 20 lb Dual Latch LVDT 72
Figure 4-32: 40 lb Dual Latch Load Cell 73
Figure 4-33: 40 lb Dual Latch LVDT 74
Figure 4-34: 10 lb Closing Test (Load Cell) 75
Figure 4-35: 10 lb Closing Test (LVDT) 76
Figure 4-36: 15 lb Closing Test (Load Cell) 76
Figure 4-37: 15 lb Closing Test (LVDT) 77
Figure 4-38: Clasp Extension Sleeve 78
Figure 4-39: Pin and Clasp Starting Orientation 78
Figure 4-40: Fluid Drying 79
Figure A-1: Viscosity Curve 48.6% PCC in PEG 89
Figure A-2: Force Applied at Center of Pressure 90
Figure A-3: Simulated Door Displacement 90
Figure A-4: Force Applied at Handle 91
Figure A-5: Simulated Door Displacement 91
Figure A-6: Force Applied at Handle 92
Figure A-7: Simulated Door Displacement 92
Figure A-8: Steel Plate 93
Figure A-9: Internal Temperature Change 94
Figure A-10: Temperature Response of Plate 95
Figure A-11: Insulation 95
Figure A-12: Complete Scenario 96
Figure A-13: Mathcad Worksheet Page 1 97
Figure A-14: Mathcad Worksheet Page 2 98
Figure A-15: Mathcad Worksheet Page 3 99
Figure A-16: Mathcad Worksheet Page 4 100
Figure A-17: Mathcad Worksheet Page 5 101
Figure B-1: Brookfield Engineering DV-III Rheometer 102

Figure B-2: DV-III Rheometer Accessories 103
Figure B-3: Rheometer Test Section..... 103
Figure B-4: Brookfield R/S-CPS Rheometer..... 104
Figure B-5: Cone and Plate Configuration 105
Figure B-6: Peltier Thermal Regulator PTR-1..... 105
Figure B-7: C25-1 and C50-1 spindles 105
Figure B-8: Brookfield R/S-CPS Rheometer technical data from operating instructions 106
Figure B-9: Peltier Thermo Regulator PTR-1 technical data from operation manual..... 107
Figure B-10: 50 mm cone specifications from measuring system data 108
Figure B-11: 25 mm cone specifications from measuring system data 109
Figure C-1 Omega LC111-100 load cell specifications from information sheet..... 110
Figure C-2: Omega LD620-25 LVDT specifications from information sheet 111
Figure C-3: H2W NCM05-28-180-2LB voice coil specification from H2W Technologies 111
Figure C-4: Advanced Motion Controls 16A20AC PWM Brush-type servo amplifier specifications from manual 112
Figure C-5: National Instruments PCI 6221 Multi-Function DAQ analog input specifications from NI 622X specifications sheet..... 113
Figure C-6: National Instruments PCI 6221 Multi-Function DAQ analog input specifications from NI 622X specifications sheet (cont.) 114
Figure C-7: National Instruments PCI 6221 Multi-Function DAQ analog output specifications from NI 622X specifications sheet..... 115
Figure C-8: LabVIEW block diagram 117
Figure C-9: LabVIEW front panel..... 117
Figure C-10: Test Cell Output File 118
Figure C-11: Load Cell Factory Calibration..... 119
Figure C-12: Load Cell Calibration Test 120
Figure C-13: Load Cell Calibration Results 120
Figure C-14: Manufacturer LVDT Calibration..... 121
Figure C-15: LVDT Calibration Test 121
Figure C-16: LVDT Calibration Test Results..... 122
Figure C-17: Voice Coil Test Data Sheet 122

Figure C-18: Actuator Calibration 123
Figure C-19: Voice Coil Calibration..... 123
Figure D-1: Proof of Concept Prototype..... 125
Figure D-2: Proof of Concept Outer Cylinder 125
Figure D-3: Proof of Concept Lid..... 126
Figure D-4: Disassembled Commercial Prototype 126
Figure D-5: Commercial Prototype Components 127

List of Tables

Table 2-1: Original Latch Requirements 5
Table 4-1: Fluid Gap Dimensions 53

Acknowledgements

I would like to thank the many people who helped make the completion of this project possible.

First, I would like to thank my graduate advisor and major professor of my committee Dr. B. Terry Beck for his patience, his always being available to provide much needed guidance, and for encouraging me to pursue my masters in the first place. I would also like to thank professors Mo Hosni and Zhongquan Charlie Zheng for serving on my committee, for their always being available to answer questions, and for providing insights on the project that I would not have caught on my own.

Next, I would like to thank the client company, and particularly my contacts Michael Roche and Phil Czarnecki for their support of the project.

I would further like to thank Dr. Susan Sun, the Kansas State University Bio-Materials & Technology Lab, and especially Karthik Venkateshan for helping me get started with the fluids research and training me in the use of the rheometer equipment.

I would like to thank students Travis Grove and Jun Chen, for their help with researching literature and testing of the testing of the prototype fluid.

I would also like to thank both Jason Selland and Eric Wagner, previous and current MNE shop managers, for their help in designing and manufacturing the prototypes and custom pieces for the test setup. Thank you as well to the rest of the MNE department staff, Erin Carlson, Sherry Donahey, Carol Konold, Marcia Chacon, and Eric Patterson, for their help during various stages of the project.

Finally, I would like to thank my family for their constant support during the pursuit of my M.S. degree.

CHAPTER 1 - Introduction

The objective of this project was to develop a viscous latch mechanism concept, and evaluate the feasibility of this viscous latch for a commercial clothes dryer door application. The latch was to be capable of resisting fast pressure loading on the inside of the dryer door, while enabling normal opening of the door from outside the dryer compartment with a slow application of force.

1.1 Motivation for Project

The project addressed safety issues associated with commercial clothes driers. In the unlikely event of a rapid pressure rise within the dryer (on the order of hundredths of a second in duration) acting against the door has been estimated to produce internal loading forces in the range of 40-60 lbf. This level of force could possibly cause premature and undesirable spontaneous opening of the door. For normal door opening with slow application of force (estimated to be approximately 1-second duration), code requires that the door be capable of being opened with a force no greater than 15 lbf.

1(a) Door-Mounted Component 1(b) Unit-Housing Receptacle

Figure 1-1: Washer Door Latch Mechanism

2(a) Unit-Housing Receptacle 2(b) Door-Mounted Component

Figure 1-2: Dryer Door Latch Mechanism

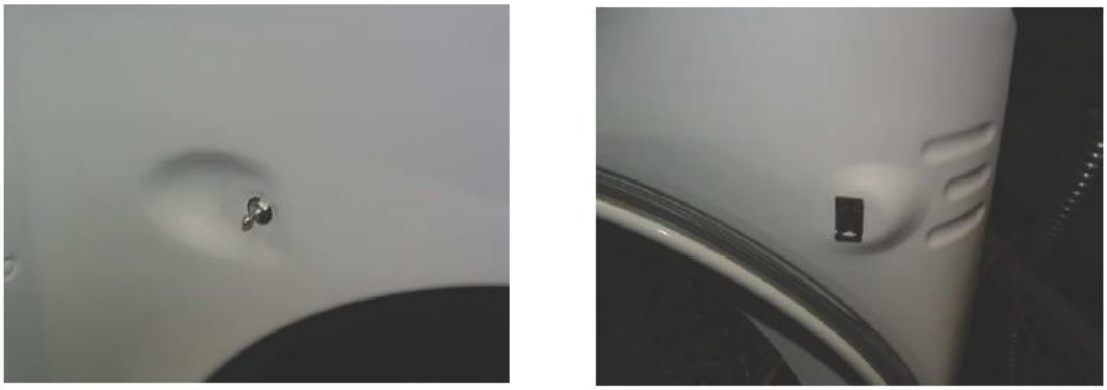

3(a) Unit-Housing Component 3(b) Door-Mounted Receptacle

Figure 1-3: Dryer Door Latch Mechanism

Examples of existing commercial washer and dryer door latch mechanisms are shown in Figures 1-1, 1-2 and 1-3. These are all relatively simple mechanical spring-loaded latch devices. These latches do not exhibit the desired protection against internal pressure pulse loading described above.

1.2 Design Objectives

The primary objective of the proposed project was to come up with a viable latch design that would fulfill the dryer door latch loading and operating requirements. In addition to the basic operating force and pulse-load resistance requirements, there were space limitations. Typical available space in a dryer door for a latch mechanism is illustrated in Figure 4. In terms of rectangular space available for the original set of requirements, the region within the door

available for the latch mechanism was approximately 3in x 1.5in x 2in, although the physical design of the latch need not be restricted to a rectangular geometry. A simplified latch mechanism provided by the client that fits the above basic rectangular geometry is displayed in Figure 1-4.

Figure 1-4: Dryer Door Latch Space Limitations

The key features of this design are that the approximately linear motion of the door is tied to the rotational motion of a shaft. With this early latch concept, some type of viscous damper would be attached to the shaft about which the latch arm pivots. This latch is actually somewhat similar in operation to the simple mechanical latch mechanisms shown in Figures 1-1, 1-2, and 1-3 above, except for the presence of the viscous damper. The viscous damper design, and determination of the required properties of the viscous fluid within the damper, was the focus of the project. The maximum environmental temperature anticipated for the door latch mechanism is expected to range from about 32 F to about 160 F during operation, with a low-end temperature limit of about -40 F to be possibly encountered during shipment of the dryer unit.

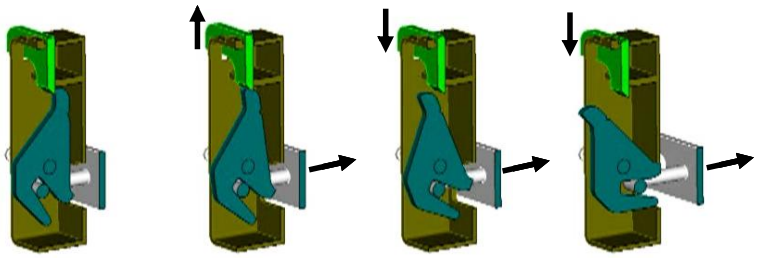

(a) Latch Opening Sequence

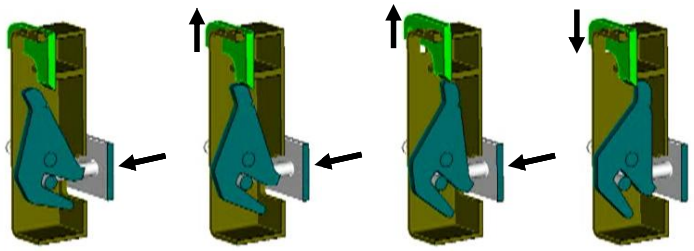

(b) Latch Closing Sequence

Figure 1-5: Viscous Latch--Basic Mechanical Concept

The project consisted of three phases. The first phase consisted of a feasibility study, identifying a potentially workable concept and investigating the basic fluid property and geometry requirements for such a device. The second phase of the work was to demonstrate a proof of concept in the form of a working model prototype. This prototype would not necessarily be of identical shape and proportions as the finalized design, but would be developed to facilitate experimental testing and evaluation of performance under the desired operating conditions. Finally, the third phase will be to develop the transition to a producible product through appropriate modifications, as necessary, to the prototype design.

CHAPTER 2 - Phase I: Background/Feasibility Study

As stated in the previous chapter the objective of the project was to develop a viscous latch mechanism concept, and evaluate the feasibility of this concept for a commercial clothes dryer door application. The first phase of the project involved performing background research on the subject and performing preliminary analysis in order to determine if the concept was feasible enough to be worth taking the project to the next phase.

2.1 Identification of All Relevant Latch Specifications

The latch had to be capable of resisting fast pressure loading on the inside of the dryer door, while enabling normal opening of the door from outside the dryer compartment with a slow application of force. The original desired specifications are listed in Table 2-1 below.

Table 2-1: Original Latch Requirements

Space constraints: • Apparatus must fit space of 3x1.5x 2 inches
Prevent opening during containment test: • Plastic components must have melting temperature greater that 500 F • Must be able to resist impulse force between 40-60 lbs
Easy to open: • Door must be free of latch after 5 mm of travel • Door must open when force of less than 15 pounds is applied for 1 second.
Door Seal: • Will not open if force of less than 6 pounds is applied • Latch must be able to operate in a temperature range from -40F to 500F • Door must take longer than 1 second to open while a force between 15 - 40 lbs is applied
Closes easily: • Closing force equal to opening force • Rate must not be restricted
Operational life:

• Closes and latches 30000 cycles
Able to withstand environment: • Storage temperature ranging from -40F to 150 F • Resistant to chemicals and humidity in environment.
Able to withstand abuse: • Door slam and over torque

2.2 Literature Review

Review of Latch Damping Mechanisms

Viscous damping devices using Newtonian fluids have been successfully implemented for various applications. Several of these are described below.

Viscous Damped Hinge

A viscous damped hinge was developed by (Rude & Brokowski, 2006) in order to minimize the occurrences of damage to laptop screens and monitors mounted in a similar fashion when slammed shut. The hinge configuration consists of two cylindrical surfaces separated by a layer of viscous damping fluid. Due to the fact that the friction force from the damping fluid is velocity dependant if the screen is closed at a high velocity, the damping force will slow to an acceptable level.

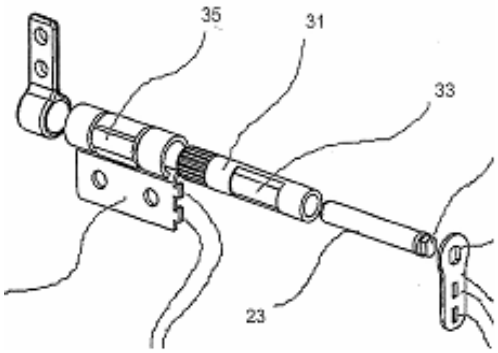

Figure 2-1: Viscous Damped Hinge. Modified From Rude & Brokowski (2006)

Viscous Coupling Unit

A viscous coupling unit can be found in the center differential of all-wheel drive vehicles (Drew & Davis, 2010). An example of this device is shown in Figure 2-2. This device is composed of alternating circular plates mounted in a sealed drum filled with a shear thickening fluid. There are two sets of plates, and when they rotate in unison the fluid stays in a liquid state. When the plates start rotating at two different speeds, the shear effect of the disks will cause the fluid to solidify. In this state the fluid will essentially glue the plates together, and transmit power from one set of plates to the other.

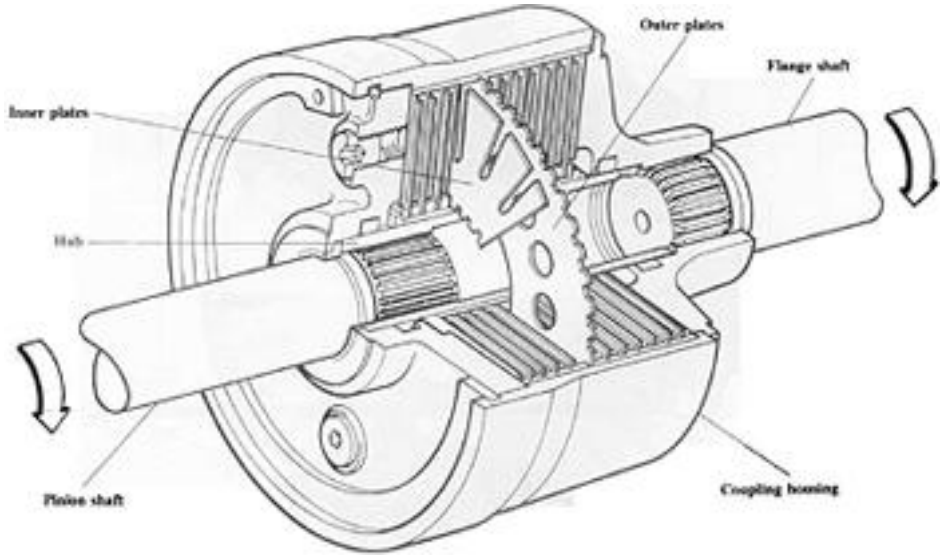

Figure 2-2: Viscous Coupling Unit from Drew and Davis (2010)

Fluid Damped Vehicle Door Latch

A fluid damped door latch is used to reduce the noise and shock caused by a spring loaded car door handle returning to rest position when released. The damping action is caused by movement of a vane mounted on a central rotating shaft, in a cavity filled with a viscous fluid such as silicone. An example of the device (McFarland, 2000) is shown in Figure 2-3.

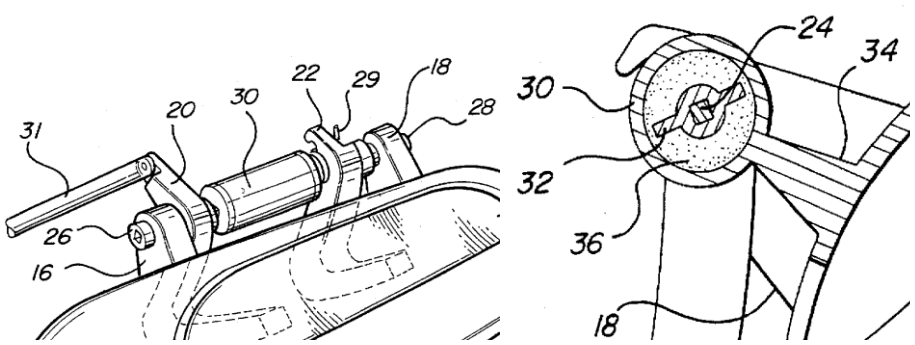

Figure 2-3: Fluid Damped Vehicle Door Latch. Modified From: McFarland (1998)

Shear Thickening Fluids

This section documents the different mechanisms for shear-thickening behavior in fluids. In many cases shear thickening behavior is the result of the interaction between small particles or polymers within the fluid which react in a particular manner when subjected to shear stress.

Suspensions

Suspensions of particles are another source of shear thickening behavior. In order for a fluid with suspended particles to have shear thickening behavior, according to Raghavan and Khan (Raghavan & Khan, 1997) two criteria must be met. First, the volume fraction of the solid particles suspended in the fluid must be very high. Secondly, the particles must be either of neutral electrical charge or repel each other so the particles remain freely throughout the fluid. The shear thickening behavior, as stated by Shenoy and Wagner (Shenoy & Wagner, 2005), is the result of the formation of clusters of the solid particles in the compressive axis of the fluid flow when viscous forces overcome the forces between the particles. The increase in viscosity is the result of fluid forces of the liquid having to squeeze through gaps between the compacted particles. Cases of discontinuous shear thickening, where the suspension quickly changes from a fluid to a solid like material at a certain shear rate, are the result of the particle clusters jamming. This behavior is represented in the diagram shown in Figure 2-4.

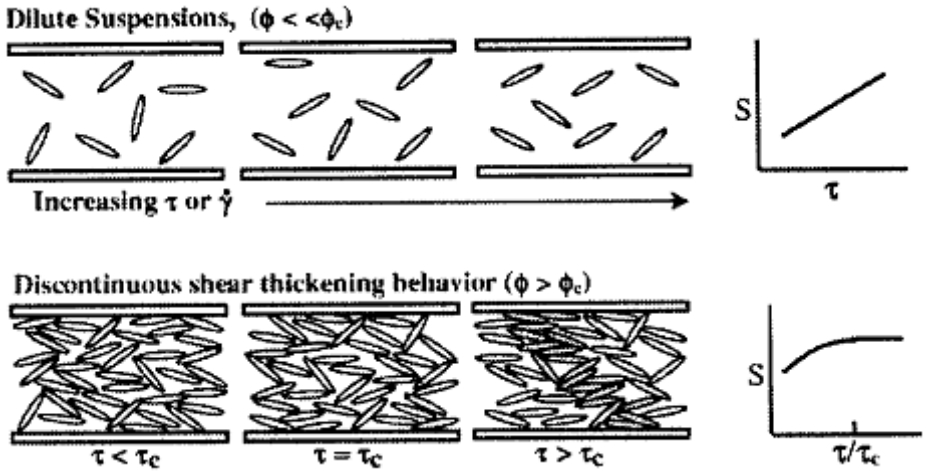

Figure 2-4: Behavior of particles in suspensions, Modified from: (Egres, Netteshein, & Wagner, 2006)

Surfactant Solutions

Shear thickening can occur in very dilute surfactant solutions, having volume fractions near 10^{-3}. Surfactants are substances whose molecules are amphiphilic, which means that the "heads" of the molecules are hydrophilic while their "tails" are hydrophobic (Sigma-Aldrich, 2010). This characteristic causes the surfactant molecules in the solution to arrange themselves into structures known as micelles. According to (Berret, Gamez-Corralez, Oberdisse, Walker, & Linder, 1998) the proper concentration for shear thickening to occur is when cylindrical and elongated micelles form. It is the interaction between these particles under shear that causes the thickening behavior. For the current project, shear thickening suspensions were pursued in favor of surfactant solutions due to the fact that the shear thickening behavior of suspensions seemed to be more significant based on test data from (Shenoy & Wagner, 2005) and (Berret et al., 1998).

Ionomer Fluids

Another possible source of shear thickening behavior is with ionomer fluids. Ionomers are a type of polymer with ions attached along the polymer chain. Some solutions with very low concentrations of ionomer have constant viscosities as temperatures increase, and in some cases the viscosities even increase with temperature (R. D. Lundberg & Makowski, 1980),(R. D. Lundberg, 1982). Still other ionomer solutions have been shown to have shear thickening

properties (R. D. Lundberg & Duvdevani, 1989). This brings up the possibility of adding ionomers to a dilatant suspension to decrease temperature effects, or of finding a temperature resistant solution with the desired shear thickening properties.

Desired Fluid Properties

An ideal shear thickening fluid would behave like a Newtonian fluid with a constant viscosity until a certain critical shear rate. At this critical rate the fluid would begin to act like a solid, as suggested in Figure 2-5.

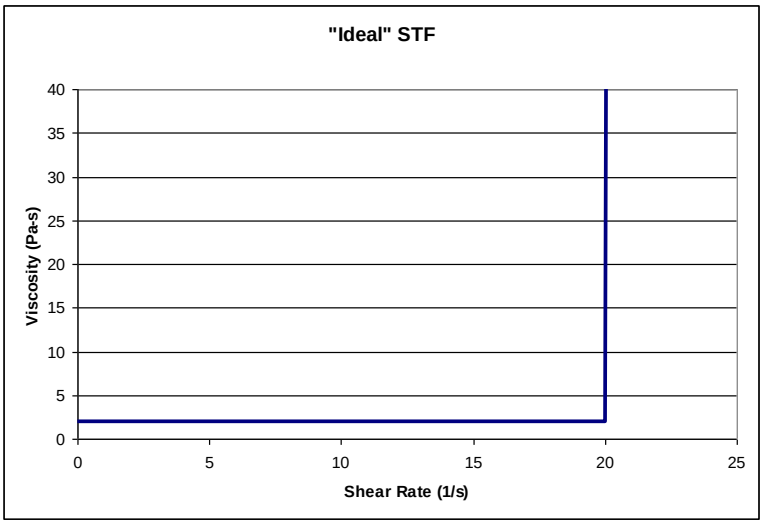

Figure 2-5: Ideal Shear Thickening Fluid

However, the actual behavior of shear thickening fluids can be much more complex. Figure 2-6 shows an example of an actual fluid, which has shear thinning behavior at low shear rates and a gradual thickening slope after the "critical" shear rate. Another interesting behavior to observe is that some fluids have a maximum viscosity that can be achieved by shear thickening. Beyond a certain shear rate the fluids will fracture or begin shear thinning. These characteristics all depend on variables such as the size, shape, hardness, and concentration of particles used in the dispersion. The data shown in Figure 2-6 is from an actual shear thickening suspension composed of 48.6% by volume Precipitated Calcium Carbonate particles in Polyethylene Glycol.

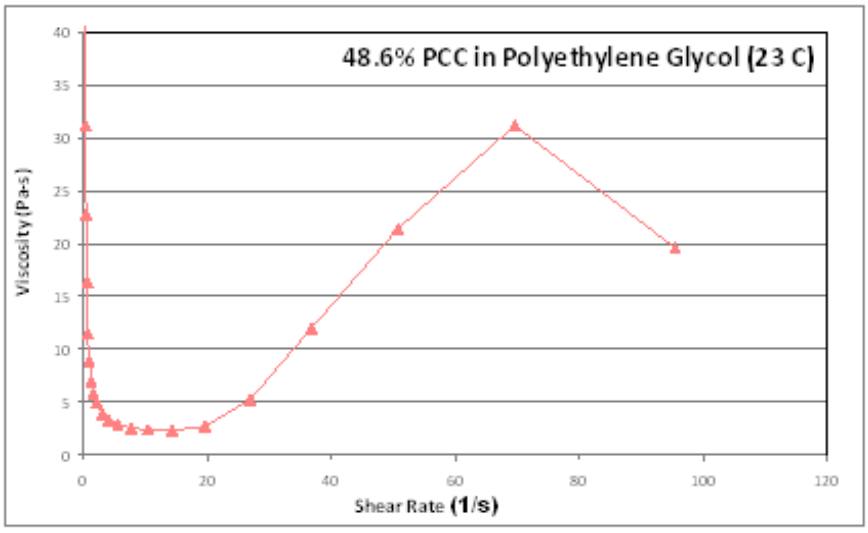

Figure 2-6: Actual Shear Thickening Behavior

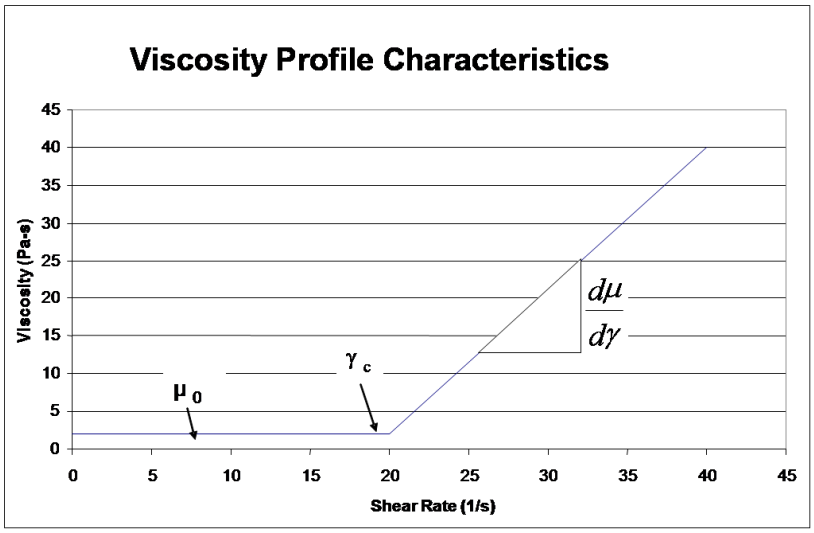

Figure 2-7: Simplified Model for a Real Shear Thickening Fluid

Figure 2-7 shows a simplified model for a real shear thickening fluid, and the primary properties of a fluid that need to be known in order to design a damper using it. The first property is μ_0, the fluid's average initial viscosity before shear thickening occurs. The next is the critical shear rate γ_c, the "break point" where significant shear thickening begins to occur. The final characteristic is the rate at which the viscosity increases with respect to shear rate once shear thickening begins. Theories have been proposed to predict all the characteristics, based on the

suspension fluid and the particle characteristics (Lee & Wagner, 2006), (Boersma, Laven, & Stein, 1990).

The behavior of shear thickening suspensions can also be highly sensitive to temperature. This is largely due to the change in viscosity of the suspension fluid medium with respect to temperature (Shenoy & Wagner, 2005).

2.3 Fluid Testing and Selection

Identification of Viable Shear Thickening Fluids

For the proof of concept phase, it was necessary to find a fluid that was stable, was readily available, and one that had good shear thickening properties. Based on these requirements it was determined that particle suspensions were the most likely group from which to find a suitable fluid, based on research described in Section 2.2.2. A suspension of precipitated calcium carbonate (PCC) particles (Magnum Gloss ® M, Mississippi Lime Company) in a medium of polyethylene glycol (PEG) with a molecular weight of 200, was chosen due to availability of the required materials and due to its good shear thickening characteristics. This fluid is similar to the fluids used by (Wetzel et al., 2004)

Viscosity Testing

The fluids tested in this first round of tests were dispersions of precipitated calcium carbonate (PCC) particles in polyethylene glycol. These tests were performed to help provide a good understanding of the shear thickening behavior, as well as to gather actual data for use in a simulation model. The mixture percentage (%) refers to the percentage of the mixture volume that is composed of the PCC particles. A comparison of the mixtures tested is seen in Figure 2-8.

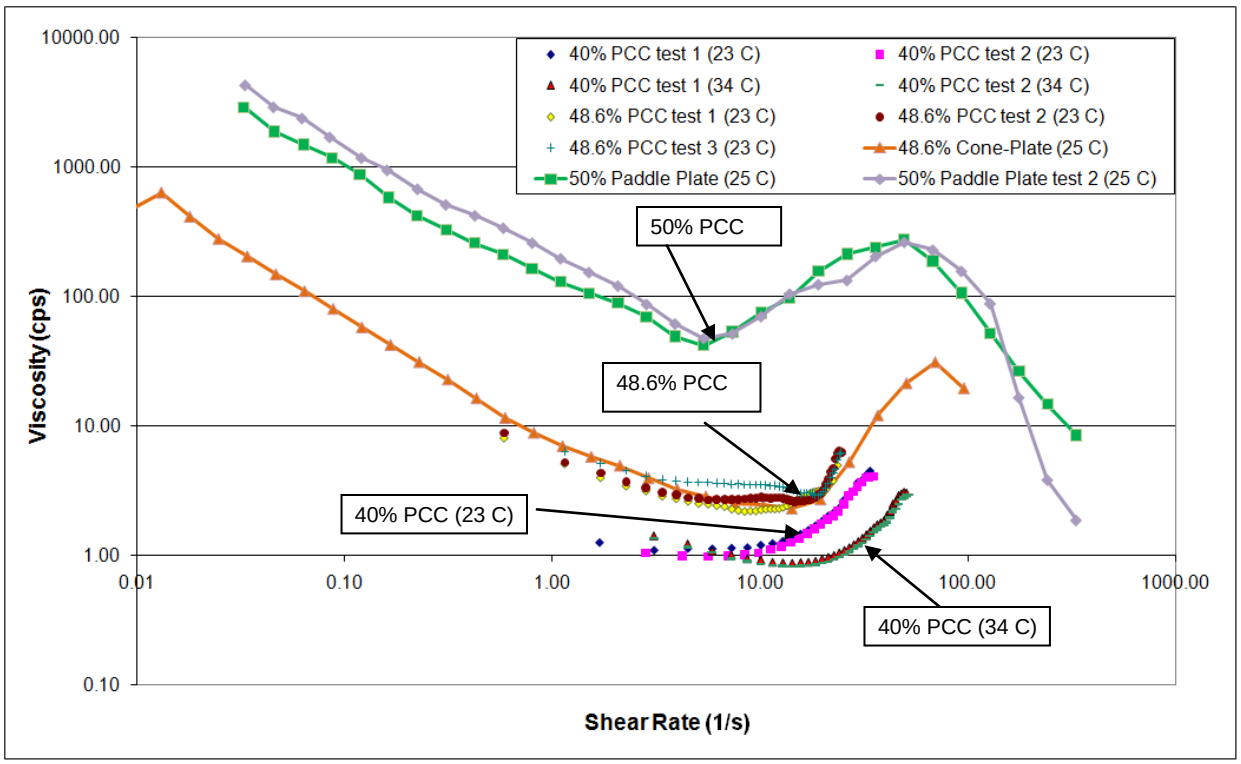

Figure 2-8: Rheometer Test Data

From this testing it was determined that the 48.6% mixture shown in Figure 2-6 had the best properties for use with the proof of concept application due to its relatively high rate of shear thickening and low initial viscosity.

2.4 Damper Design Process

The damping forces used in the development of the initial design concepts came from the behavior of shear thickening fluids in simple Couette flow, neglecting fluid inertia effects. This is illustrated in Figure 2-9. The viscous shear reaction force of the fluid layer counteracts the force acting to open the door. The fluid shear stress is a function of the fluid's dynamic viscosity (μ), and the time rate of strain (velocity gradient normal to the surface, dV/dy) that the fluid is subjected to.

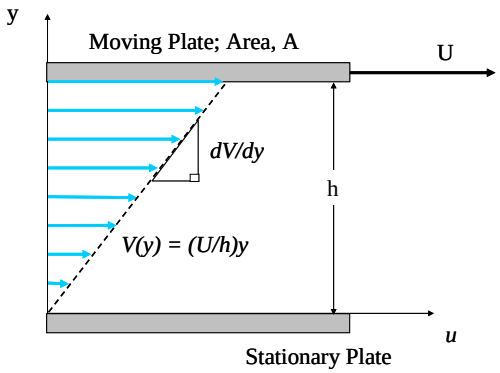

Figure 2-9: Couette Flow

$$\tau = \mu(dV/dy) \cdot dV/dy = \left(\frac{N \cdot s}{m^2}\right)\left(\frac{m/s}{m}\right) = \frac{N}{m^2} \qquad (2\text{-}1)$$

By using a non-Newtonian fluid, a damper can be designed where the resistance force actively changes to counteract the external force applied. This will be described below.

Early Concepts

The preliminary designs presented below all involve transferring the opening motion of the door to the plate over plate motion of the latch. The designs all boil down to Couette flow of an STF as represented in Figure 2-9 above.

Cylinder

A cylinder aligned with the rotating axis mounted within a larger cylinder with a thin layer of damping fluid between the two cylinders forms the basis for one damper design. This concept is shown in Figure 2-10. Multiple cylinders can be lined up within each other in this fashion to increase effectiveness (i.e. surface area) and save space

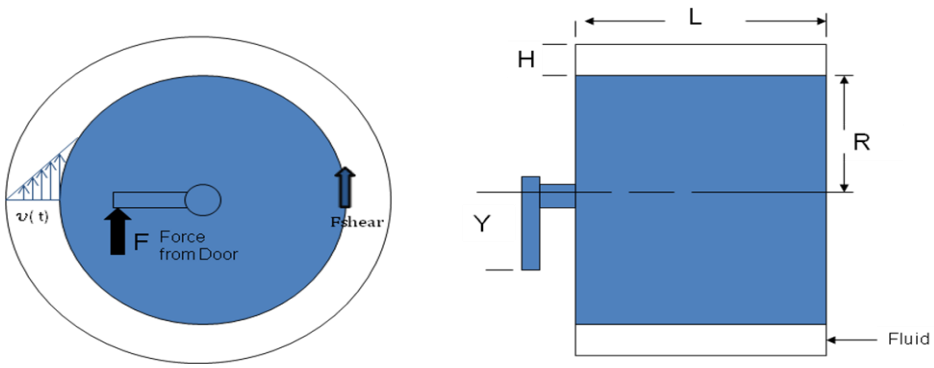

Figure 2-10: Fluid Damped Cylinder

Disk

The simplest form of a disk-based design consists of two disk plates, one fixed and, one linked with the rotational axis. A thin film of damping fluid is sandwiched in between. Like the cylindrical design, multiple moving and stationary disks could be utilized to increase damper effectiveness. This basic concept is shown in Figure 2-11.

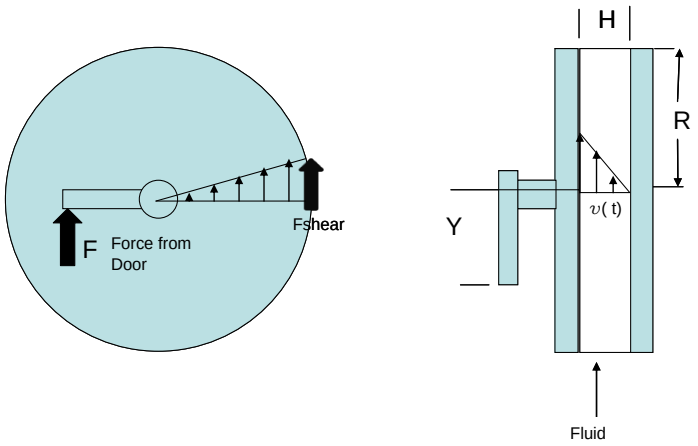

Figure 2-11: Fluid Damped Disks

Paddle Wheel

A third rotational shear thickening fluid design consists of a paddle wheel connected to a rotational shaft suspended in a damping fluid. This design is shown in Figure 2-12. As with the above designs the number of fins is variable and could be increased to increase effectiveness of the damper. The damping effect of this design will be more difficult to model, as it is more complex than simple Couette flow.

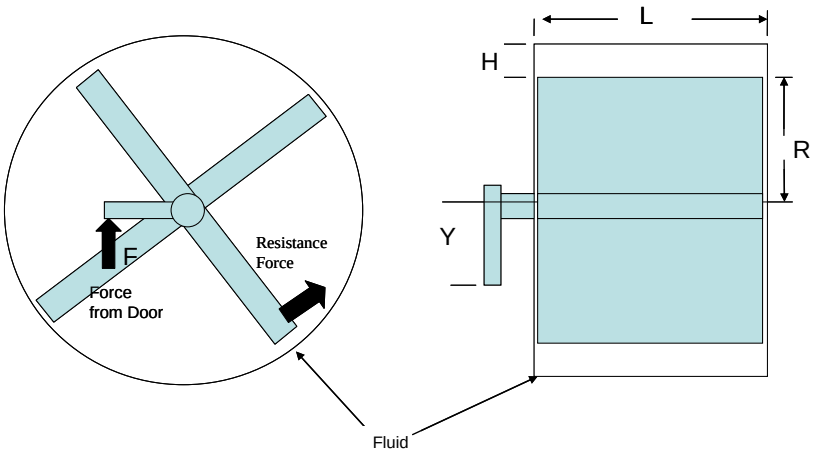

Figure 2-12: Fluid Damped Paddlewheel

Linear Latch

Other possible configurations for a viscous latch include the use of linear motion, such as that shown in Figure 2-13. Like some of the rotational designs, the effectiveness could be increased by increasing the number of plates.

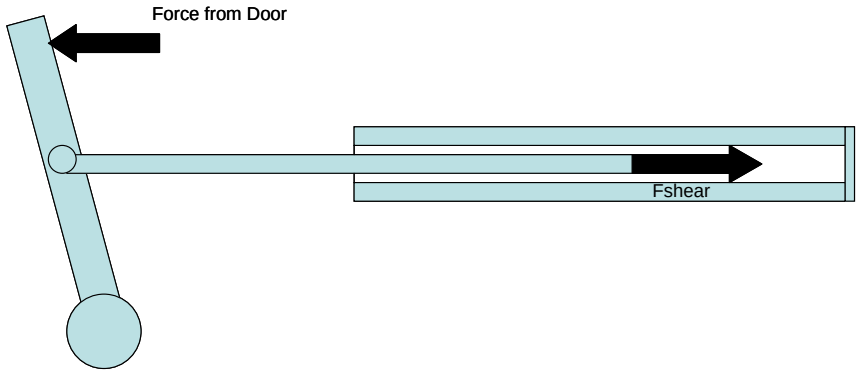

Figure 2-13: Linear Latch

2.5 Prediction Model

Ultimately, the cylindrical geometry in Figure 2-10 was chosen for the first prototype damper design. It was chosen for its ease of construction and its simplicity in modeling. Using this geometry a simple prediction model was developed from the methodology described below.

Step 1: Conservation of Momentum for Door

The first step is to take into account the forces acting on the door.

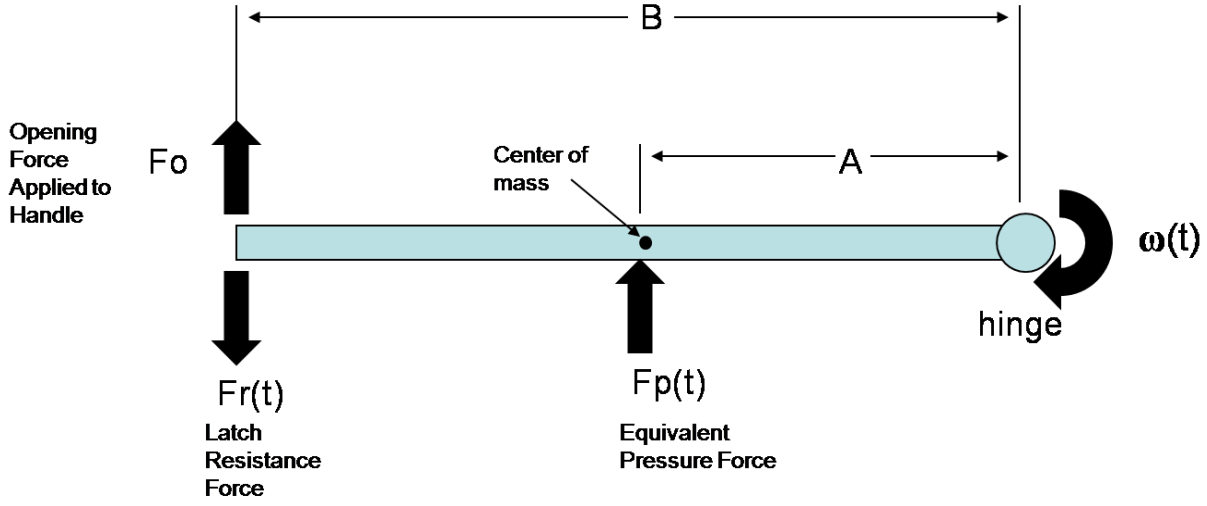

Figure 2-14: Door Hinge Force-Moment Diagram

Nomenclature:

Fr(t)= resistance force provided by the viscous latch,

Fo(t) = Opening force being applied to the handle

ω(t) = angular velocity of the dryer door rotating about its hinge,

Area = area of door subjected to pressure within dryer,

B = distance from handle to hinge,

A = distance from center of door to hinge,

Mass = mass of door,

P(t) = internal pressure,

The angular velocity of the door can be found using Equation 2-2.

$$A \cdot Fp(t) - B \cdot Fr(t) + B \cdot Fo(t) = I_{Door} \frac{d\omega}{dt} \tag{2-2}$$

This equation could be modified to take into account additional forces acting on the door by simply adding or subtracting the appropriate force-moment component into the Equation 2-2, and properly accounting for whether it is acting clockwise or counterclockwise about the hinge.

Approximating the door as a thin plate to find its mass moment of inertia, I, it yields

$$I = (\frac{1}{12} \cdot Mass \cdot B^2 + Mass \cdot A^2) \tag{2-3}$$

Substituting into Equation 2-2, and relating Fp(t) to applied pressure inside the door, yields

$$A \cdot (P(t) \cdot Area) - B \cdot Fr(t) + B \cdot Fo(t) = (\frac{1}{12} \cdot Mass \cdot B^2 + Mass \cdot A^2) \frac{d\omega}{dt} \tag{2-4}$$

Rearranging Equation 2-4 in order to find the angular acceleration results in Equation 2-5 as follows

$$\frac{d\omega(t)}{dt} = \frac{A \cdot (P(t) \cdot Area) - B \cdot Fr(t) + B \cdot Fo(t)}{\left(\frac{1}{12} \cdot Mass \cdot B^2 + Mass \cdot A^2\right)} \tag{2-5}$$

Using Equation 2-5 the angular velocity of the door can be solved in discreet form using small time steps; thus

$$\omega(t + \Delta t) = \frac{d\omega(t)}{dt} \cdot (\Delta t) + \omega(t) \tag{2-6}$$

Step 2: Correlation between Movement of Door and Latch Rotation

The displacement of the door at the point where it engages the damper will be the same as the displacement at the end of the damper arm.

Assuming X(t) << B, the motion can be approximated as essentially translation rather than rotation.

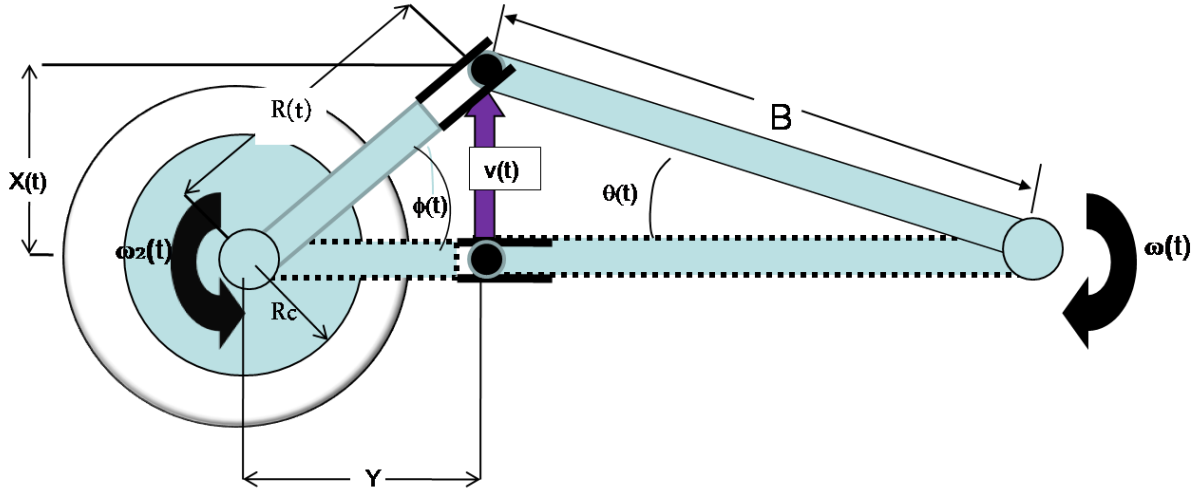

Figure 2-15: Damper Travel

Figure 2-15 shows the damper travel, where, assuming small angular displacement of the door, it is easily shown that

$$\omega(t) = \frac{d\theta}{dt} \cong \frac{dX}{dt} \cdot \frac{1}{B} \tag{2-7}$$

Integrating Equation 2-7 using discrete time steps yields

$$X(t+\Delta t) = \int_{t}^{t+\Delta t} \omega(t) \cdot B \cdot dt \tag{2-8}$$

Since the angular velocity is found in Equation 2-6, the discreet form of Equation 2-8 for use in the model is

$$X(t+\Delta t) = (\omega(t+\Delta t) \cdot (t+\Delta t) - \omega(t) \cdot t) \cdot B \tag{2-9}$$

Noting that X(t) of the door is the same as X(t) for the latch arm gives

$$\omega 2(t) = \frac{d\phi}{dt} = \frac{d}{dt}\left(\tan^{-1}\left(\frac{X(t)}{Y}\right)\right) \tag{2-10}$$

Equation 2-11 is the discreet form of Equation 2-10

$$\omega 2(t) = \frac{\tan^{-1}\left(\frac{X(t+\Delta t)}{Y}\right) - \tan^{-1}\left(\frac{X(t)}{Y}\right)}{\Delta t} \tag{2-11}$$

Due to the "cam-like" motion of the damper shown in Figure 2-16, the effective radius transmitting the velocity, v(t), changes with position while the force moment arm remains approximately constant.

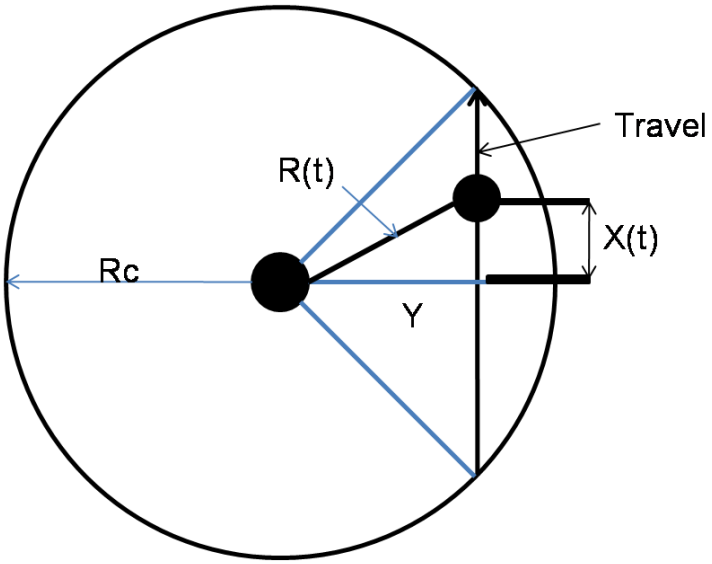

Figure 2-16: Cam Motion

Since the door opening velocity v(t) is a function of angular velocity of the damper ω2(t) and the radius of the moment arm is R(t), the following is attained:

$$v(t) \cong \omega 2(t) \cdot R(t) \tag{2-12}$$

where

$$R(t) = \sqrt{X(t)^2 + Y^2} \tag{2-13}$$

The "effectiveness" of the damper actually changes with the opening position. This means that the farther the latch rotates, the faster is the opening velocity, v(t).

Step 3: Determine Resistance Force of Latch

It is assumed that the mechanical and fluid inertia of latch are negligible.

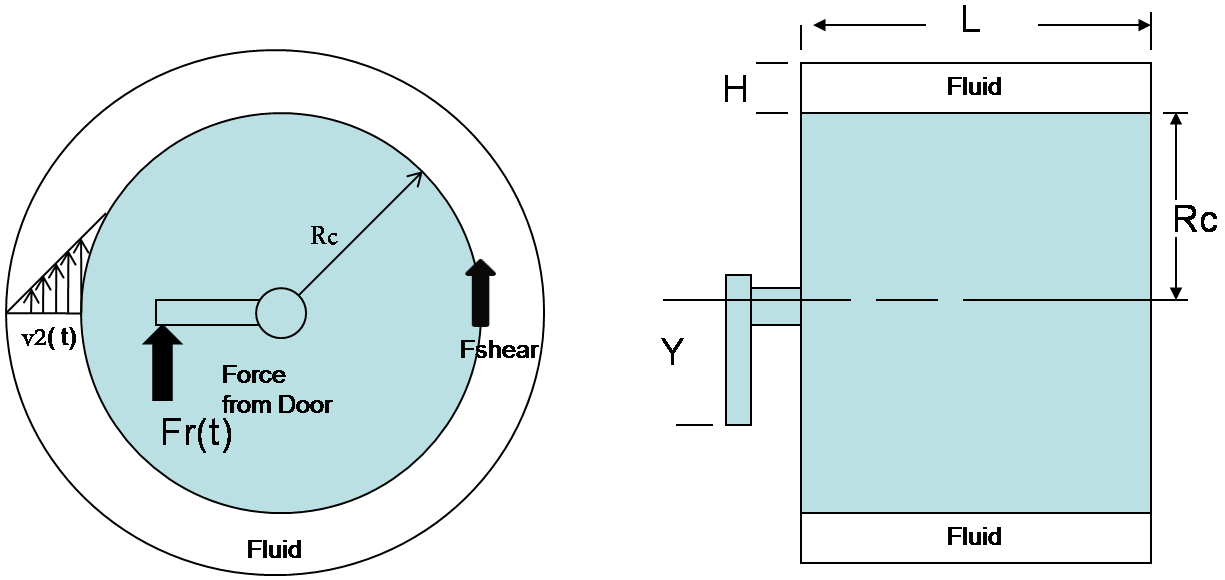

Figure 2-17: Latch Resistance

The resistance force of the latch can then be determined using Newton's law which gives the following for the shear stress:

$$\tau = \mu \frac{dV}{dy} \tag{2-14}$$

The shear rate $\gamma(t)$ is then given by

$$\gamma(t) = \frac{v2(t)}{H} = \frac{\omega 2(t) \cdot Rc}{H} \tag{2-15}$$

Now, the viscosity is dependent on shear rate, so $\mu = \mu(\gamma)$.

The resisting shear force in the fluid layer is thus given by

$$Fshear(t) = \mu(\gamma) \cdot (\gamma(t)) \cdot (SurfaceArea) \tag{2-16}$$

or,

$$Fshear(t) = \mu(\gamma) \cdot \gamma(t) \cdot (2\pi \cdot Rc \cdot L) \tag{2-17}$$

The resisting torque is given by,

$$T(t) = R_c \cdot Fshear(t) = Y \cdot Fr(t) \tag{2-18}$$

therefore the resistance force acting on door is,

$$Fr(t) = Fshear(t) \cdot \frac{Rc}{Y} \tag{2-19}$$

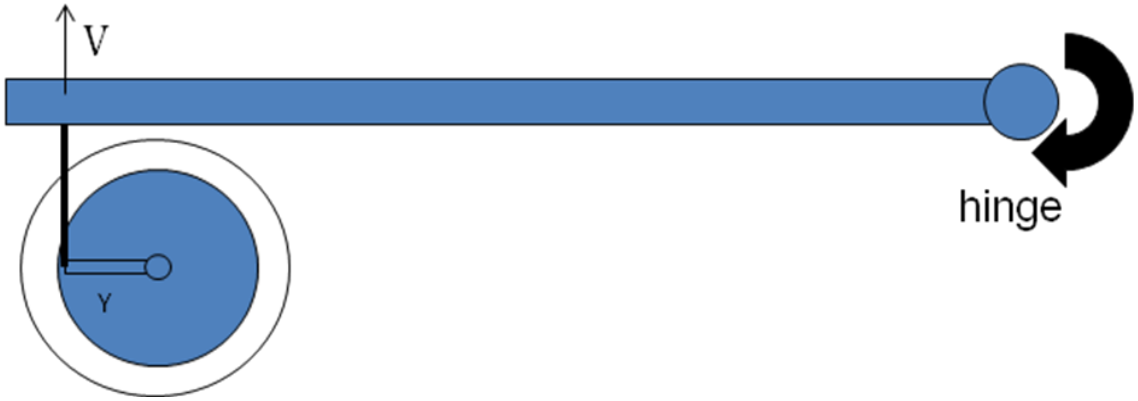

Figure 2-18: Door Resistance

Performance predictions

Using the prediction model described in detail above, as well as the viscosity versus shear rate curve of the 48.6% PCC/PEG suspension found from rheological testing, a Matlab program was developed to estimate how the viscous latch would perform under different loadings. The code for the program, as well as the detailed results, can be found in appendix A. The geometry of the door and damper used in the model is given in Figures 2-19 and 2-20. Response predictions for certain door opening conditions will be presented in the next section.

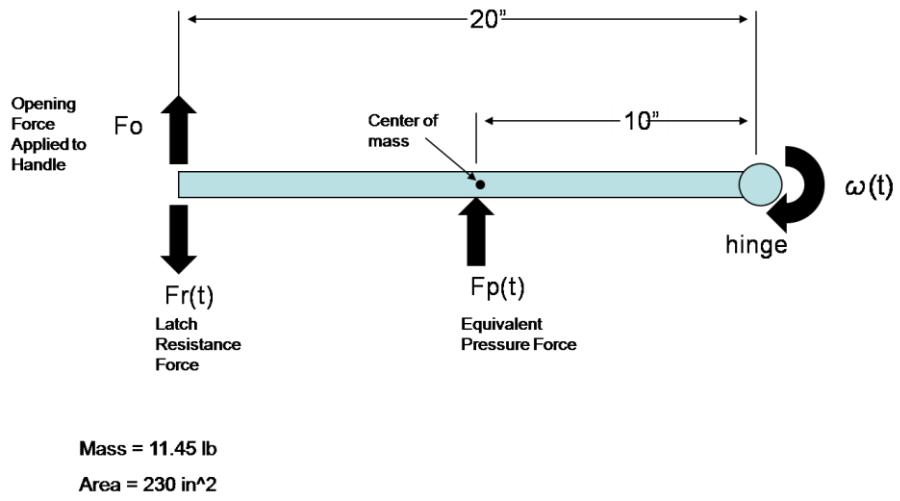

Figure 2-19: Door Geometry for Dynamic Model

The door is considered fully disengaged when the displacement X(t) = 0.2 inches.

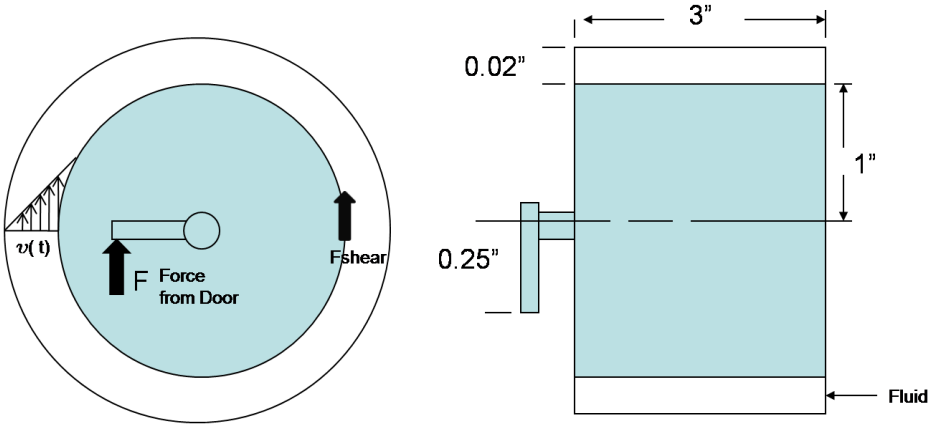

Figure 2-20: Damper Geometry for Dynamic Model

Worst Case Pressure Pulse

The average pressure buildup within a dryer during an event is on the order of 1.6 to 1.8 inches of water, lasting for 0.3 to 0.5 seconds. The worst case pulse recorded was 5.2 inches of water. Hence, the "worst case" is a pressure of 5.2 inches of water lasting for 0.5 seconds. Figure 2-21 (a) shows the input pulse, and 2-25 (b) shows the response. As seen in Figure 2-21 the door does not open for this input.

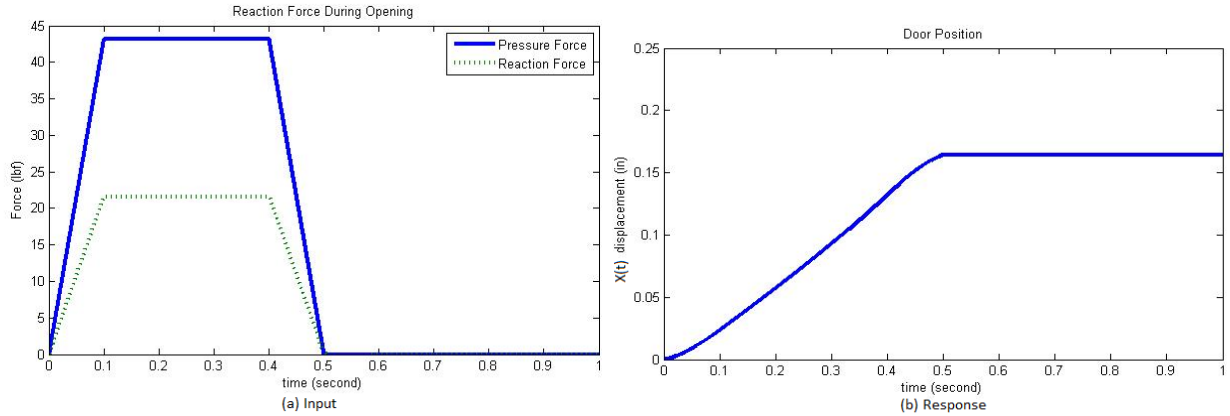

Figure 2-21: Door Displacement and Forces for Worst Case Pressure Pulse

User Opening

According to the design specifications, a person must be able to open the door in 1 second by applying a force of no more the 15 pounds and no less than 6 pounds.

Figure 2-22 shows that applying 15 pounds of force would cause the door to open in approximately 0.6 seconds. While Figure 2-23 demonstrates that the 6 pound force will cause the door to open in 0.85 seconds, both within the acceptable time duration.

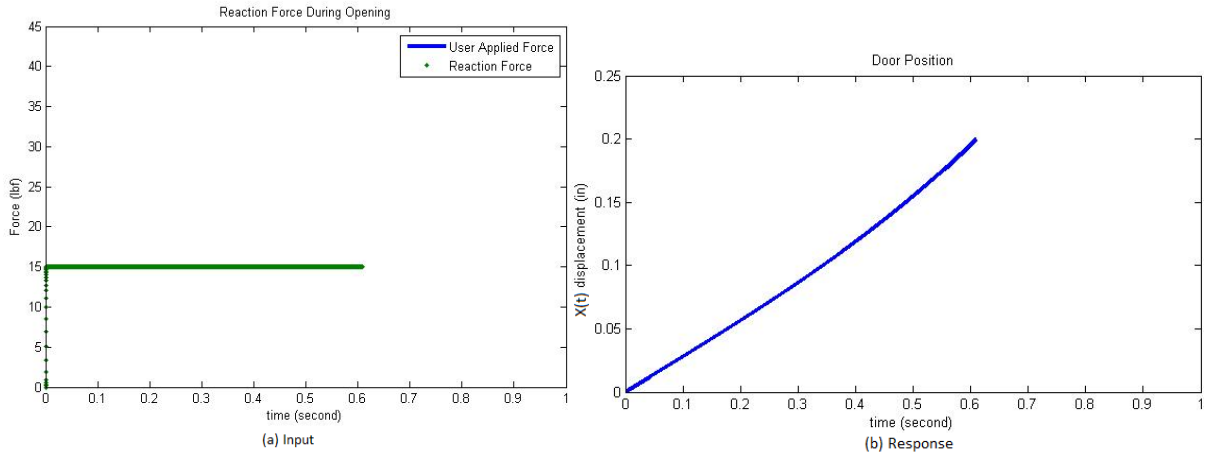

Figure 2-22: Door Displacement and Forces for 15 Pound Opening Force

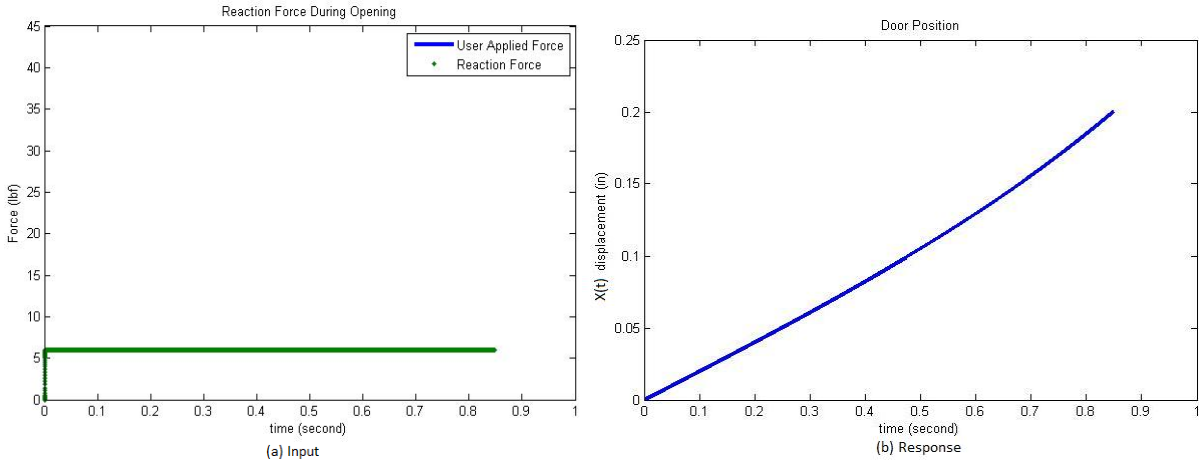

Figure 2-23: Door Displacement for 6 Pound Opening Force

2.6 Shielding Latch from Temperature Pulse

Due to the possible issues of temperature sensitivity in the latch operation, it was important to determine if the latch could be adequately thermally shielded from the temperature pulse within the dryer which accompanies the pressure pulse during an event. In other words, could the latch remain cool enough for a long enough period to perform its purpose, i.e., preventing the door from opening?

In order to simulate a temperature pulse which the hinge could possibly experience, the following assumptions were made: the hinge was assumed to be thermally shielded from the interior of the dryer by a 1/4 inch thick glass fiber blanket insulation with a thermal resistance per unit area of 1h-ft^2-F/Btu (0.18 m^{2}K/W), and a 1/32nd inch layer of steel simulating the door wall construction. The initial internal temperature was treated as the steady state operating temperature of the dryer at 150 ^{o}F, with the maximum air temperature inside the dryer during an event taken to be at 1000 ^{o}F. The temperature pulse for this analysis lasted 0.5 second, ramping up from 150 to 1000 ^{o}F and back down to 150 °F. After the pulse, the temperature was maintained at 150 °F for the remaining duration of the transient.

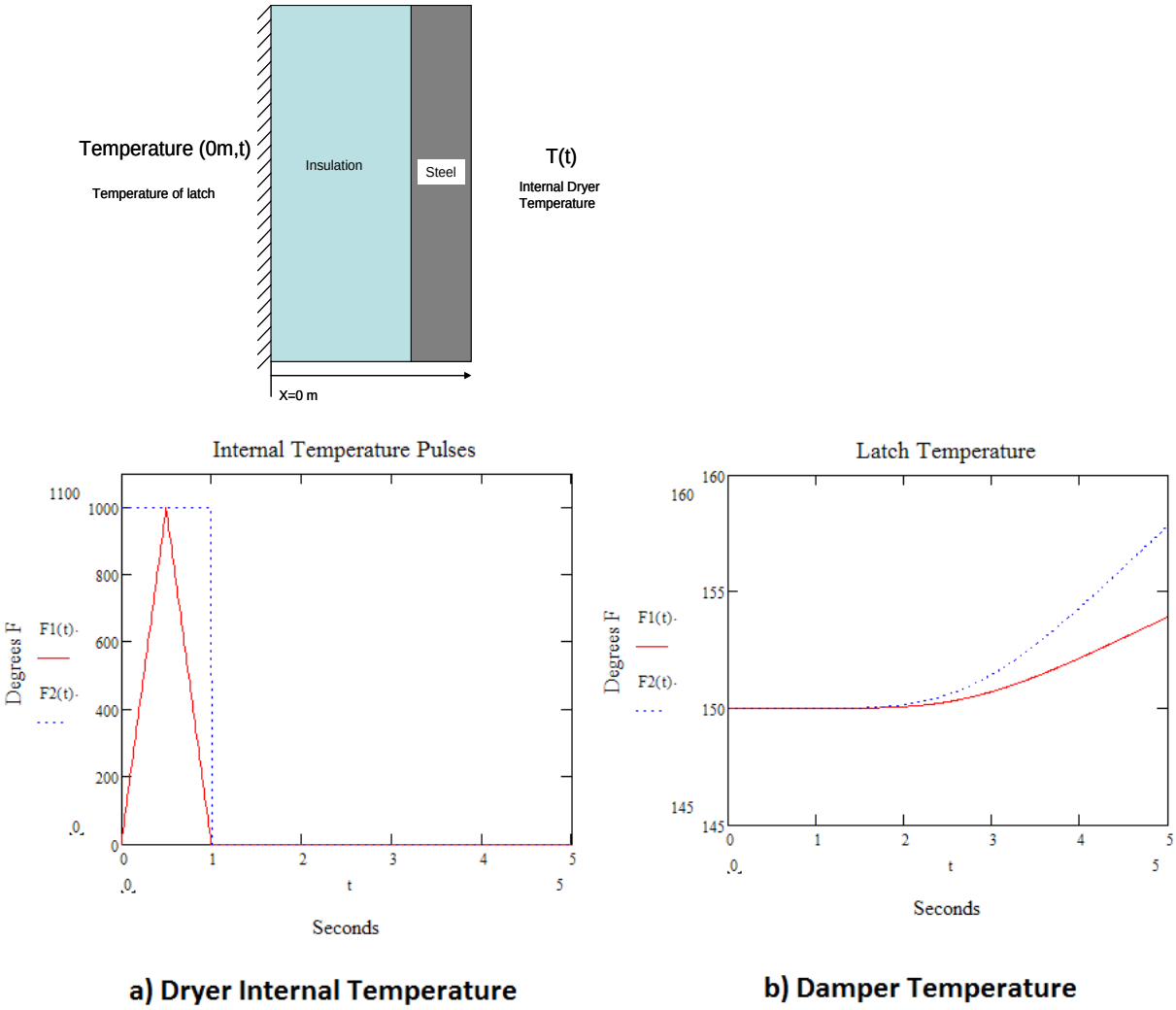

Figure 2-24: Temperature Pulse Results

As seen in Figure 2-24 the latch temperature is shown to not exceed 160 °F over a period of several seconds- long enough to ensure protection of the latch. Thus, it is feasible to shield the latch from a temperature pulse for at least long enough for it to withstand the likely accompanying pressure force. The temperature analysis is described with more detail in Appendix A.2.

2.7 Thermal Expansion to Control Fluid Layer Thickness

Another situation that was investigated during the feasibility evaluation was the possibility of compensating for temperature effects on the latch fluid viscosity using thermal expansion of the housing. Figure 2-25 shows estimated temperature effects on the shear thickening behavior of a 40% PCC shear thickening fluid. The concern is that these viscosity

changes within the normal ambient operating temperature range (50-104 degrees F) will degrade the shear thickening behavior rendering the viscous behavior of the latch unacceptable.

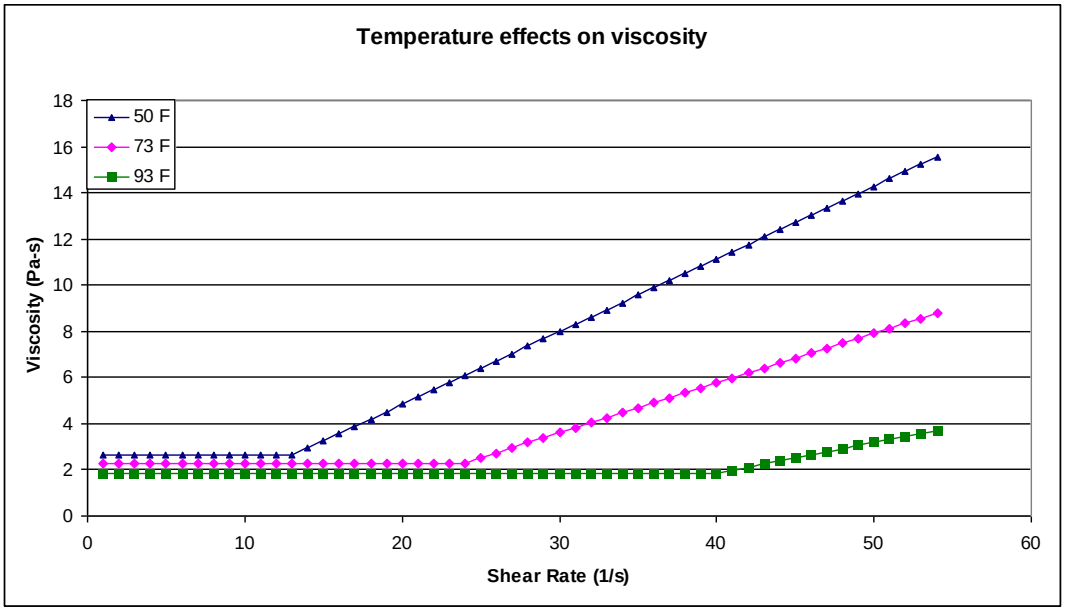

Figure 2-25: Estimated Shear Thickening Behavior

What needs to remain constant for the latch to have sustained behavior as the temperature changes is the shear stress in the fluid layer. For Couette flow the shear stress is a function of viscosity (μ), fluid layer thickness (H), and velocity of the upper plate (U):

$$\tau = \mu(\frac{U}{H}) \cdot \frac{U}{H} \qquad (2\text{-}20)$$

In theory if the fluid layer thickness (H) were to expand and contract sufficiently with temperature, the effect of changes in the shear stress vs. velocity gradient could be minimized and the latch viscous performance could then be maintained.

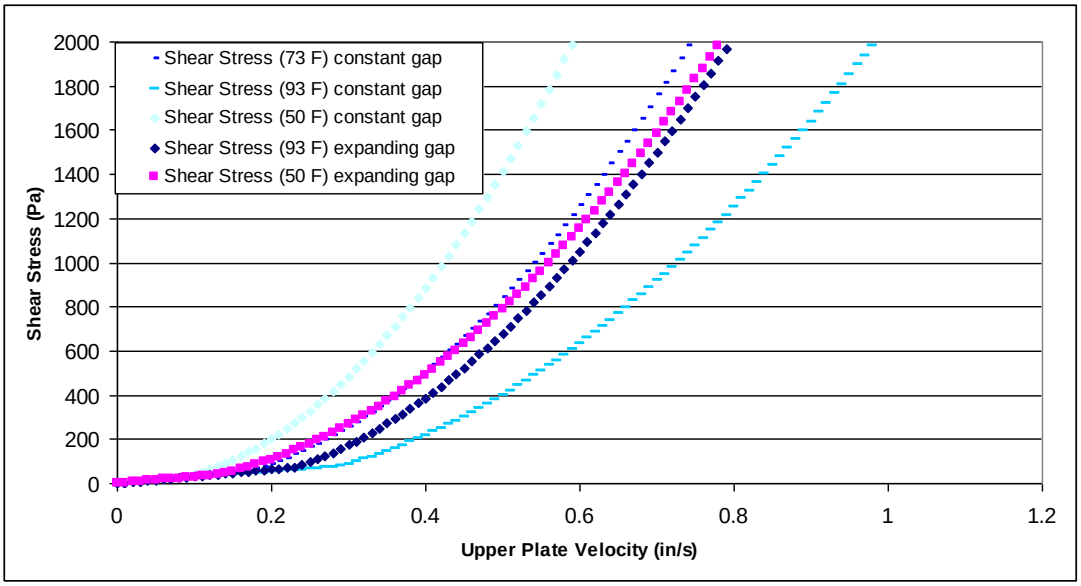

Figure 2-26: Effectiveness of Thermal Expansion

Figure 2-26 shows a comparison of behavior with fixed gap to one with a thermal expansion housing to attempt some compensation for the temperature effects. This technique is dependent on having the fluid layer thin enough that the thermal expansion causes a significant change in gap H. For the above example, the H was 0.007 inch (0.0178 cm) at 77 F and was changed by 5.9e-5 in/F representing the behavior of a 1 inch (2.54 cm) layer of Nylatron. This simulated a case where the inner rotating spindle was a solid cylinder of Nylatron with a 1 inch radius.

2.8 Phase I Summary

Based on this preliminary research and analysis, the feasibility of the latch concept was established, and it was deemed appropriate to move forward to the proof of concept phase. This preliminary phase also brought to light some of the challenges that would be faced throughout the rest of the project-specifically the challenge of addressing the temperature requirements of the project.

CHAPTER 3 - Phase II: Proof of Concept

The focus for the second phase of the project was to demonstrate a proof of concept in the form of a working model prototype. This prototype would not necessarily be of identical shape and proportions as the finalized design, but would be developed to facilitate experimental testing and evaluation of performance under the desired operating conditions. It was also necessary to design and construct the test setup for the dynamic testing of the door opening.

3.1 Initial Prototype Latch Design

The driving factors for the design of the first prototype were to make it as easy to use with as flexible range of use as possible. Features implemented into the design to meet these goals included the possibility for interchangeable spindles to change the inner rotating geometry and the ability to switch the damping fluid that will allow testing/verifying the proposed dynamic opening model and determine the most effective fluid and geometry.

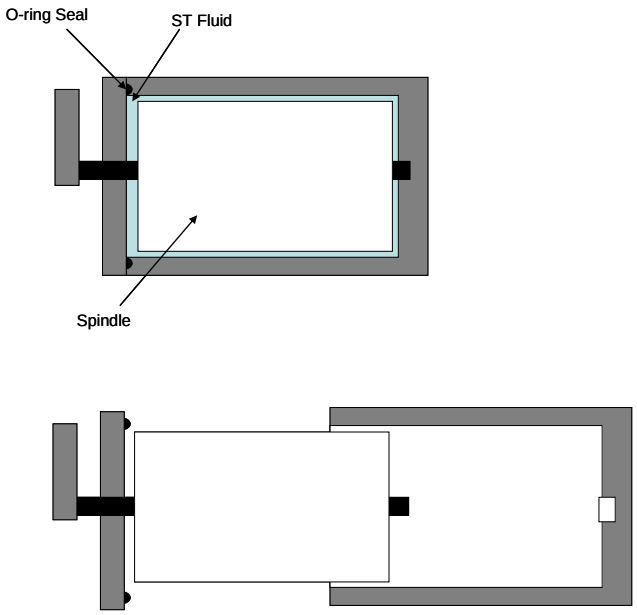

Figure 3-1: Damper Cut-Away

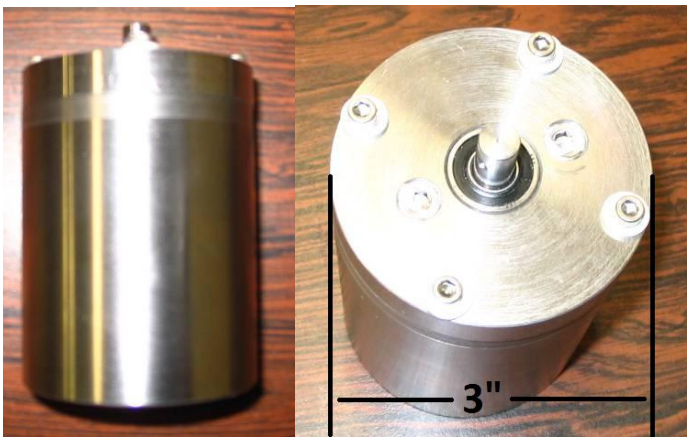

Figure 3-2: Viscous Latch

Prototype Spindle

The prototype shown in Figure 3-2 and 3-3 was designed in order to test multiple combinations of internal geometries and shear thickening fluids by being able to switch out the rotary shaft component and change out the fluids with relative ease.

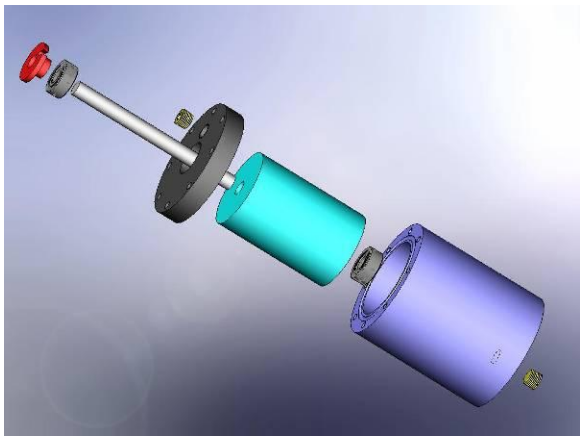

Figure 3-3: Exploded View of Damper Model

The shaft used in the damper for the testing was a simple cylinder. This shaft resulted in a 0.02 inch (0.0508 cm) thick layer of the fluid being sheared between the rotor and the housing. This spacing was designed so that when the damper is filled with a shear thickening dispersion of calcium carbonate (CaCO3) and polyethylene glycol (PEG) with a volume fraction of 48.6% CaCO3, it should meet the physical opening and closing rate requirements to act as proof of concept for the project.

Spindle Engage Mechanism

In order to transfer the linear opening motion of the door to the rotary motion of the latch a cam type mechanism is used. A catch is attached to the shaft of the damper as shown in Figure 3-4.

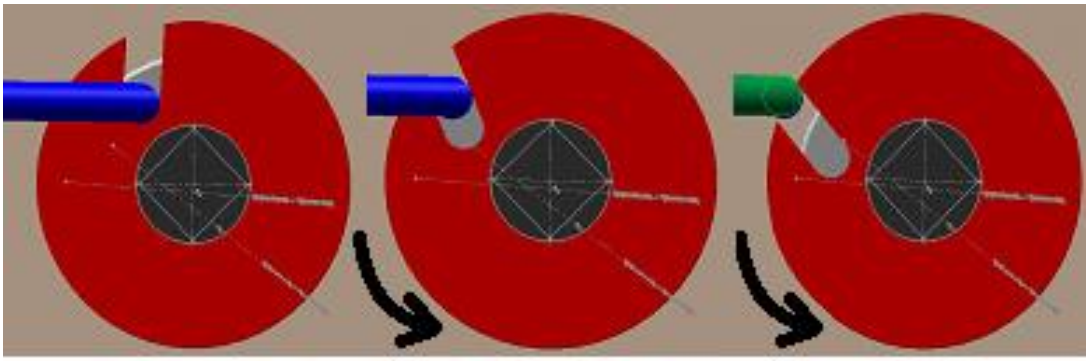

Figure 3-4: Catch Diagram

The catch has a slot milled into it to receive a pin tied to the dryer. For the first proof of concept testing, the pin remained in the slot since testing the effectiveness of the damper doesn't require the door to open entirely. For initial testing, the ring was connected rigidly to the shaft. A one-way rotating apparatus was implemented between the catch and shaft in the next prototype to allow for unobstructed closing of the door.

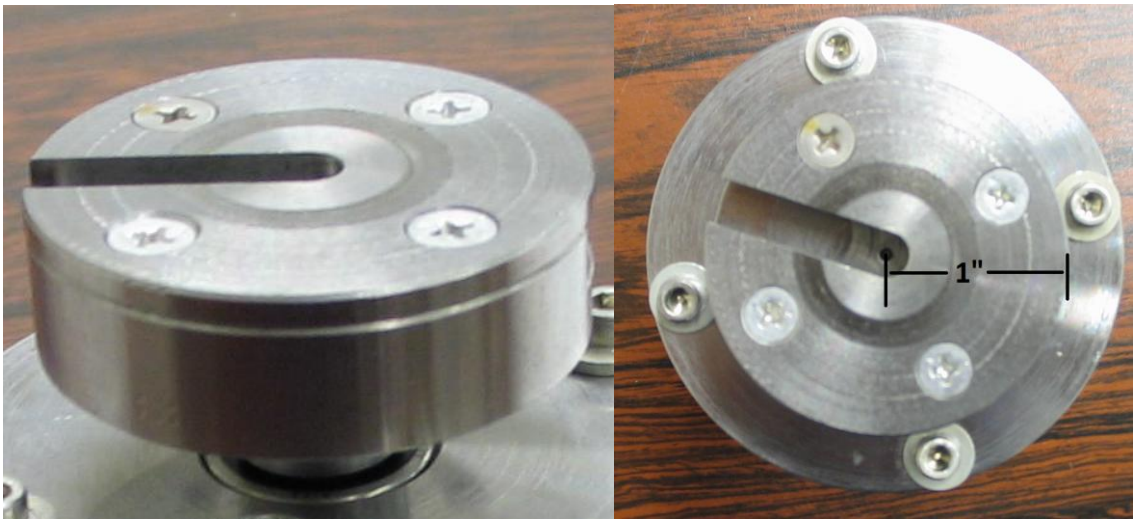

Figure 3-5: First Prototype Catch

Latch Support Structure

The proof of concept prototype was too large to fit properly inside a dryer door. Therefore, the viscous damping latch was mounted in the dryer door as shown in Figure 3-6. The linkage that ties the opening motion of the door to the rotational motion of the latch was bolted directly to the test frame, due to the fact that the front panel from the dryer flexed too much for the linkage to operate properly if connected directly to it.

Figure 3-6: First Prototype Mounting

3.2 Dryer Door Test Setup

In order to properly evaluate the performance of the prototype, the test setup had to be able to perform the following functions:

- Measure linear door opening position as a function of time.
- Measure force applied as a function of time.
- Replicate door opening rate and forces accurately according to design requirements

In order to best replicate actual conditions during testing, it was decided that the best course of action would be for the setup to consist of an actual dryer door mounted in a simple frame for stability with the necessary equipment and instrumentation attached. A simple representation of how the instruments were attached to the door is shown in Figure 3-7.

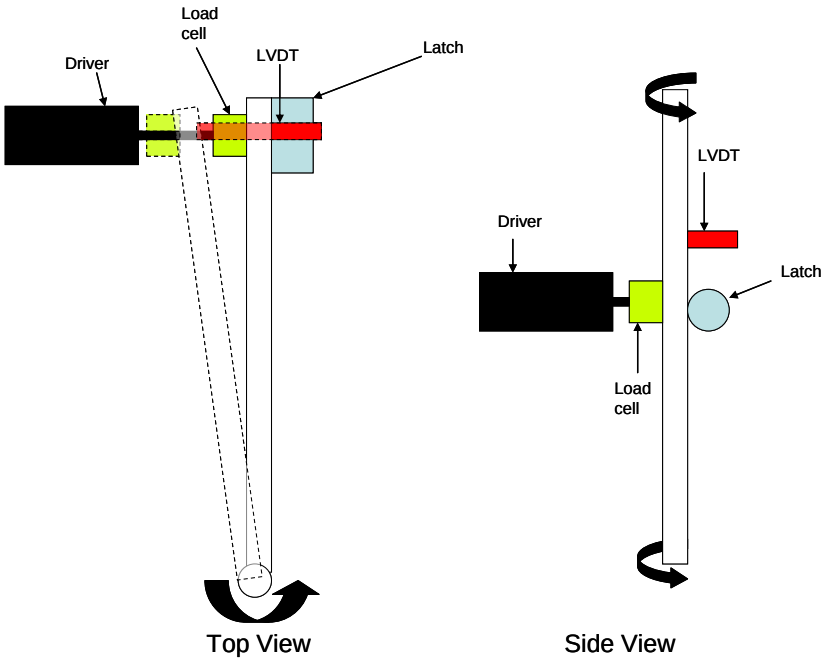

Figure 3-7: Instrumentation

Dryer Door Support Structure

The support structure serves the function of providing a basic framework for the mounting of instrumentation and drivers, as well as rigidly supporting the front panel/door assembly from the dryer. Steel strut channel was selected for construction of the frame because it is relatively easy to work with, easy to attach mounting points for instrumentation to, and is a fairly simple matter to modify the frame to work with different front panel assemblies. A photograph of the frame support structure is shown in Figure 3-8.

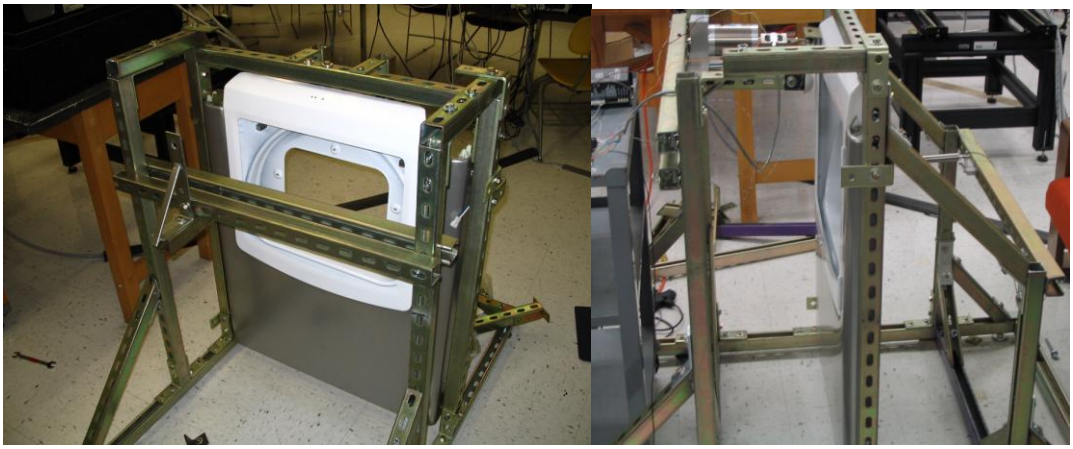

Figure 3-8: Support Structure

Instrumentation

Actuator

In order to properly simulate the dryer door opening, closing, and pressure pulse conditions, a driver control system was needed that could react quickly and to provide a force and displacement that could be precisely controlled. For these reasons it was decided to use a voice coil linear actuator. A photograph of the actuator is shown in Figure 3-9. Some of the benefits of choosing the voice coil over a pneumatic or electromechanical actuator include:

- Fast acceleration
- Small mass and inertia
- Precise force and position control
- Compact size, easy setup
- Ideal for small displacement

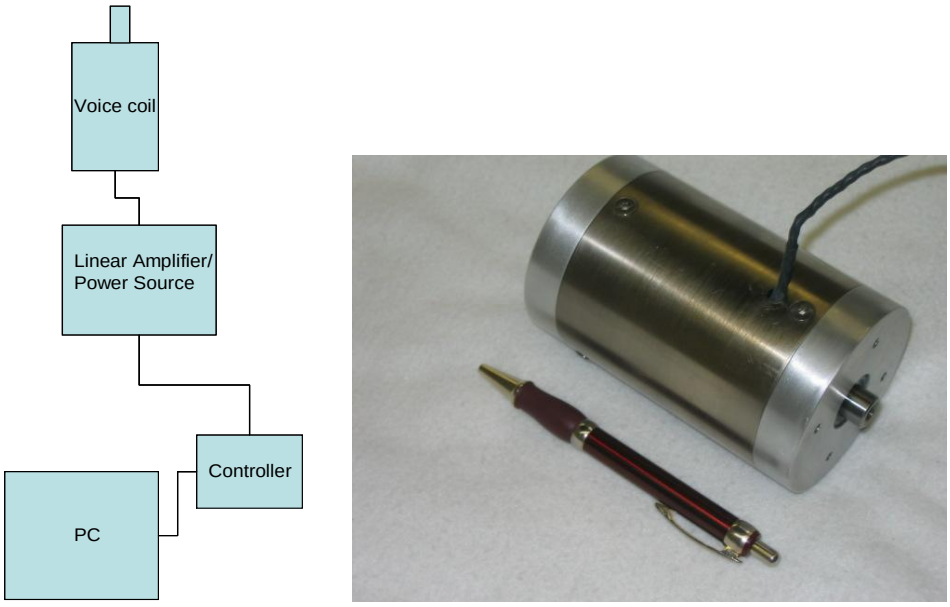

Figure 3-9: Voice Coil Linear Actuator

Force Measurement

In order to monitor force applied to the door from the actuator, an S-beam type load cell was chosen because it was durable, easy to mount, and could read forces in both tension and compression. The load cell was mounted as a linkage between the voice coil and door as shown in Figure 3-10.

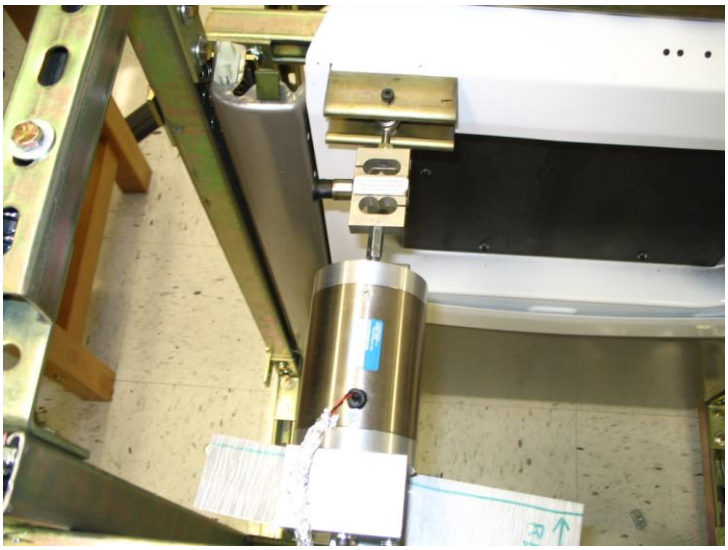

3-10: Mounted Load Cell and Actuator

Displacement Measurement

Finally, in order to measure and record the displacement of the door with respect to time during the opening test, a linear differential transformer (LVDT) was used. LVDT's have a very fine resolution, making it an ideal choice to monitor these tests where 0.2 inch (5 mm) is considered the maximum. The LVDT was attached to the back of the door using an eyelet adaptor allowing the door to move freely, as shown in Figure 3-11.

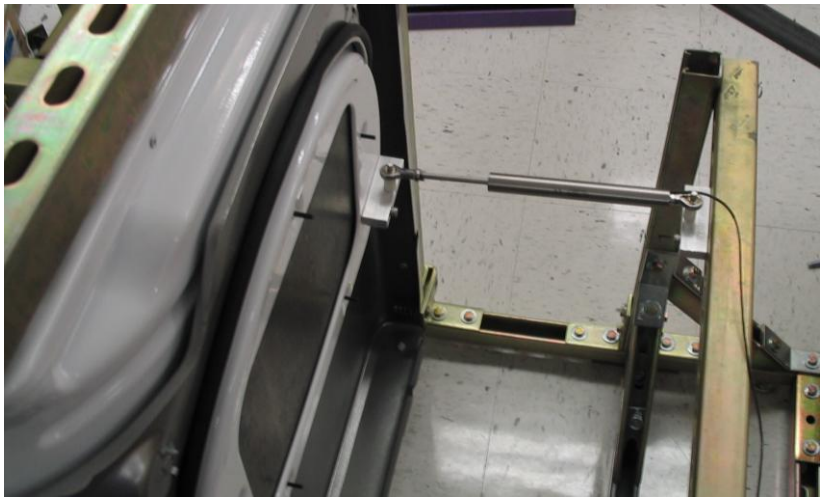

3-11: LVDT Mounting

Data Acquisition

The control signal for the linear actuator, as well as the data signals from the LVDT and load cell, were processed using LabVIEW software.

3.3 Test Results

Three sets of tests were run using the test setup:

(1) The standard mechanical latch currently used on the door as a basis for comparison

(2) The viscous latch prototype

(3) Door with no latch in order to observe it's inertia during acceleration.

The tests were all run using the 3 pulses shown in Figure 3-12. The positive forces represent the forces applied by the voice coil pulling on the door to open it, while the negative forces represent the voice coil acting in the opposite direction pushing the door closed. In these tests the -5 lbs of force level was applied in order to keep the door closed during the viscous and "no latch" tests since the door would slowly drift open when no force was applied.

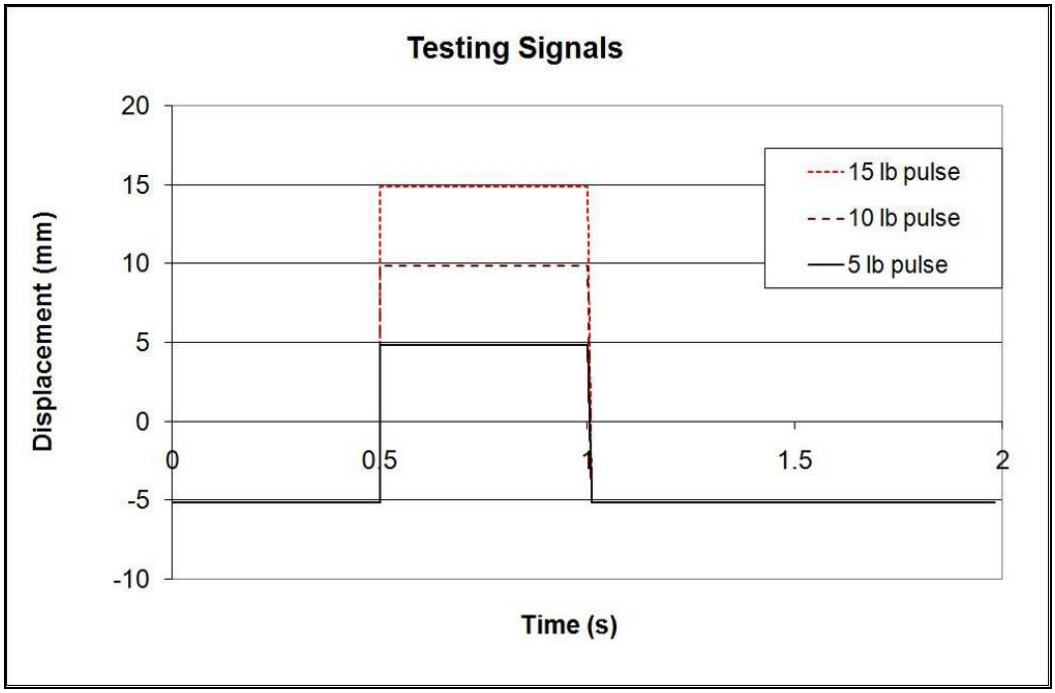

Figure 3-12: Door Testing Force Control Signals

Mechanical Latch Tests

The data from the mechanical latch tests are presented in Figures 3-13 through 3-15 below. The results show that as long as a force greater than 5 lbf is applied to the handle, the door opens with relatively little resistance.

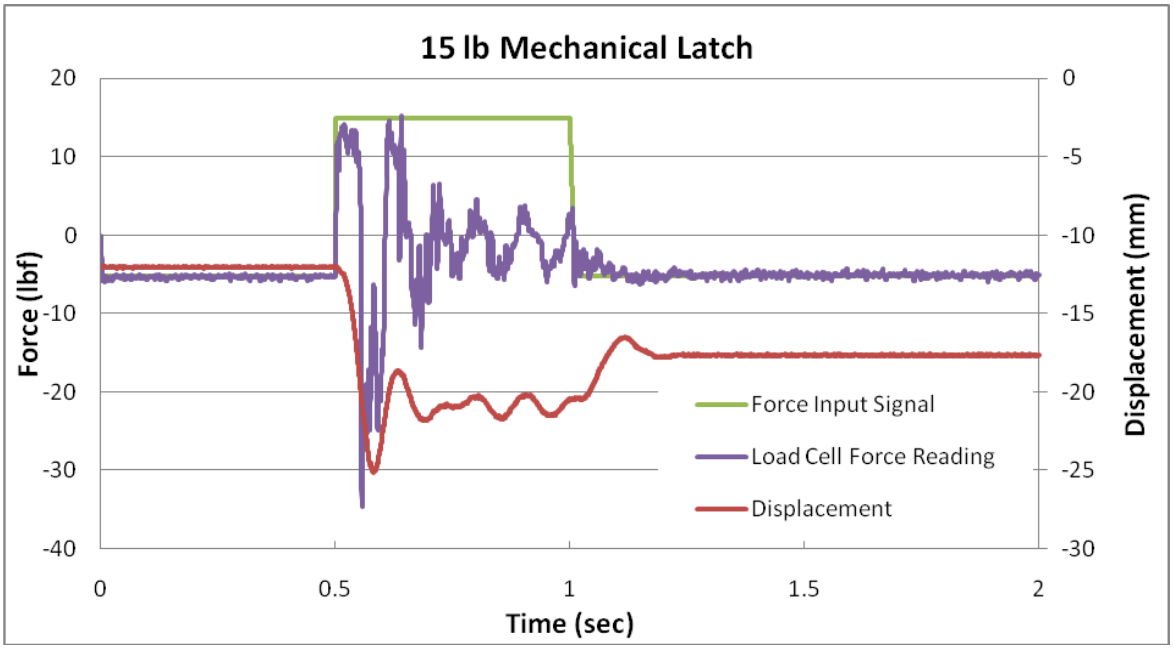

Figure 3-13: 15 lb Mechanical Latch

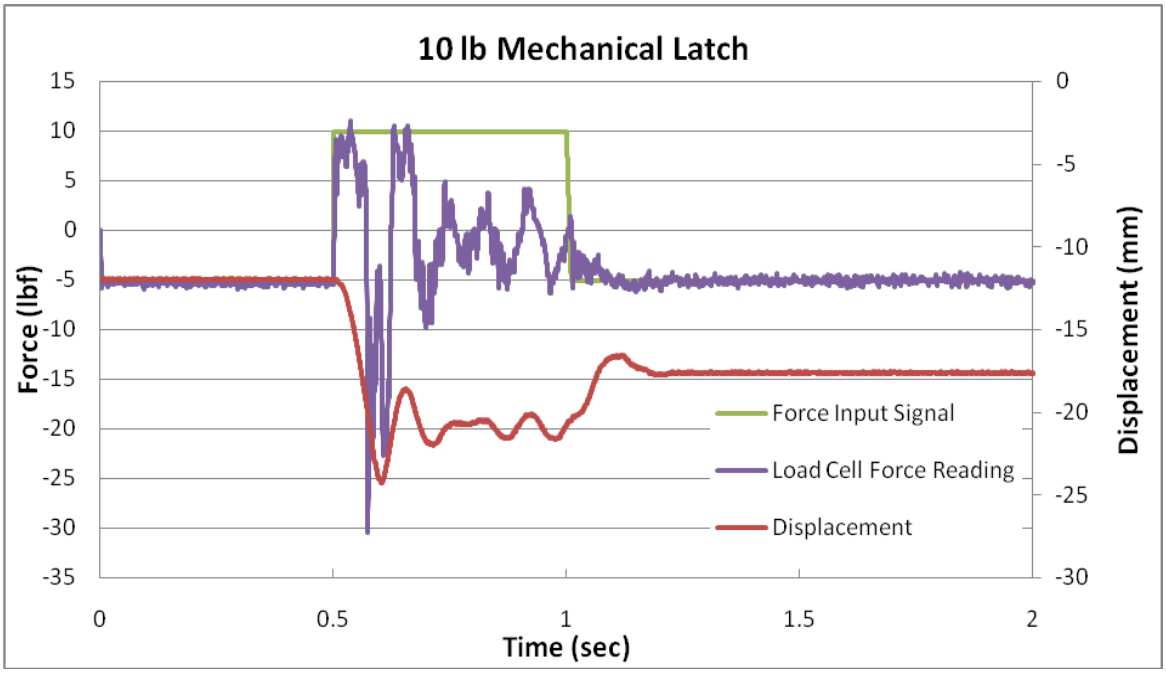

Figure 3-14: 10 lb Mechanical Latch

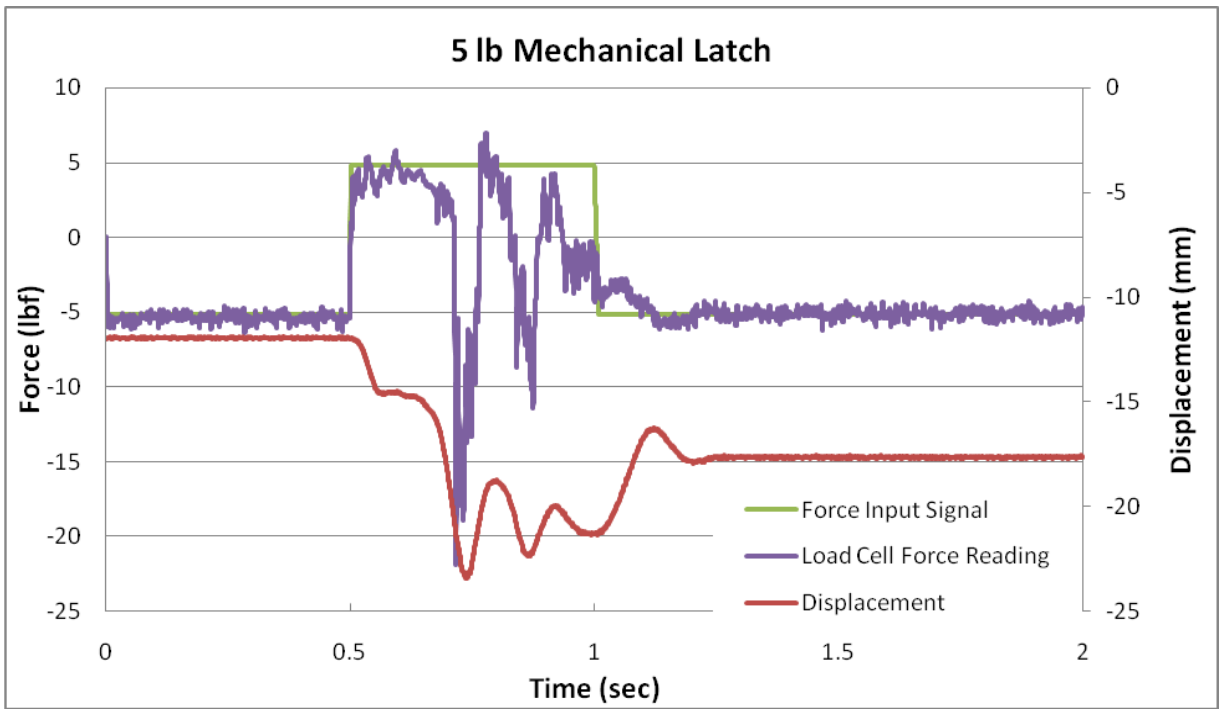

Figure 3-15: 5lb Mechanical Latch

Dynamic Testing Without Latch

As shown in Figures 3-16 through 3-18, without any latches to provide resistance, the door opens and closes in a very short time span, going from the closed to open and back to closed positions. The oscillations that can be seen in the force and displacement plots are due to mechanical vibration that occurs when the door hits its stops.

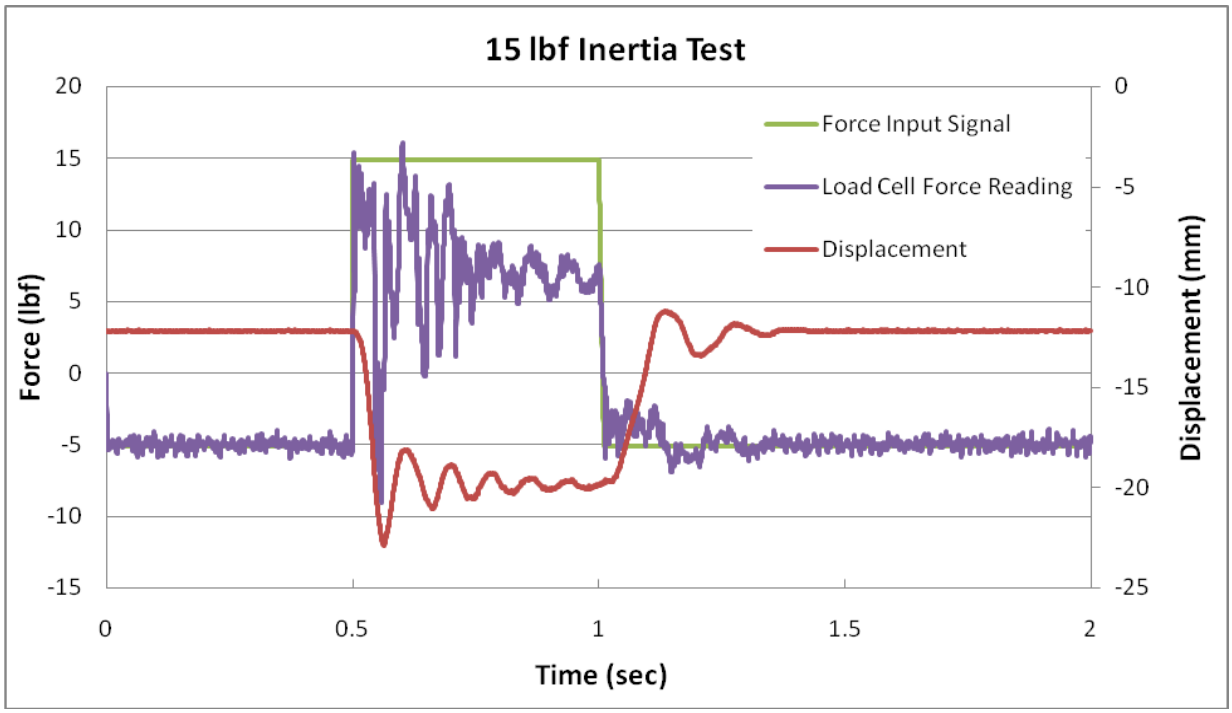

Figure 3-16: 15 lb No Latch

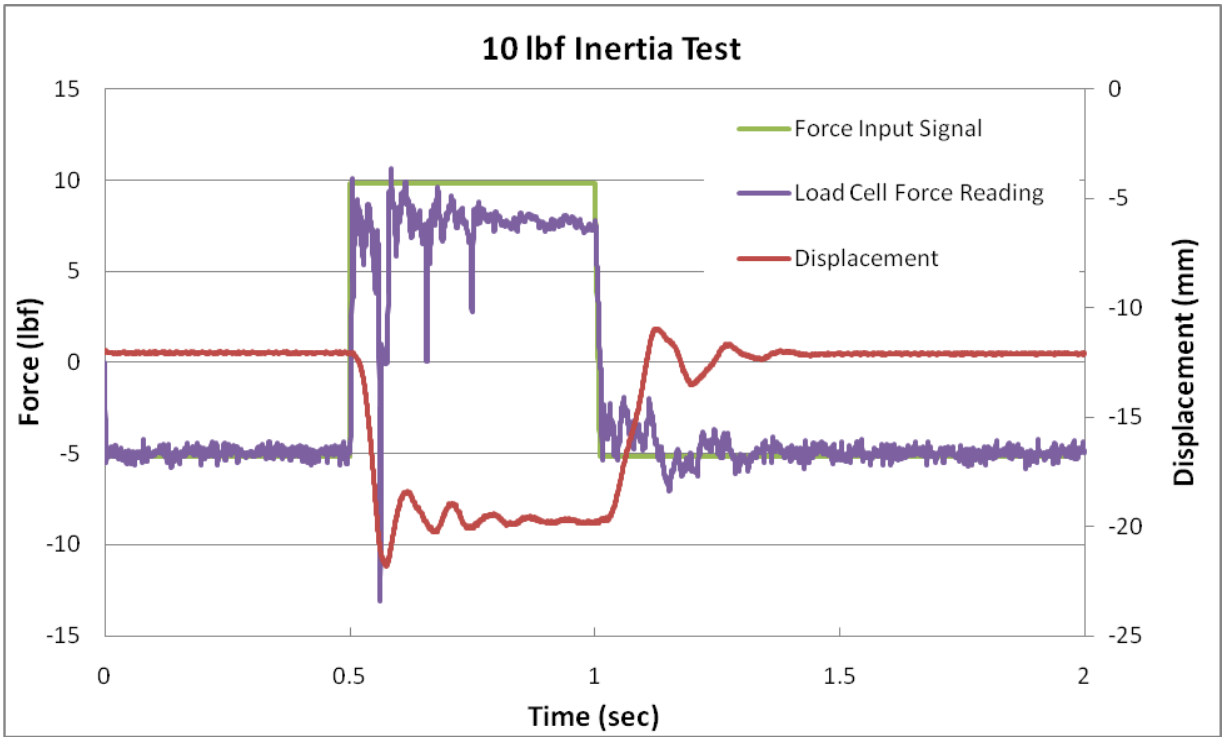

Figure 3-17: 10 lb No Latch

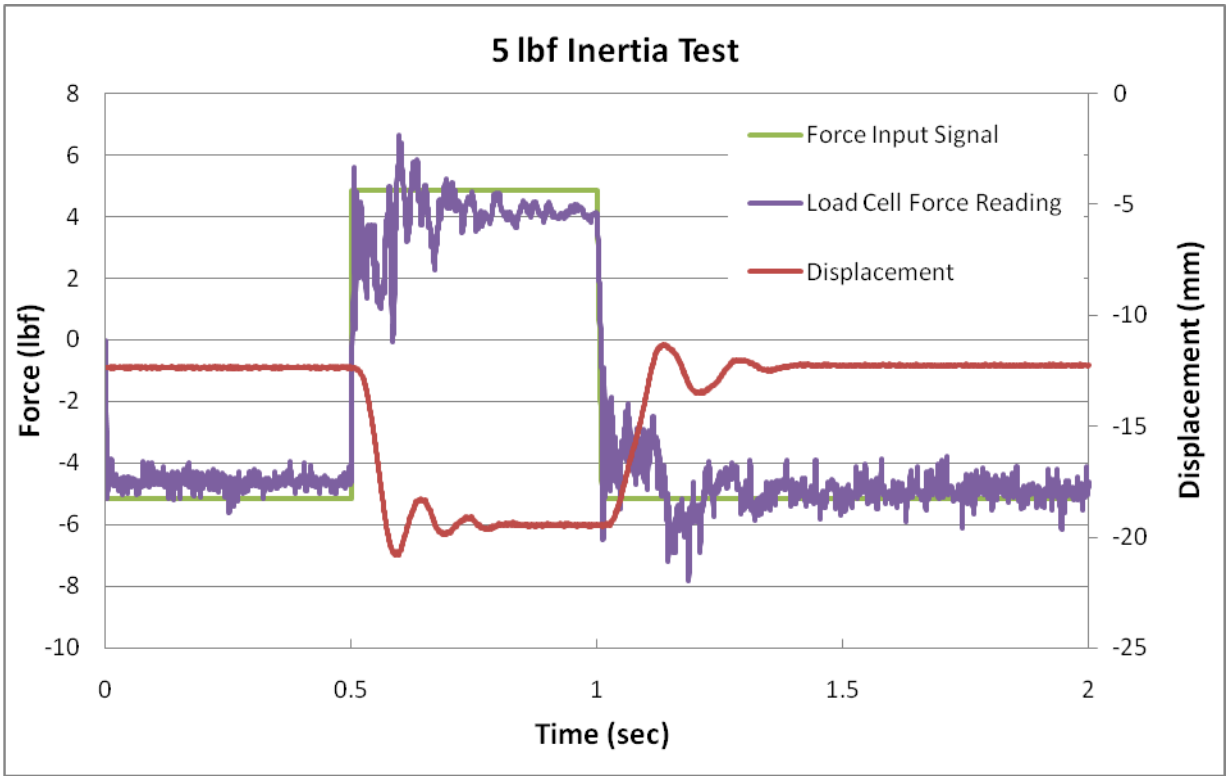

Figure 3-18: 5 lb No Latch

Figure 3-19 shows the LVDT displacement readings for all three inertia tests superimposed on each other. The LVDT was positioned at -12 mm displacement when the door is closed during these tests.

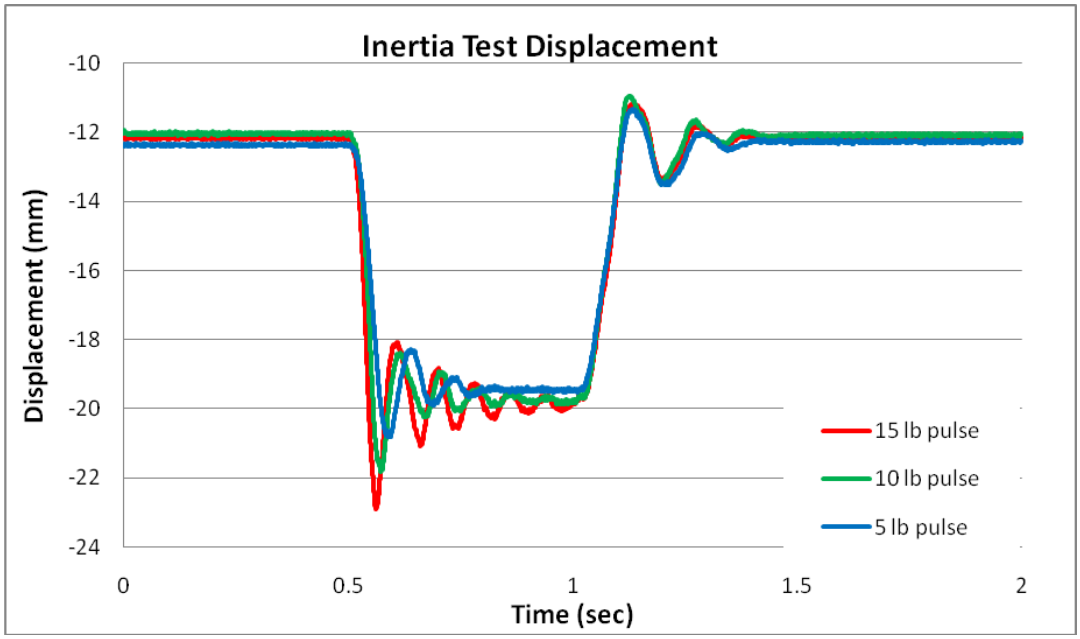

Figure 3-19: Inertia Test Displacement

Figure 3-20 is a zoomed in view of Figure 3-19 during the 0.5 to 0.75 second time interval, in order to show the movement of the door while it is swinging open. A simple Matlab mathematical model was used to predict the behavior during this initial part of the opening process.

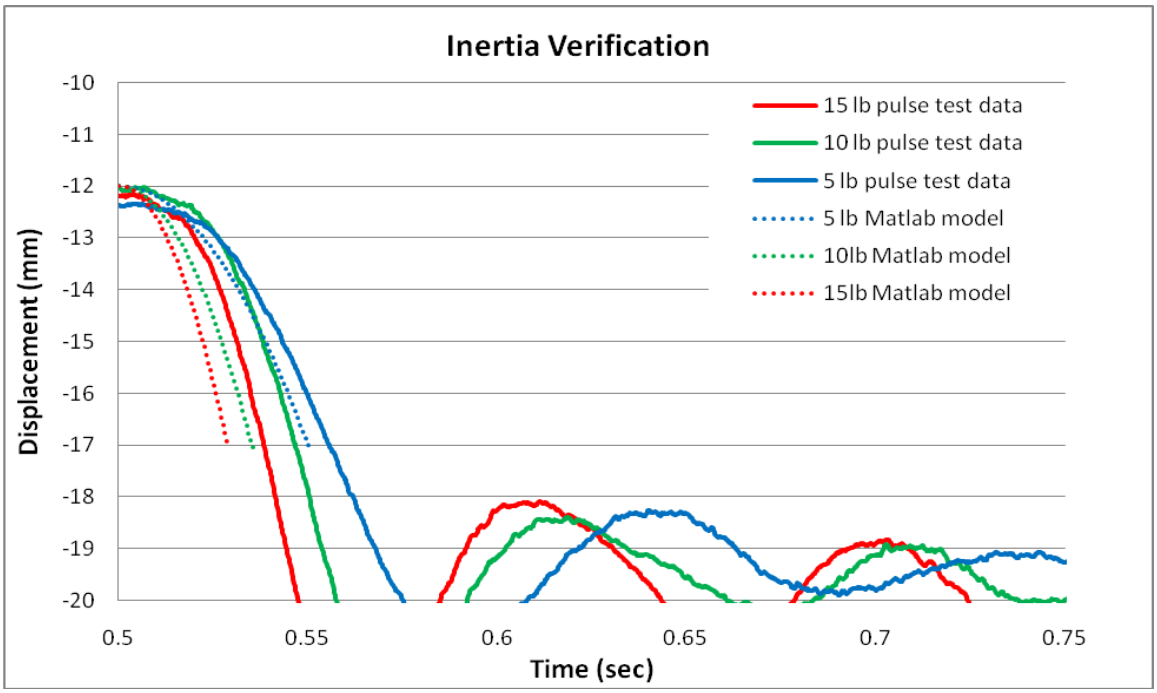

Figure 3-20: Inertia Verification

The solid lines in Figure 3-20 are from the actual test data, while the dashed lines represent a preliminary approximation to the inertia behavior of the door. Looking back at Figure 3-20, the approximate model seems to agree with the test data within roughly 20% error indicating that the basic physics of the model is consistent with the tests.

Dynamic Testing With Viscous Latch

Figures 3-21 to 3-23 show the test results for the door using the viscous latch. The viscous test results show that the load cell force readings match the force input signal extremely well. This is because the latch doesn't release the door. This shows two things; first that the damper can produce enough resisting torque to keep the door from opening, and second that the cam and linkage applying the torque on the damper work well and do not slip.

Looking at the LVDT displacement readings for the door, there are really three different behaviors that can be immediately observed. Two of these behaviors, i.e. flexing and vibration,

are linked in the dryer door and front panel and the third is directly due to the viscous damper behavior.

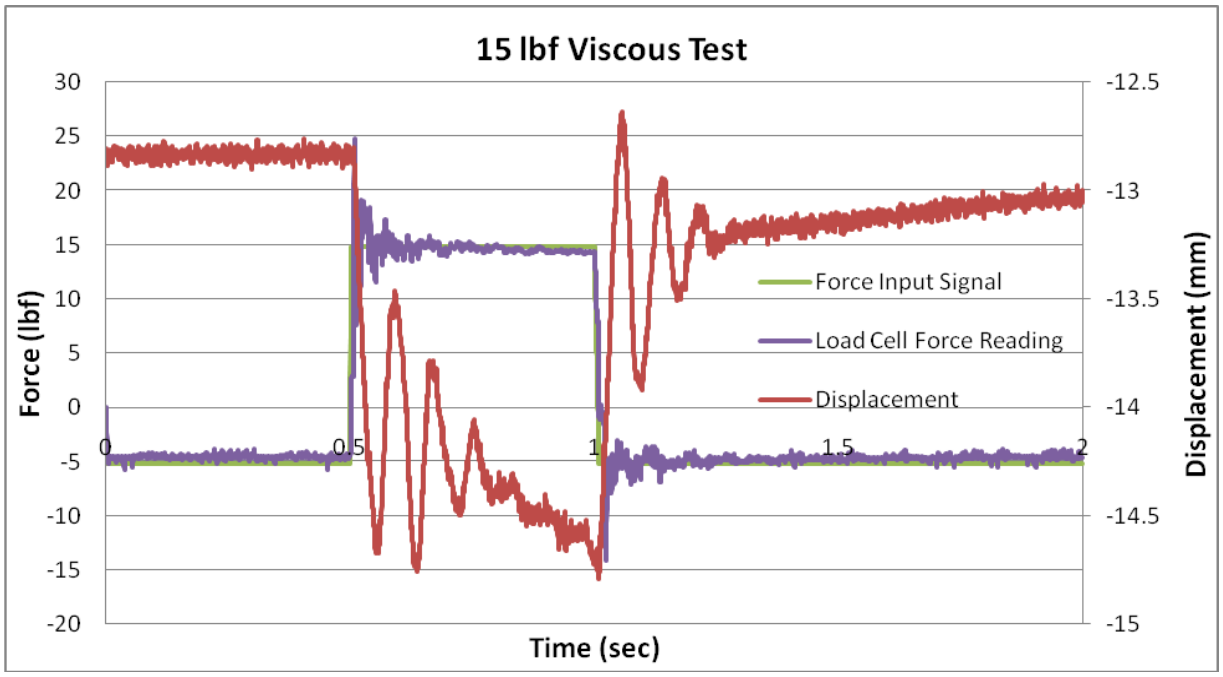

Figure 3-21: 15 lb Viscous Latch

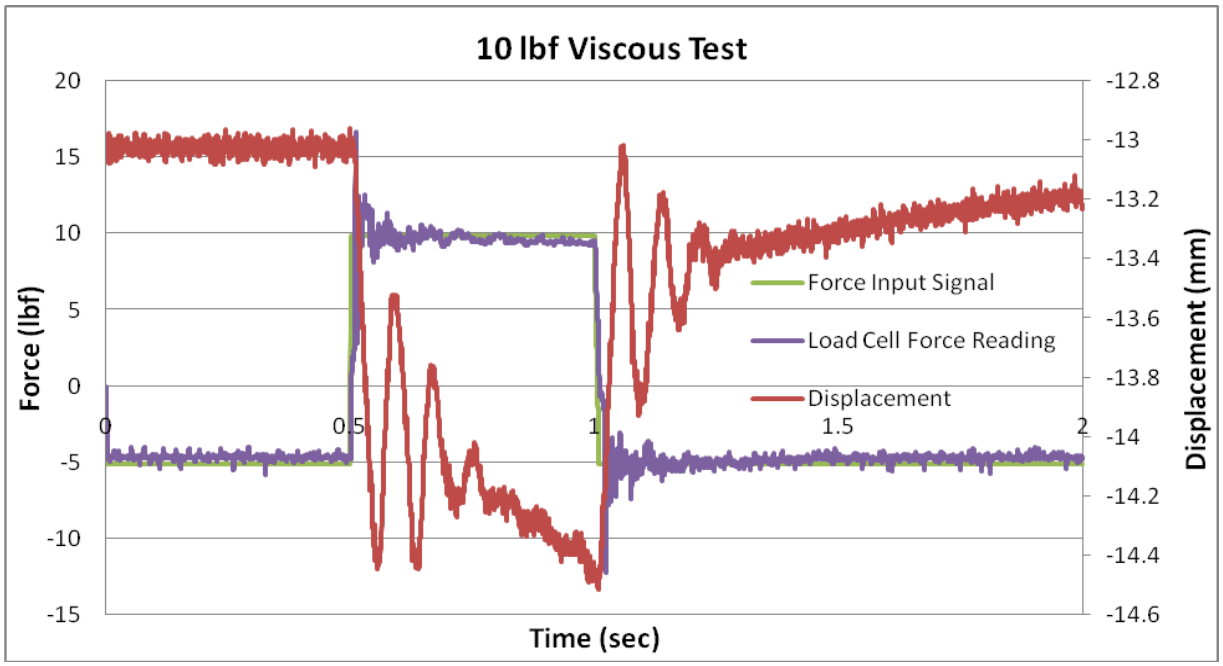

Figure 3-22: 10 lb Viscous Latch

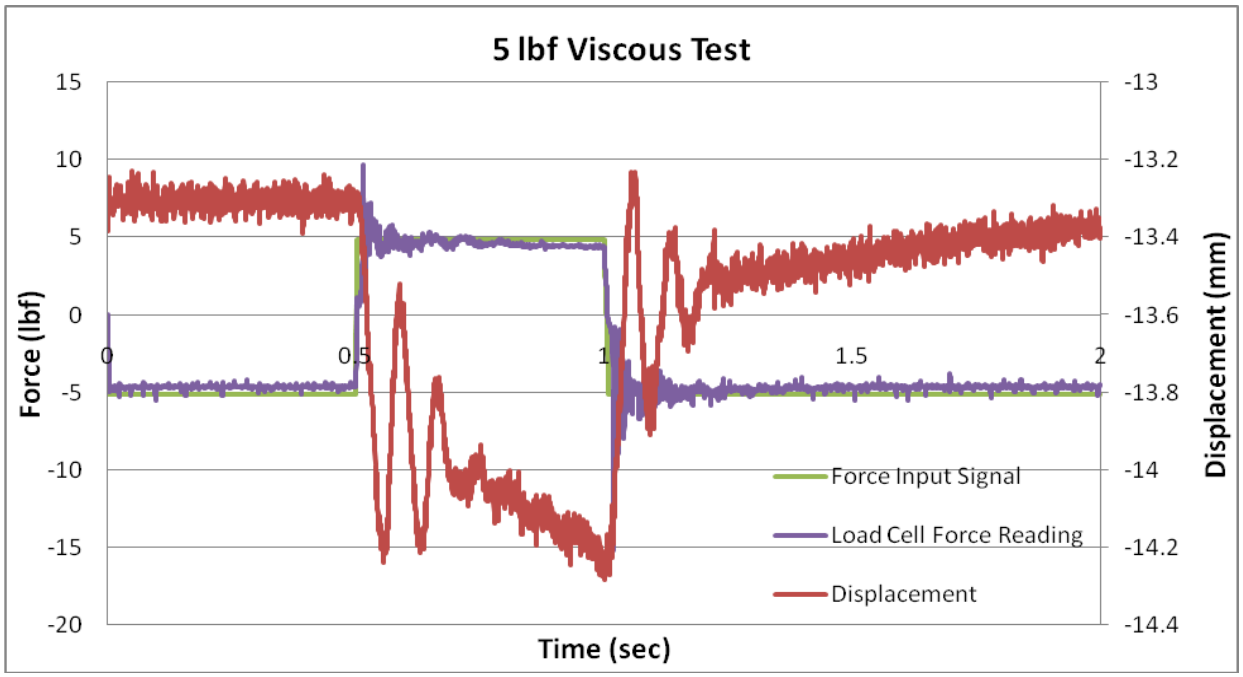

Figure 3-23: 5 lb Viscous Latch

The first behavior is the immediate jump in displacement that coincides with the step changes in force from the load cell. These jumps read by the LVDT are most likely the result of the door rocking or flexing slightly before the damper engages. This jump is small (on the order of 0.5 to 1 mm) and by observing Figure 3-24 one can see it is force dependant. Overall, due to its small size, this behavior does not negatively influence the performance of the damper.

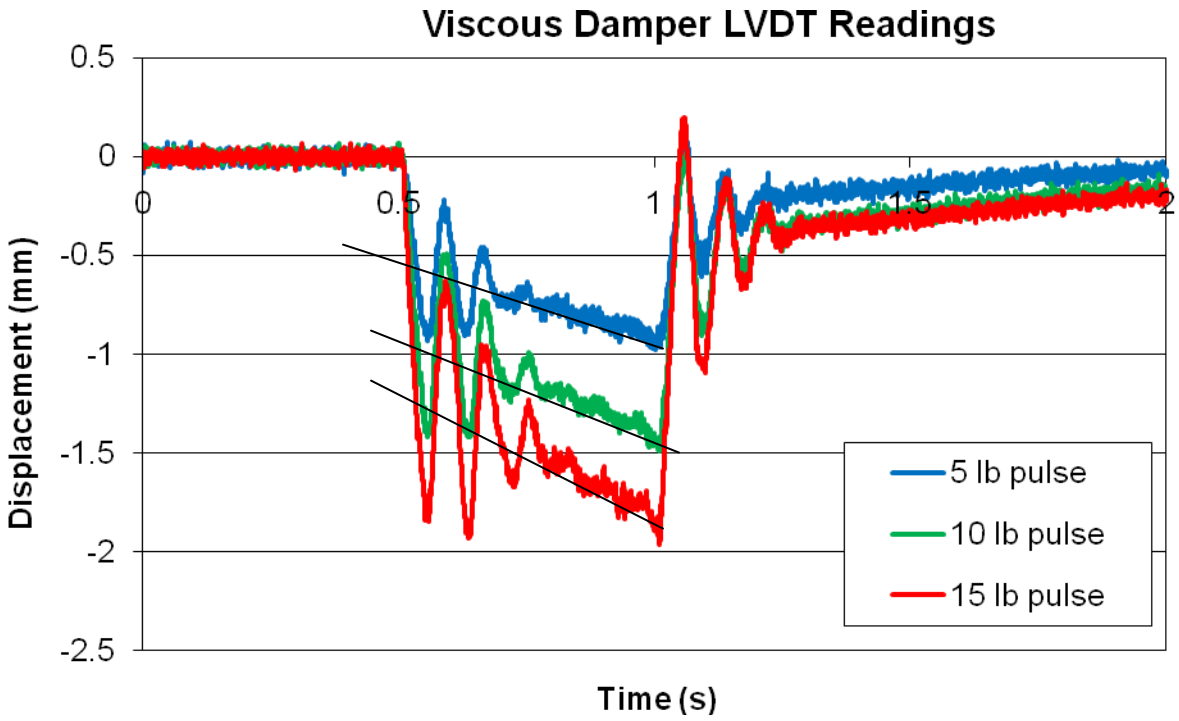

Figure 3-24: Viscous Damper LVDT Readings (Superimposed)

The second behavior is simply the vibrations that can be observed in the LVDT reading like those in the inertia tests due to vibration in the door and panel when a sudden force is applied. A "spring constant" was estimated for the door and panel based on its deflection when force was applied. Using this approximate spring constant the period of oscillations was estimated to be approximately 0.1 seconds. Measuring peak to peak the period of the oscillations for the viscous testing was found to be around 0.08 second, and 0.095 second for the inertia test oscillations.

The final behavior is associated with the opening rates allowed by the damper at different forces. The damper limits the rate the door can open depending on the force applied. Figure 3-25 shows the opening rates of the door during the viscous damper test calculated based on the LVDT data.

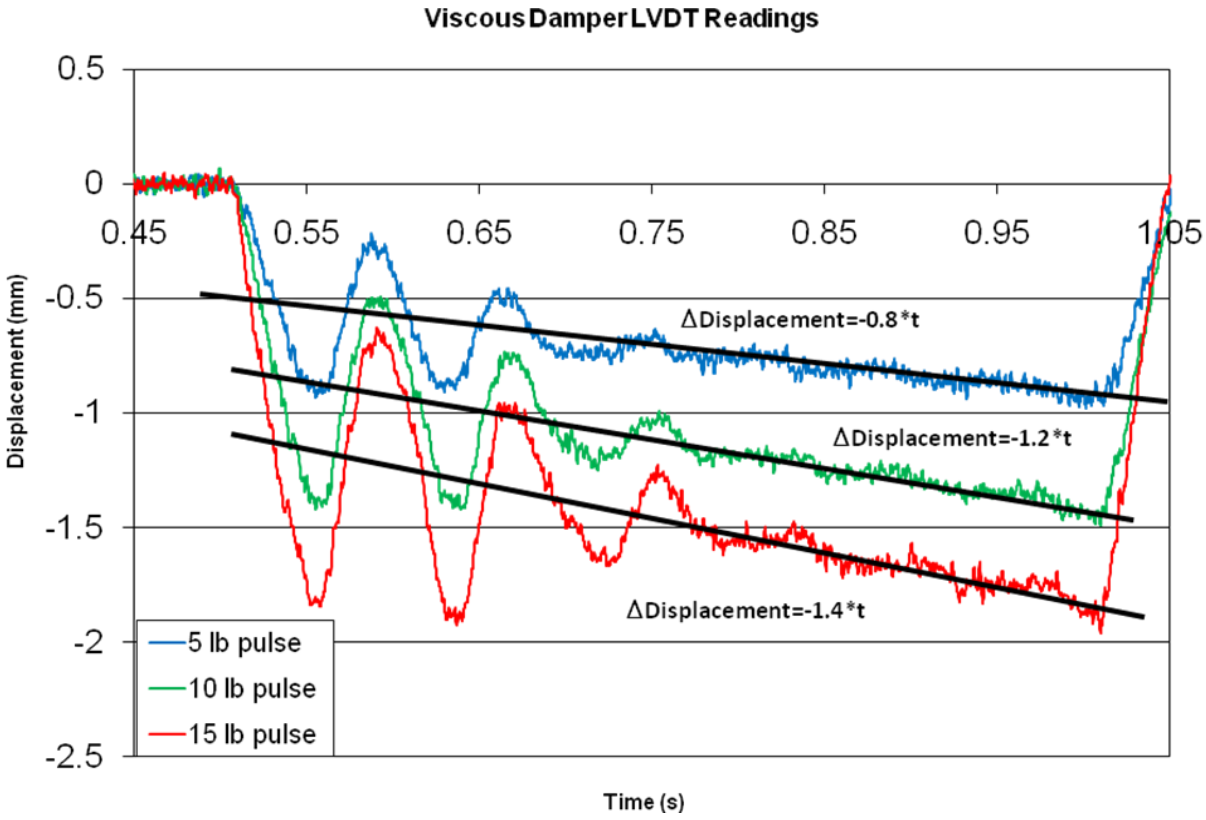

Figure 3-25: Experimental Opening Rates

The comparison between the actual door opening rates shown in Figure 3-25 and the estimated opening rate from the Matlab simulation is shown in Figure 3-26.

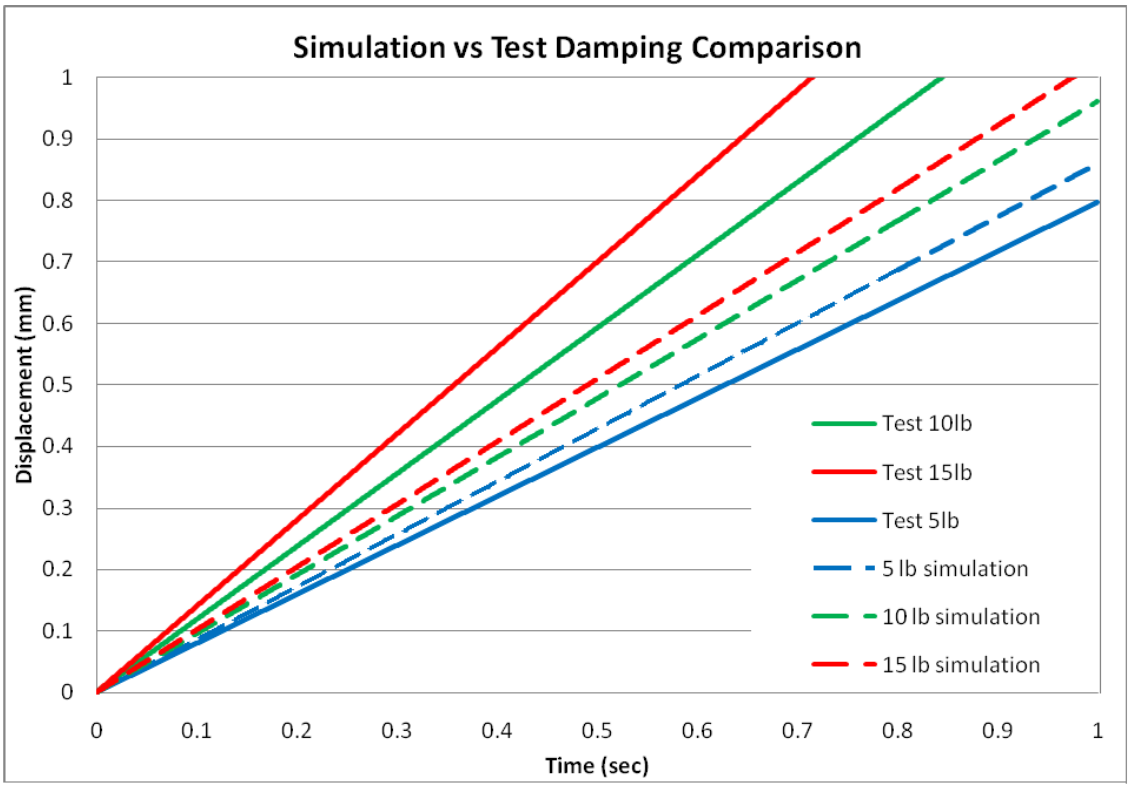

Figure 3-26: Experimental and Calculated Opening Rate Comparison

The solid lines represent the actual opening displacement versus time behavior of the door, while the dashed lines represent the predicted opening rates from the Matlab simulation. The Matlab estimations are within about 15-20% of the actual displacements, which seems quite reasonable considering the difficulty in accurately estimating slopes of the experimental results. The main difference between the actual and predicted is that the predicted slopes are more tightly clustered together than the actual slopes.

3.4 Static Testing

Preliminary tests on the latch have been conducted by using the steady-state test setup shown in Figure 3-27 and timing the rotations.

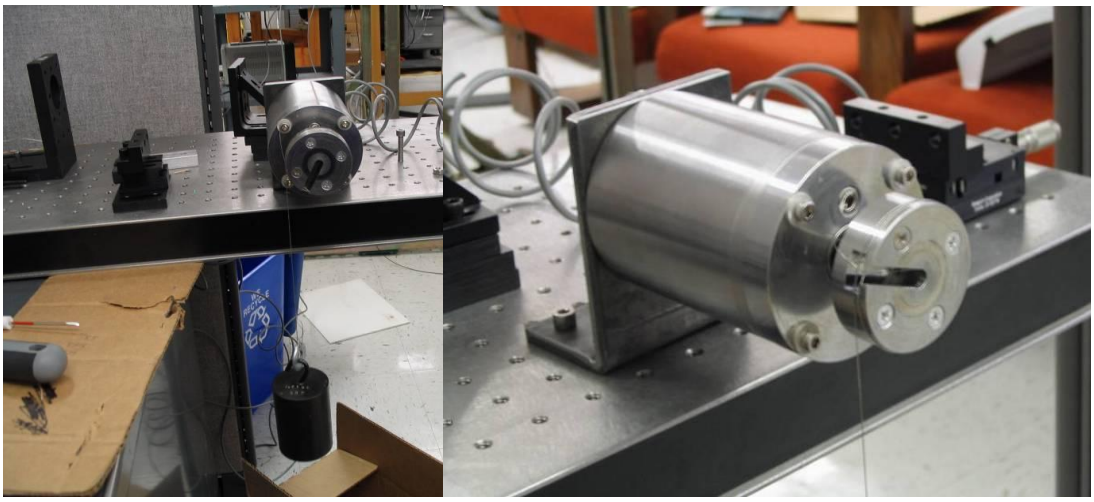

Figure 3-27: Static Damper Test

Room Temperature Static Testing

The static test results of this test at room temperature are presented in Figure 3-28. Tests were performed by winding a wire around the cam of the prototype, hanging a known weight from the wire, and timing the rotations as the wire unwound. The shear thickening fluid used was thicker than expected, resulting in slower than ideal rotation; however, the Non-Newtonian action of the latch can still be clearly observed.

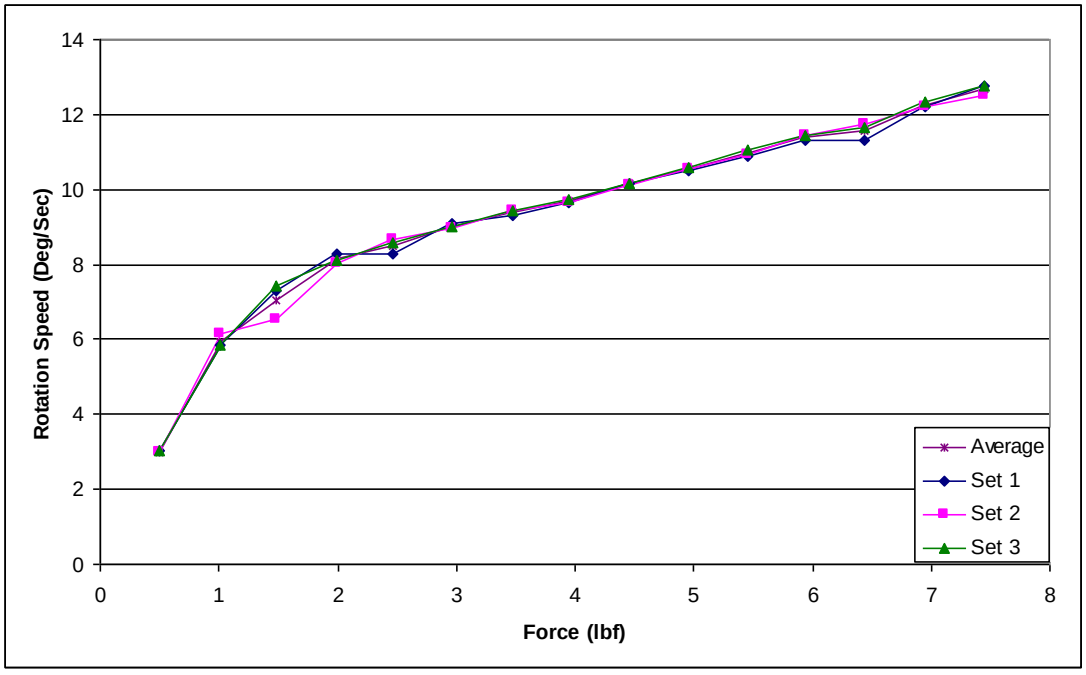

Figure 3-28: Room Temperature Static Test Results

Non-Room Temperature Testing

In order to determine the effect of temperature on the damper's performance, tests were conducted by using the steady-state test setup and timing the rotations. Temperatures less than ambient conditions were achieved by putting the damper in a freezer and allowing it to come to steady state, upon removal the damper was well insulated and the tests were performed. For high temperatures the damper was wrapped in a patch heater and insulated allowing the temperature to be actively controlled. The damper's temperature was monitored using thermocouples attached at different points on the damper to ensure even, steady-state temperature distribution.

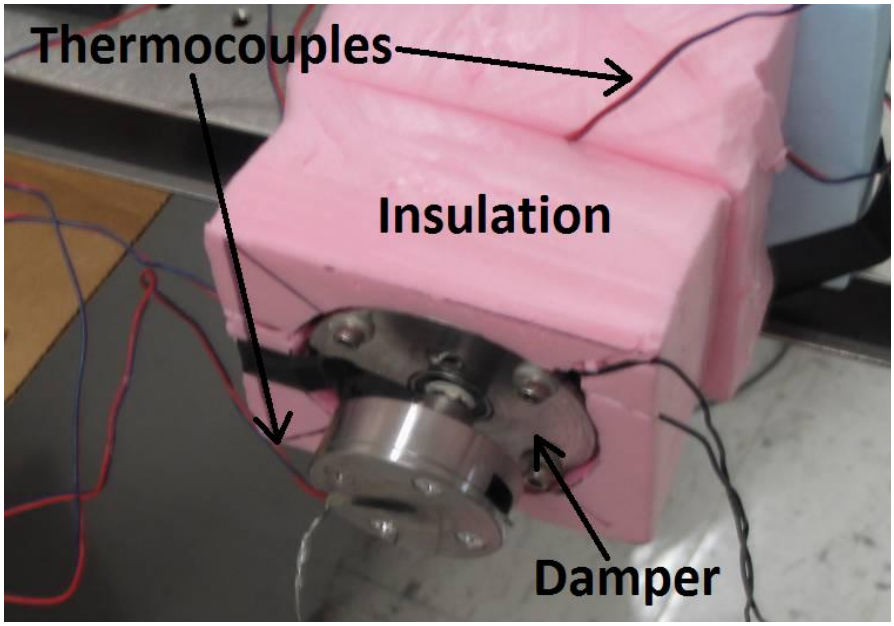

Figure 3-29: Temperature Control

The results shown below reveal that, with the Polyethylene Glycol based fluid in the damper, the damping action is extremely reduced as temperature increases. And as the damper is cooled the damper becomes very stiff.

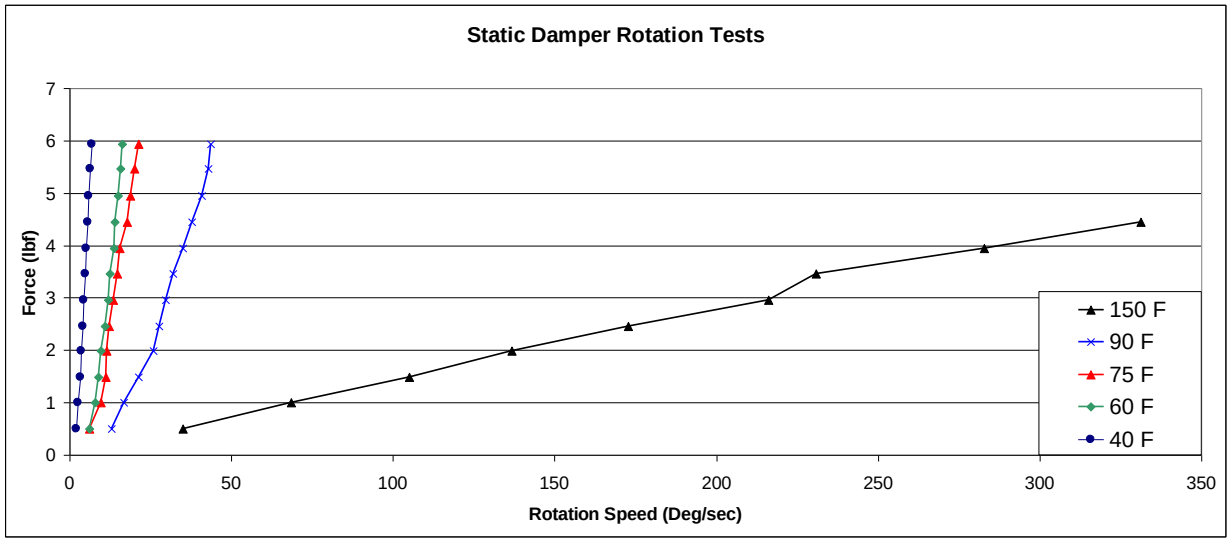

Figure 3-30: Temperature Effects

This temperature sensitivity is a direct result of the temperature sensitivity of the Polyethylene Glycol based shear thickening fluid. Figures 3-30 and 3-31 show that at high temperatures this particular fluid has no significant shear thickening behavior, the temperature sensitivity of the fluid is at least partially due to the temperature sensitivity of the solvent in which the particles are dispersed.

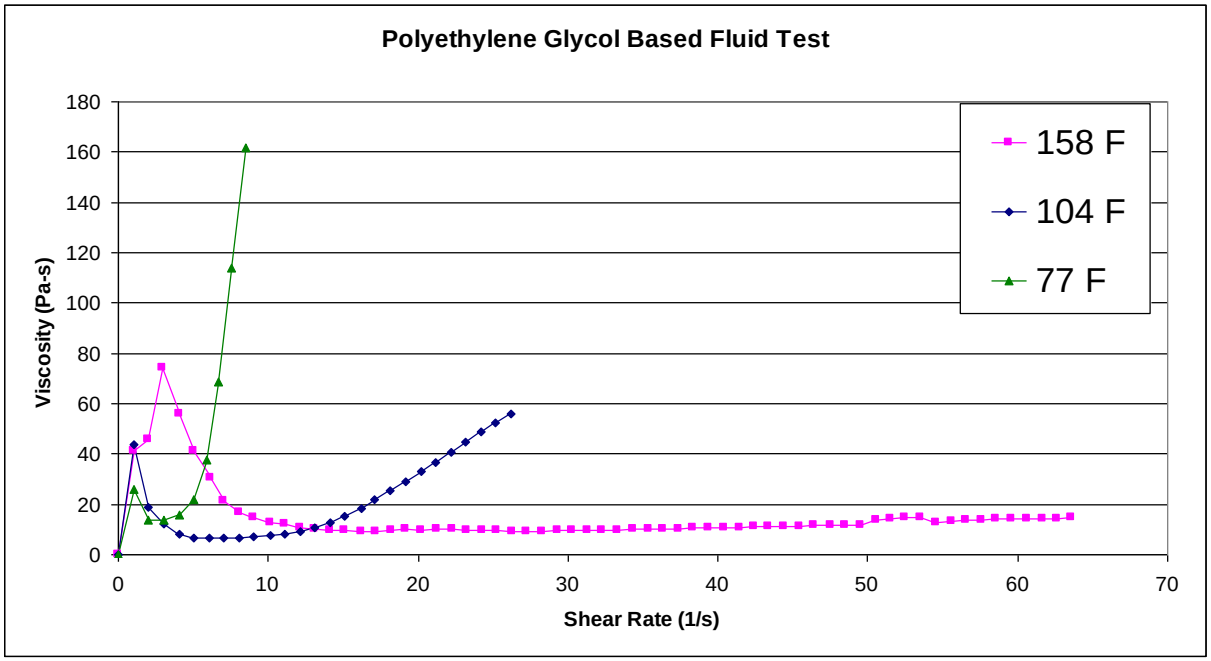

Figure 3-31: Viscosity Curves at Elevated Temperatures

3.5 Phase II Summary

The testing of the first prototype successfully verified that the viscous latch had the desired damping behavior, and provided some initial verification of the mathematical models for the prediction of the door and latch behavior. These tests also illustrated the behavior and possible problems arising from flexing of the door and panel. But, overall they seem to clearly provide a proof of concept for the basic desired viscous damper behavior in resisting large abrupt forces applied to the dryer door.

CHAPTER 4 - Phase III: Transition to Commercial Product

The objective of the second prototype was to improve upon the original in order to prove the validity of a viscous latch beyond the proof of concept phase in a form closer to what is desired for the commercial product.

4.1 Second Prototype Design

The target improvements for the commercial prototype were as follows:

- Reduce size and design the latch to fit within a particular unit provided by the client
- Incorporate a one-way ratcheting device into the latch to allow unrestricted closing of the door
- Have an operational testing range from 70-120 degrees Fahrenheit

Size Reduction

In order to reduce the size of this prototype from the original proof of concept prototype, two actions were taken. First, in order to maximize the surface area of the sheared fluid layer for the smaller volume, the rotating element was changed from a solid cylinder to a thin walled tube. This provided two layers of fluid resisting shear force instead of just one. Secondly, the thicknesses of the fluid layers were reduced in order to compensate for the reduction in radius and maintain a similar shear rate.

Figure 4-1: Latch Mounting

As shown Figure 4-1, the new prototype succeeds in fitting entirely into the available space in the provided door.

Gap Ratio

In order for the dual fluid layers to be as effective as one larger area layer, it is necessary that the fluid in both layers encounter the same shear rate at the same time. As stated in Equation 2-15, the shear rate of the fluid (γ) in the damper is a function of the gap thickness, angular velocity of the rotating element, and the radius of the moving surface.

$$\gamma = \frac{\omega \cdot Rm}{H} \tag{4-1}$$

Since the inner fluid layer had a slightly smaller radius than the outer layer, it was necessary to make its thickness slightly smaller to compensate. This ratio is shown in Figure 4-2 and Equation 4-2. This approach is similar to how the gap thickness in the commercial prototype had to be decreased to make up for the reduced radius from the original.

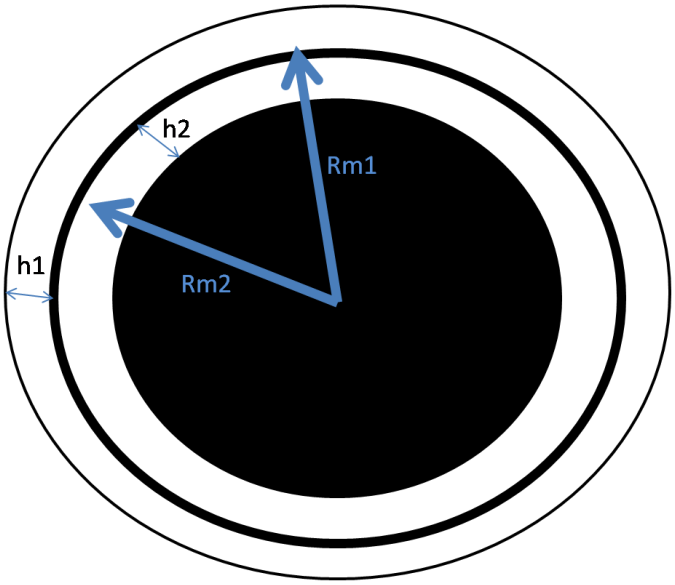

Figure 4-2: Gap Ratio

$$h1 = \frac{h2 \cdot Rm1}{Rm2} \tag{4-2}$$

Using Equation 4-2 as a guideline, the gap thicknesses and radii for the prototype are estimated and listed as in Table 4-1. Taking into account the tolerances to which the parts could be easily machined, the closest that the ratio could be achieved relative to the ideal was within 0.7 percent.

Table 4-1: Fluid Gap Dimensions

h1 = .3308 mm	Rm1 = 12.37 mm
h2 = .31 mm	Rm2 = 11.51 mm

Ratcheting Mechanism

For the ratcheting mechanism, a simple one-way needle bearing was chosen. The bearing was press fitted into the clasp piece, which was in turn placed on the end of the damper's shaft. The theoretical basis for this is that in the opening direction the bearing would lock, thereby transmitting the motion of the clasp to the damper. Alternatively, in the closing direction the bearing would spin freely bypassing the damper.

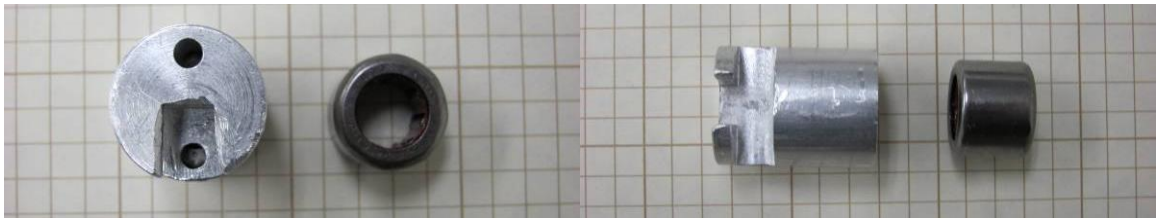

Figure 4-3: Clasp and One-Way Bearing

This mechanism worked well, but after prolonged testing the bearing had a tendency to work its way off the damper shaft since there was no collar to lock it in place. This is not a major issue, but something that should be addressed in future developments.

Filling Damper

Filling the refined prototype is a simple process; a picture of the stand used to facilitate the process is shown in Figure 4-4a. The prototype is first oriented as shown in the jig. Then the fluid is poured into the hopper in the top while a vacuum is applied through the lower tube (5-10 inches of water usually sufficed), drawing the fluid down through the damper. As seen in the disassembled damper shown in Figure 4-4b, the fluid is well distributed throughout the damper by this method.

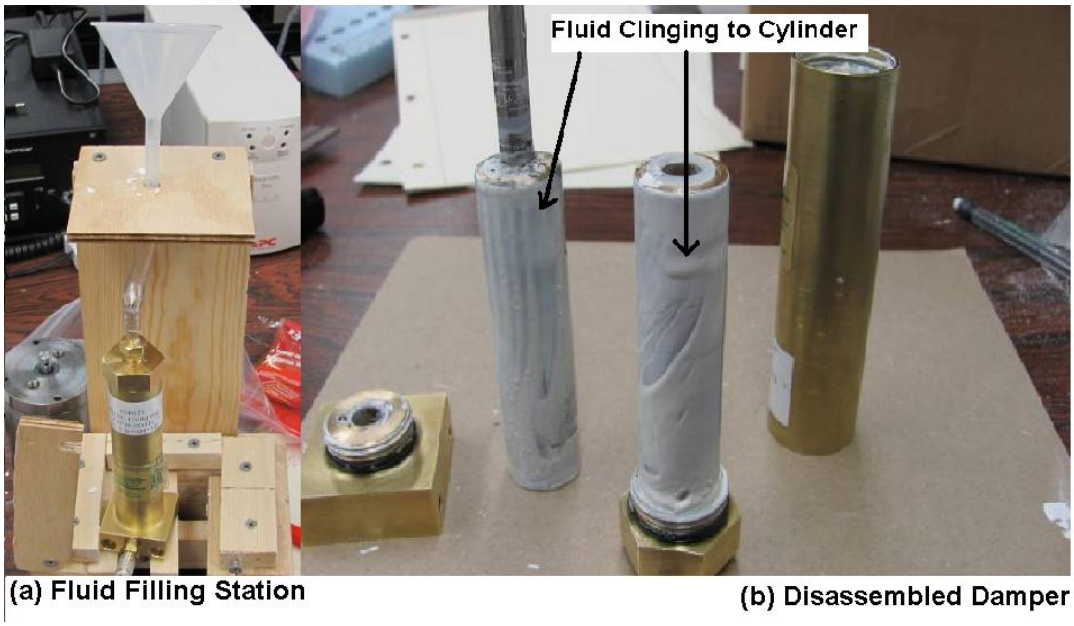

Figure 4-4: Filling Commercial Prototype

Temperature Range

The likely cause for temperature sensitivity in the polyethylene glycol based fluid is the change in the viscosity of the solvent that the particles are dispersed in. The viscosity vs. temperature curve for Polyethylene Glycol used in the prototype fluid is shown in Figure 4-5. Over the desired temperature range, the viscosity changes rather drastically from 10 cps to over 100 cps.

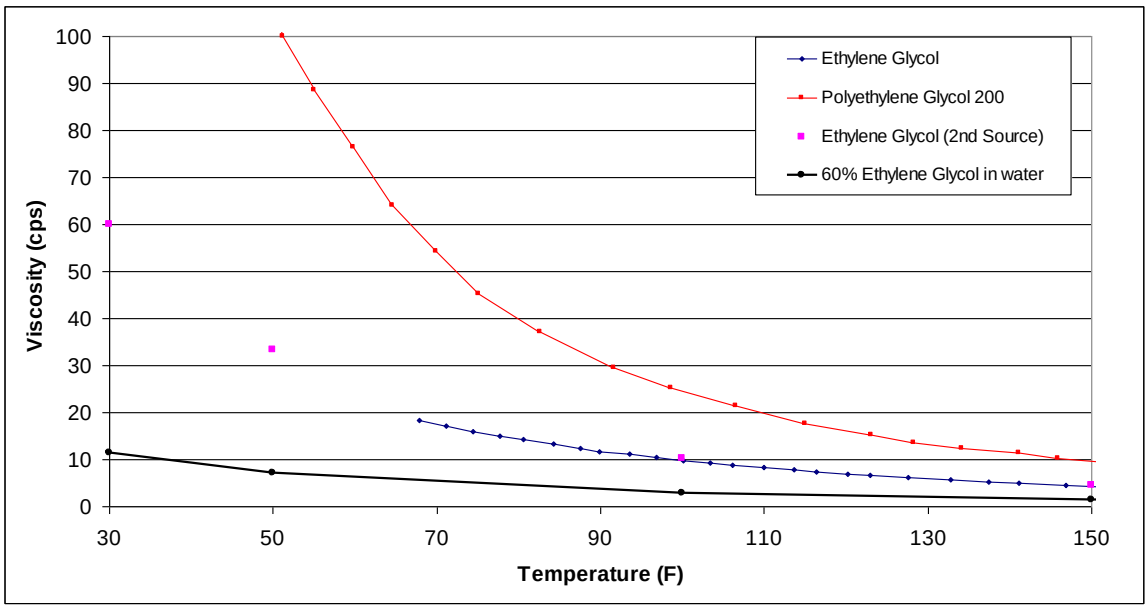

Figure 4-5: Viscosity vs. Temperature Curve

In an attempt to locate a more temperature resistant fluid, a dispersion using a mixture of 60% Ethylene Glycol and 40% Water by weight as the base fluid was tested. Precipitated Calcium Carbonate particles were also used for this dispersion, this time at a volume fraction of approximately 50%.

The results of the rheometer testing for the Ethylene Glycol based fluid are presented in Figure 4-6. As seen in Figure 4-6 the critical shear rate, shear rate where thickening begins, still varied with temperature although to a lesser degree. As an added benefit, the shear thickening is extremely rapid and significant at all temperatures. This is unlike the Polyethylene Glycol based fluid, which has a more gradual rate of shear thickening that decreases with temperature.

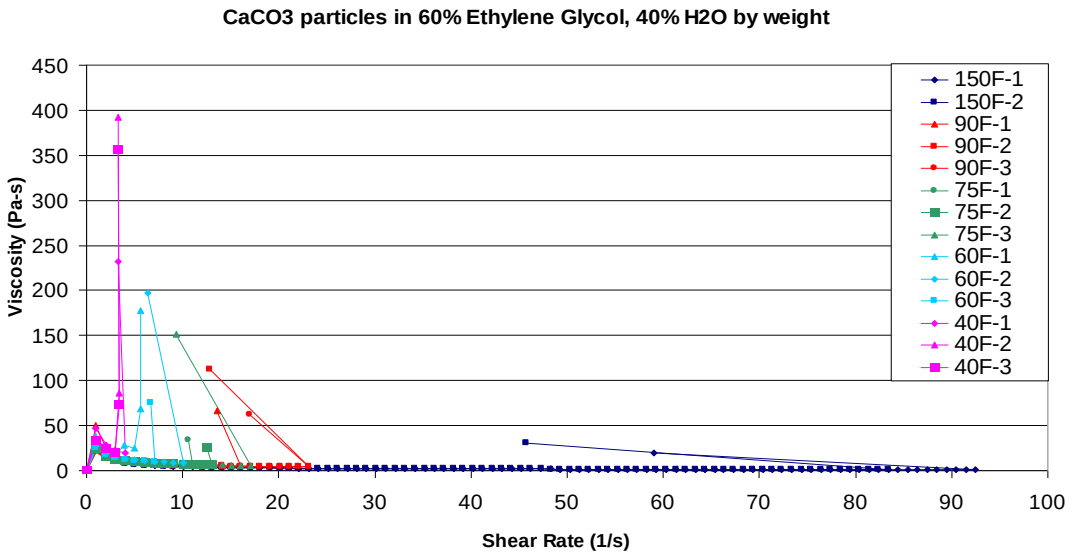

Figure 4-6: Viscosity vs. Shear Rate for Various Temperatures

While the shear thickening at 150F for the EG/H2O mix does occur at a high shear rate, it does have distinct and significant shear thickening behavior. This is unlike the Polyethylene Glycol based fluid, which has minimal shear thickening properties at high temperatures. This means that the Ethylene Glycol/Water based fluid at least has the potential for use in a damper capable of operating at high temperature with some sort of shear rate compensation, unlike the PEG fluid where the damper would become completely ineffective.

Figure 4-7 shows the correlation between the critical shear rate of the fluid and temperature for the Ethylene Glycol and Water base, while Figure 4-8 shows the critical shear rate in terms of the viscosity of the base fluid. The critical shear rates are taken from Figure 4-6.

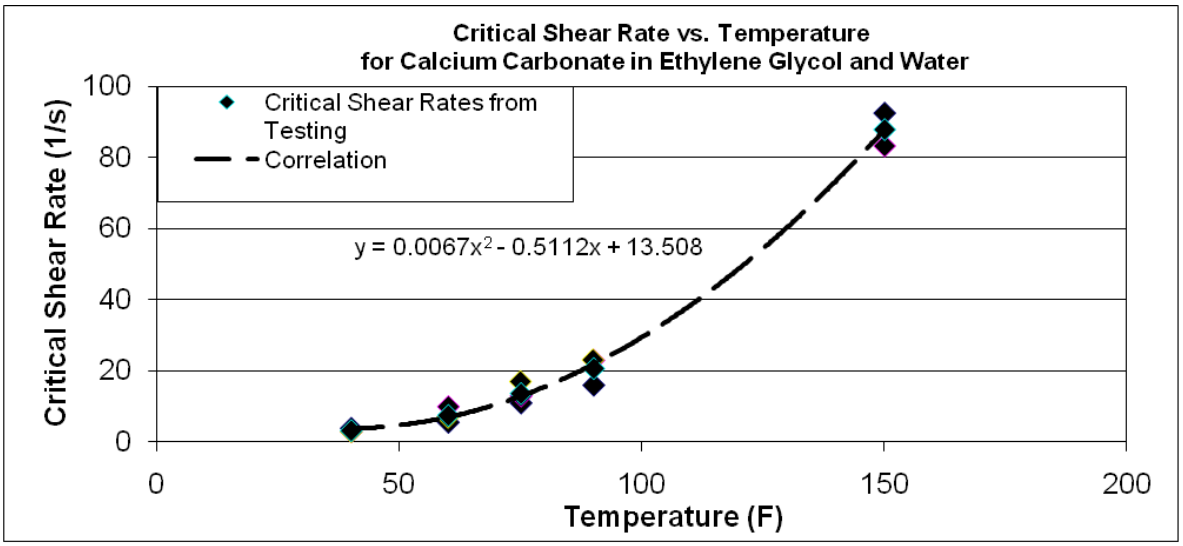

Figure 4-7: Critical Shear Rate vs. Temperature

The viscosity of the base fluid in Figure 4-8 is taken from the 60% Ethylene Glycol in water curve from Figure 4-5 corresponding to the temperature of the dispersion test.

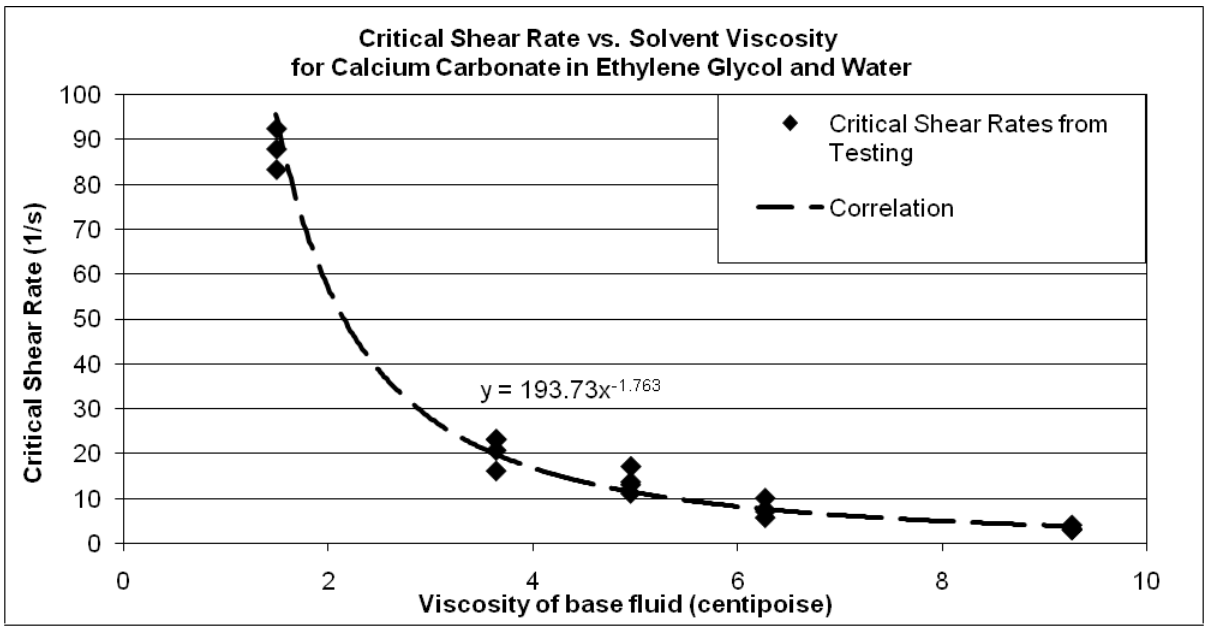

Figure 4-8: Critical Shear Rate vs. Solvent Viscosity

Looking back at Figure 4-5, even though the Ethylene Glycol and Water solution has much less absolute viscosity change over the given temperature range than Polyethylene Glycol,

there is still a fairly drastic relative change from 10 cps to 1 cps over this same temperature range. This may explain why there is still a large variation in critical shear rate with temperature, even though as far as shear thickening is concerned it is behaving better than the Polyethylene Glycol base.

In order to meet the 70F -120F temperature requirement it was decided to go with a suspension of PCC (Precipitated Calcium Carbonate) in water. The thermal expansion concept explored in Chapter 2 was infeasible due to the fact that the spindle for the new design did not have enough volume to show significant thermal expansion. While water based fluid has the drawback of drying out rapidly when exposed to air (compared to the polyethylene glycol based fluids used previously), the water based fluid has greatly reduced temperature sensitivity as well as extremely rapid and distinct thickening at all temperatures. Due to the time it took to sort out complications with the instrumentation (and issues with the mechanical door clasping mechanism), there was not an opportunity to test the upper temperature threshold. The fluid used for this prototype damper testing was 83% by mass Precipitated Calcium Carbonate (Magnum Gloss M from Mississippi Lime) in water.

4.2 Test Results

Several tests were run on the new prototype to test its effectiveness. These included a 1-second force pulse to test the opening rate, closing tests to observe the effectiveness of the newly implemented ratchet, and finally repeating the previous two sets of tests using a mechanical latch in addition to the viscous latch on the door.

Viscous Damper Only

Opening

For the opening tests, 1-second pulses of magnitudes ranging from 5-20 lbs were applied to the setup. It is important to point out that in all the LVDT readings below there is a jump in the displacement reading at the beginning and end of each pulse. These jumps are a result of the viscous damper being off axis from the handle and LVDT. Because of this, when force is applied the door pivots (or twists) about the latch, and does not affect the performance of the damper greatly. This is illustrated in Figure 4-9.

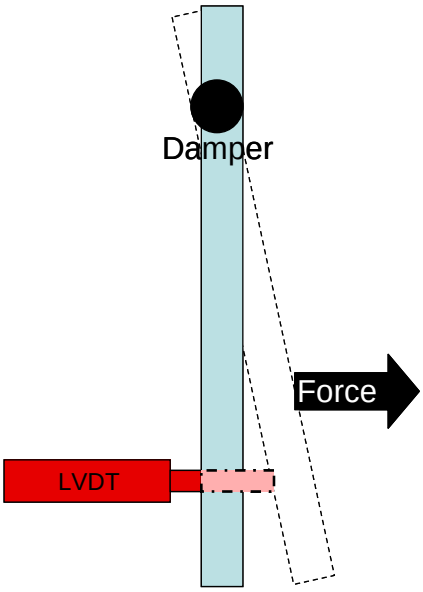

Figure 4-9: Door Pivoting

It should also be noted that this prototype and door combination does not have the problem of drifting open on its own like with the previous prototype. This is due to the fact that this door is much lighter than the one previously tested, and there is enough friction force to hold it in place. Because of this, using a mechanical latch is not absolutely necessary to keep the door closed.

The first testing scenario was to apply a 5 lb opening force to the door, the results of which are shown in Figures 4-10 and 4-11. The fact that the door shifts less than a millimeter during the tests indicates that 5 lbs is not enough to overcome the static friction forces of both the latch and the door.

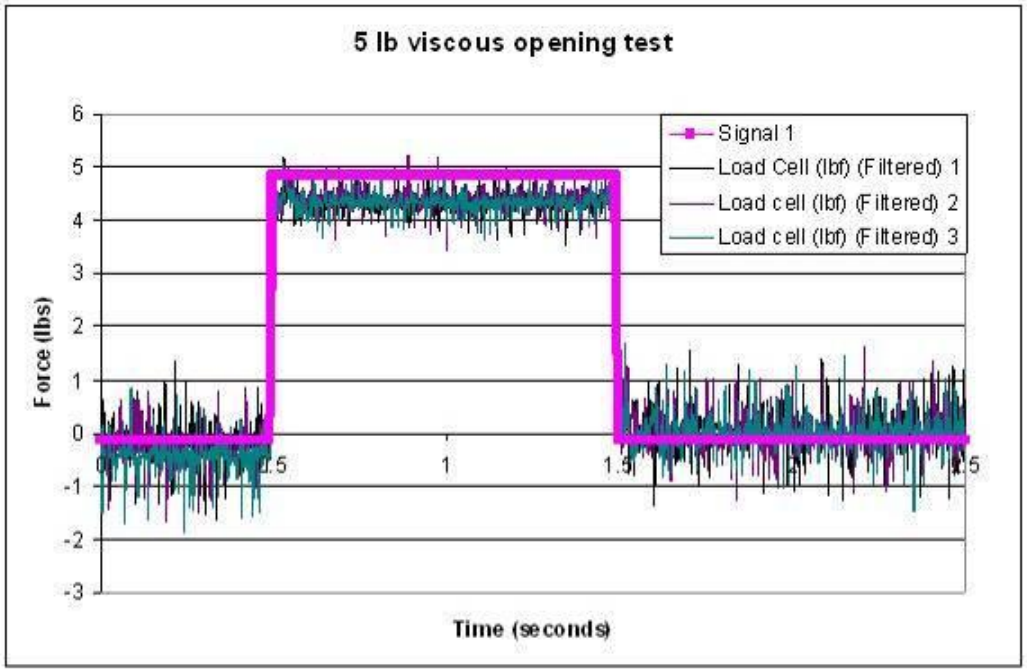

Figure 4-10: 5 lb Load Cell Readings

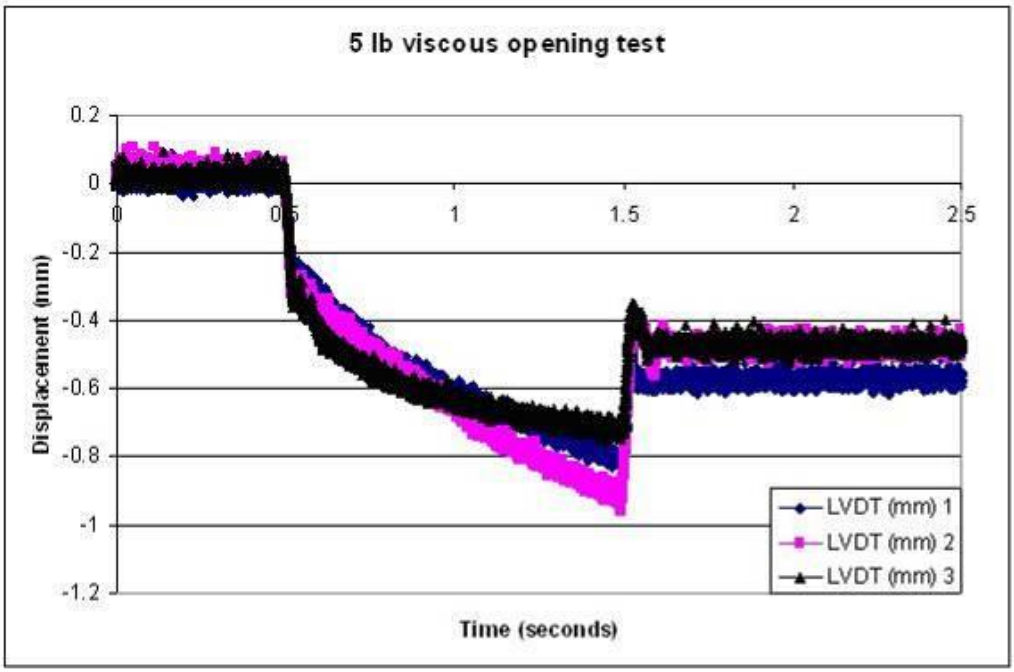

Figure 4-11: 5 lb LVDT Readings

In the force range of 10-20 lbs the damper allows the door to open at a steady controlled rate, as seen in Figures 4-12 through 4-15.

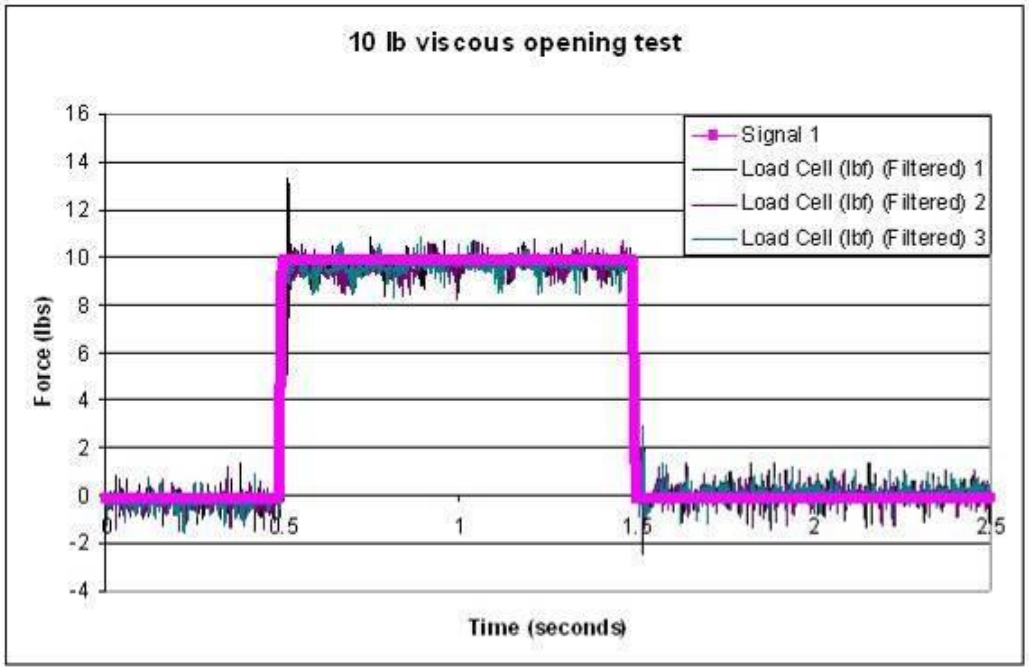

Figure 4-12: 10 lb Load Cell Readings

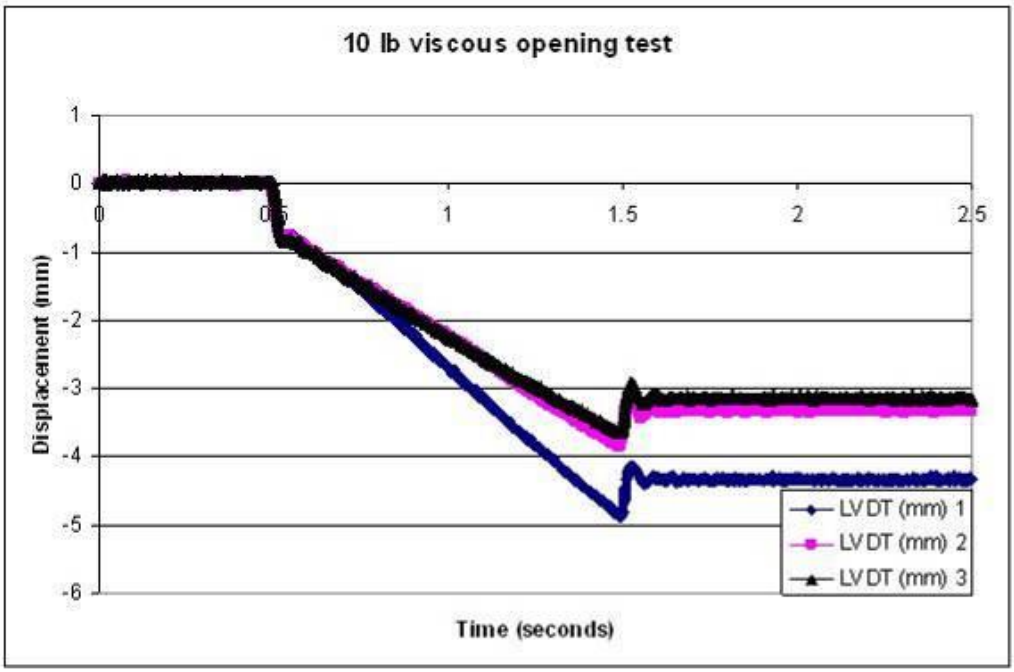

Figure 4-13: 10 lb LVDT Readings

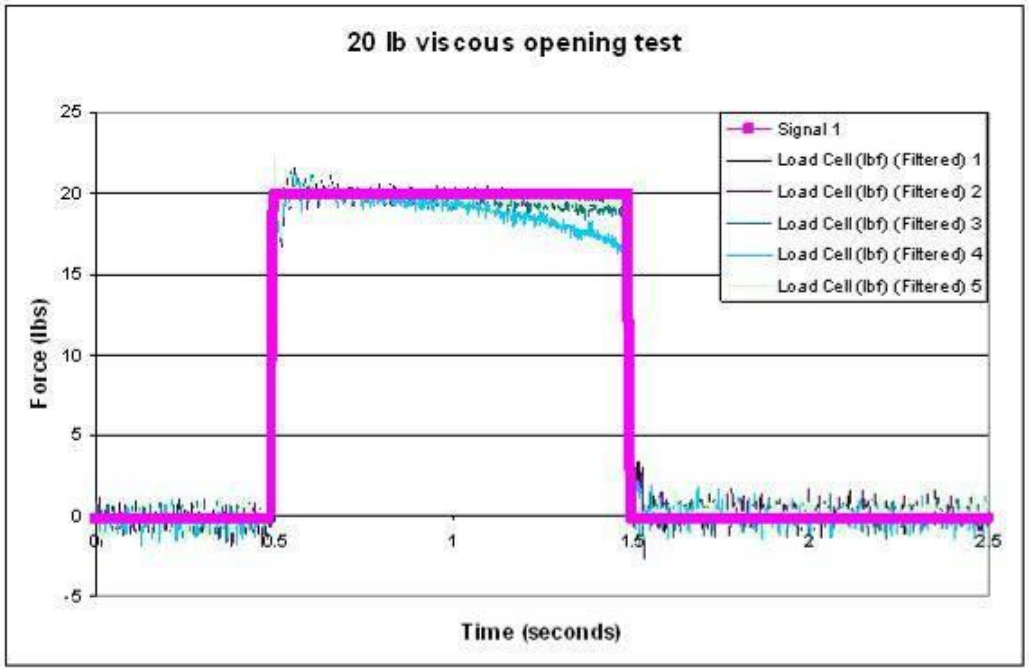

Figure 4-14: 20 lb Load Cell Readings

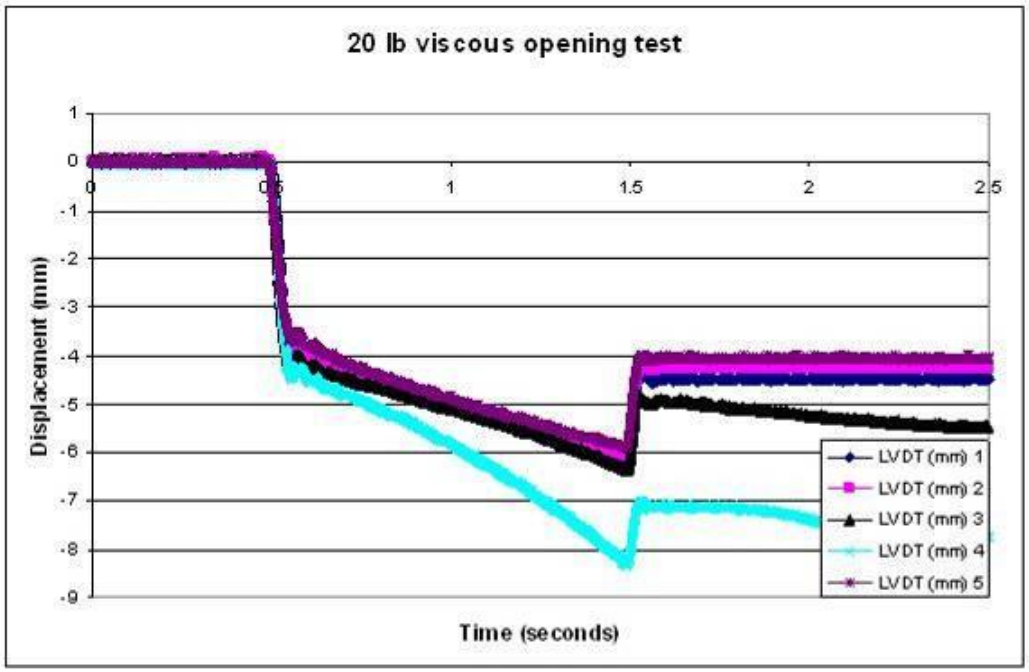

Figure 4-15: 20 lb LVDT Readings

Figure 4-16 is a comparison of the opening rates for the damper at applied forces of 10, 15, and 20 lbs. While there does seem to be a moderate amount of variation in repeatability for any given force, (between 2 to 4.5 mm per second) it is within an acceptable range. The reason

for this variation could be linked to either the fluid (during rheometer testing the water based fluids had a similar scatter for the critical shear rate) or the mechanical components.

The really interesting thing to note is that the rates remain in the same range for all three loadings. This means that the thickening rate of the fluid is significant enough such that, provided the force applied is large enough to overcome the static friction forces in the latch, the opening rate of the door is force approximately independent.

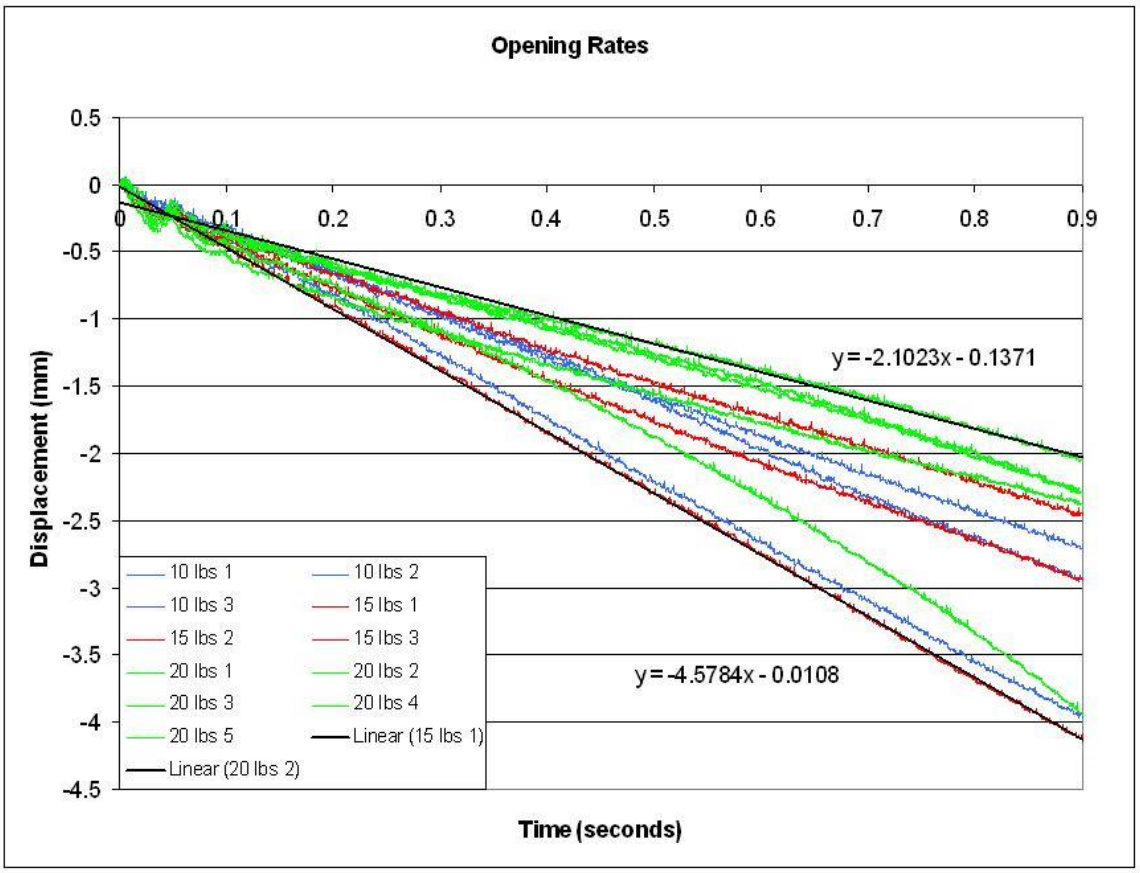

Figure 4-16: Opening Rate Comparison

Extreme Case

As a final test of the damper's rate control, an extreme case load of 40 lbs was applied to the handle for 0.5 seconds. This loading is significantly above anything the door should be subjected to in actual use. The results for this test are presented in Figures 4-17 and 4-18. The

force caused the door itself to pivot a significant amount, but the latch itself shifted (i.e., displaced) less than a millimeter.

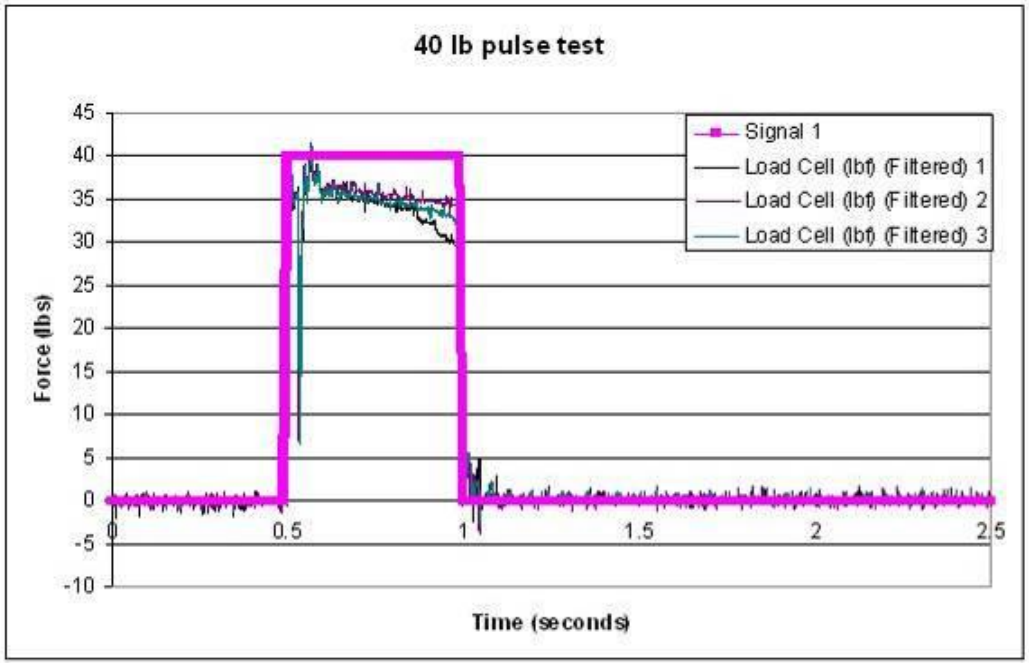

Figure 4-17: 40 lb Load Cell Readings

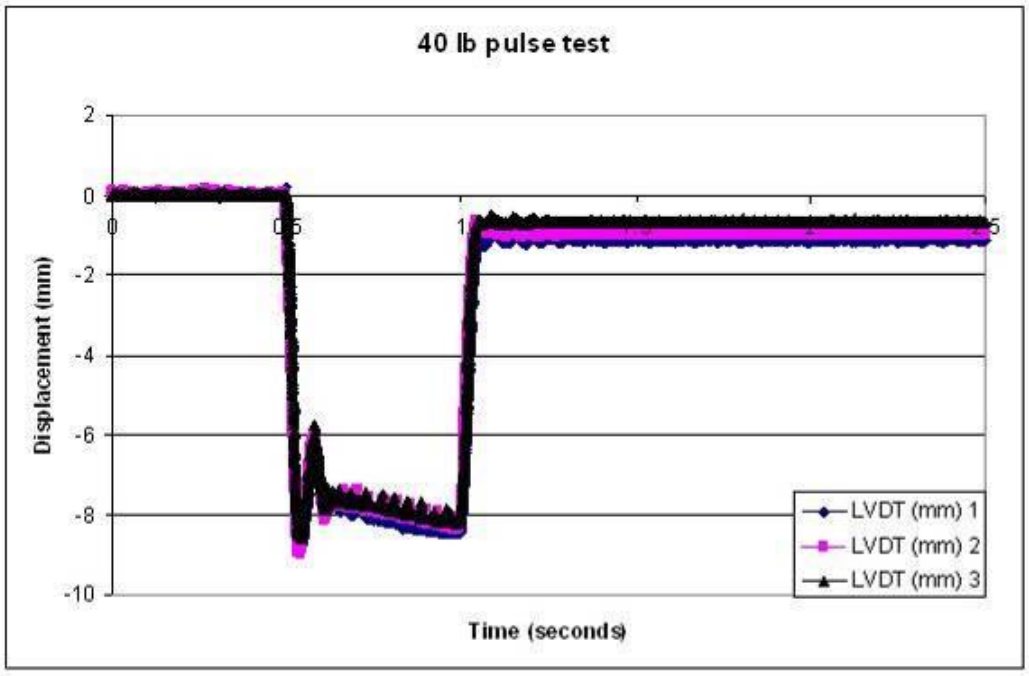

Figure 4-18: 40 lb LVDT Readings

Closing Test

In order to test the closing action of the latch, an opening force of 15 lbs was applied to the door followed by a 0.5 second duration closing force. Some of the results of these tests are shown in Figures 4-19 through 4-22.

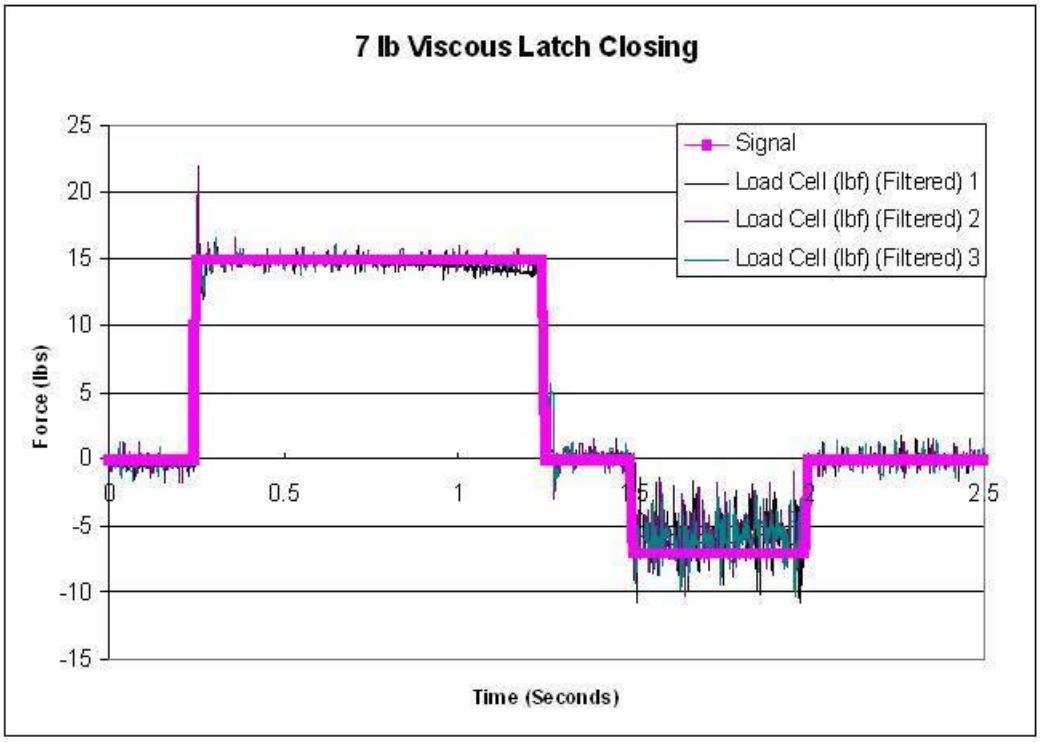

Figure 4-19: 7 lb Closing Load Cell

In Figure 4-19 from 0.25 sec to 1.25 sec the 15 lbs opening force is applied to the door followed by a -7 lbs closing force from 1.5 sec to 2 sec. The force is relieved between the two loadings so the actions can be viewed distinctly from each other. The result of this loading is shown in Figure 4-20. While the opening force is applied from 0.25 to 1.25 seconds the door opens at a constant rate, at 1.5 seconds when the closing force is applied the does not resist allowing the door to return to the closed position in a very small time duration.

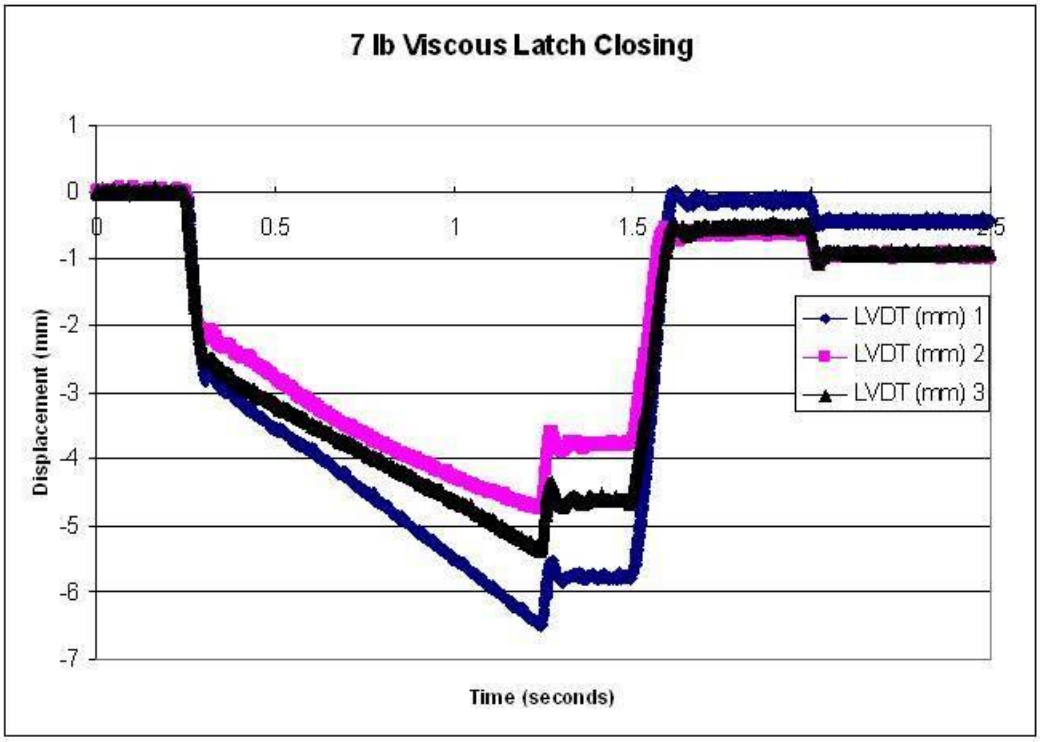

Figure 4-20: 7 lb Closing LVDT

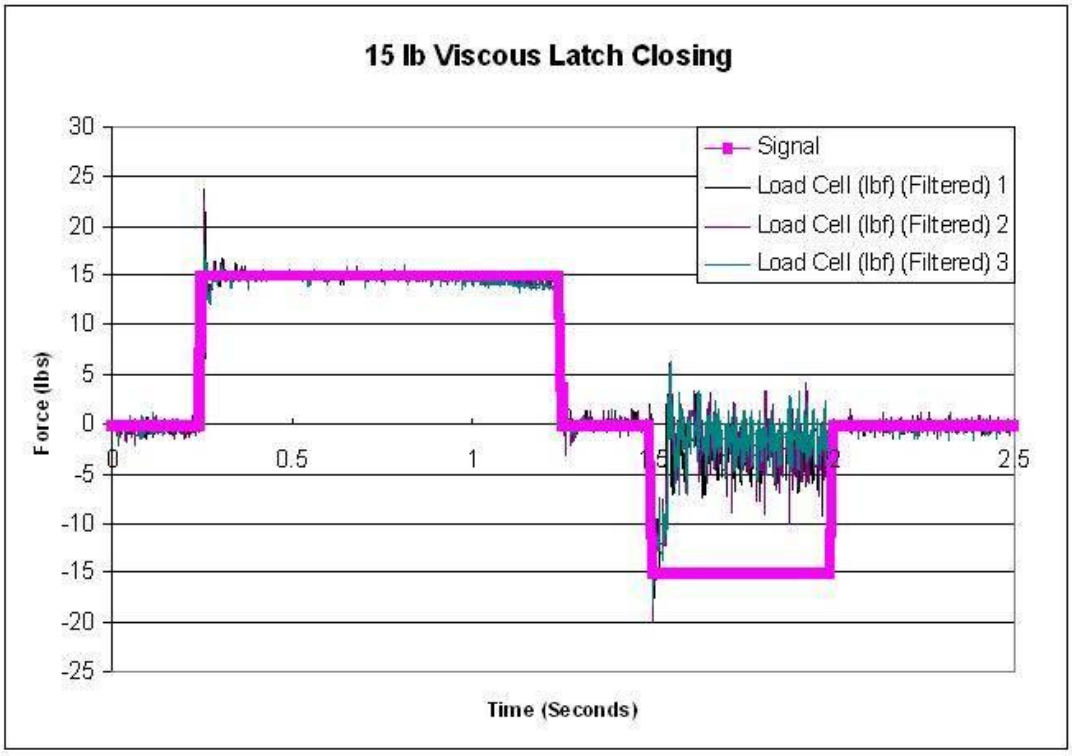

Figure 4-21: 15 lb Closing Load Cell

Figure 4-21 shows a similar door loading to Figure 4-19, however the closing force from 1.5 to 2 seconds has been increased in magnitude to -15 lbs. The load cell readings do not match the signal input during most of this time period because when the door is closed it deflects absorbing the force instead of registering on the load cell.

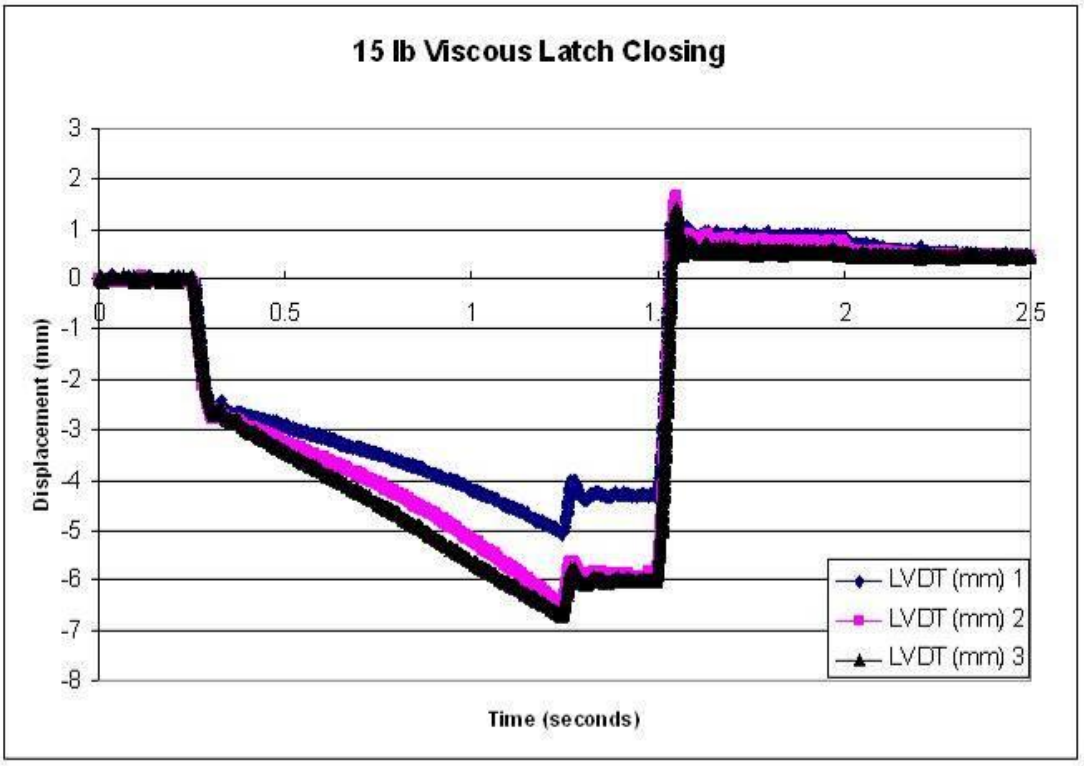

Figure 4-22: 15 lb Closing LVDT

From the closing tests, it was determined that a minimum force of 7 lbs was required to shut the door using the new prototype viscous latch. This was a marked improvement over the stock mechanical latch for the door, which requires a minimum of 15 lbs to open and close.

From the LVDT readings shown in Figures 4-20 and 4-22, provided that a force greater than or equal to 7 lbs is applied to close the door, the closing is almost instantaneous with no significant rate resistance from the damper. This means that the one way bearings are performing their intended purpose of achieving unrestricted closing for the door.

Mechanical and Viscous Latches

The next set of tests performed was to determine how well the viscous damper worked in concert with a mechanical latch.

Preliminary testing on the original mechanical latch, shown in Figure 4-23 below, determined that a force of 15 lbs was required for opening and closing. This, combined with the initial resistance force of the viscous latch, would require a force level above the acceptable range of 5-15 lbs for opening.

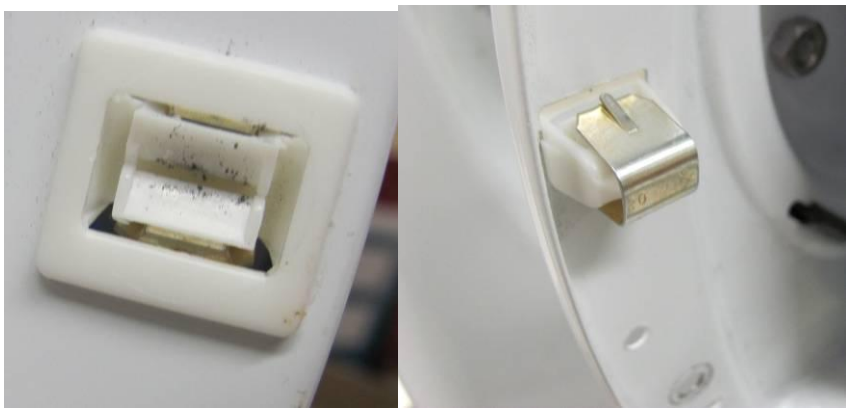

Figure 4-23: Original Mechanical Latch

In order to test a mechanical and viscous latch within the acceptable range, the mechanical latch was replaced with a weaker latch. This weaker latch was taken from the door used for testing in phase 2, which required 5-6 lbs to operate.

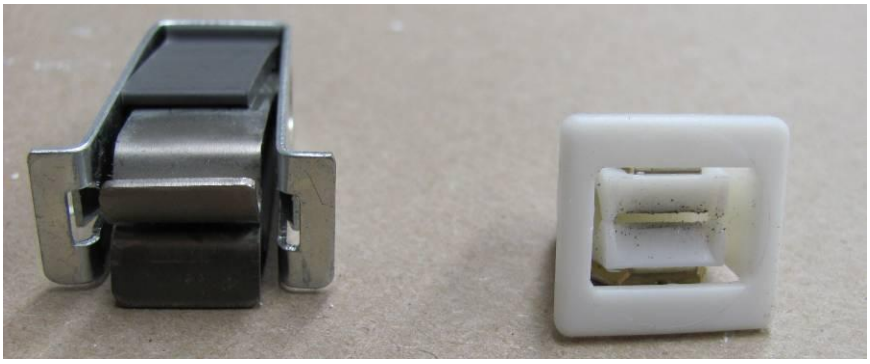

Figure 4-24: Mechanical Latches

Figure 4-25: Weak Latch

Opening

The opening tests for the dual latch configuration were conducted in the same manner as the viscous latch only tests, in that 1 second pulses of magnitudes ranging from 5-20 lbs were applied at the door handle.

As seen in Figures 4-26 and 4-27, the dual latch setup is significantly stiffer than the viscous damper only and 10 lbs is not enough to open the door.

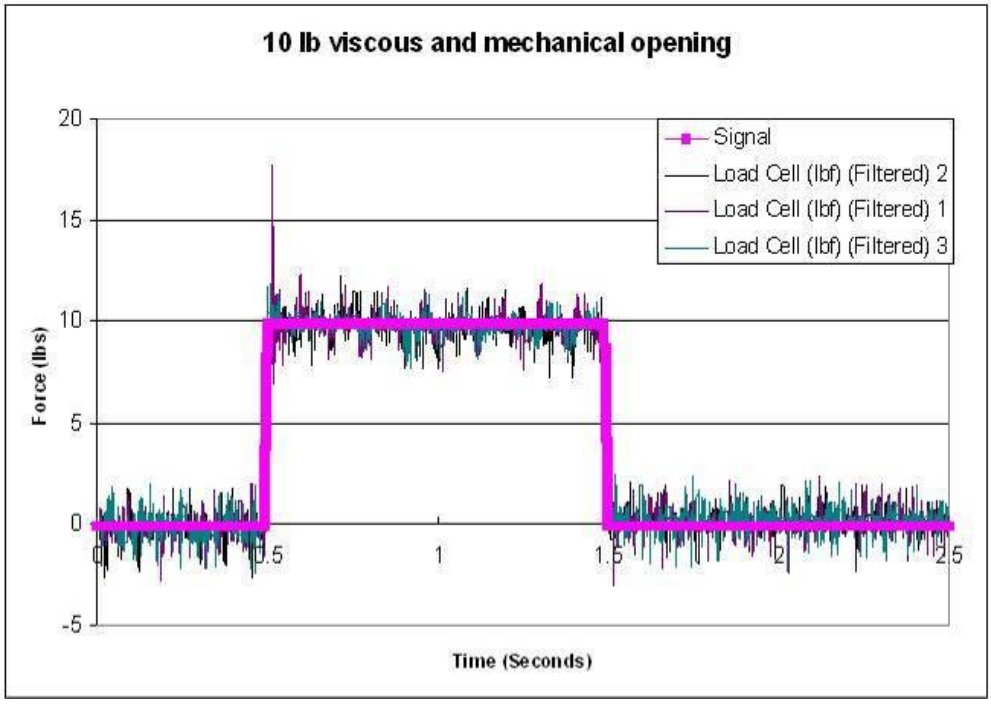

Figure 4-26: 10 lb Dual Latch Load Cell

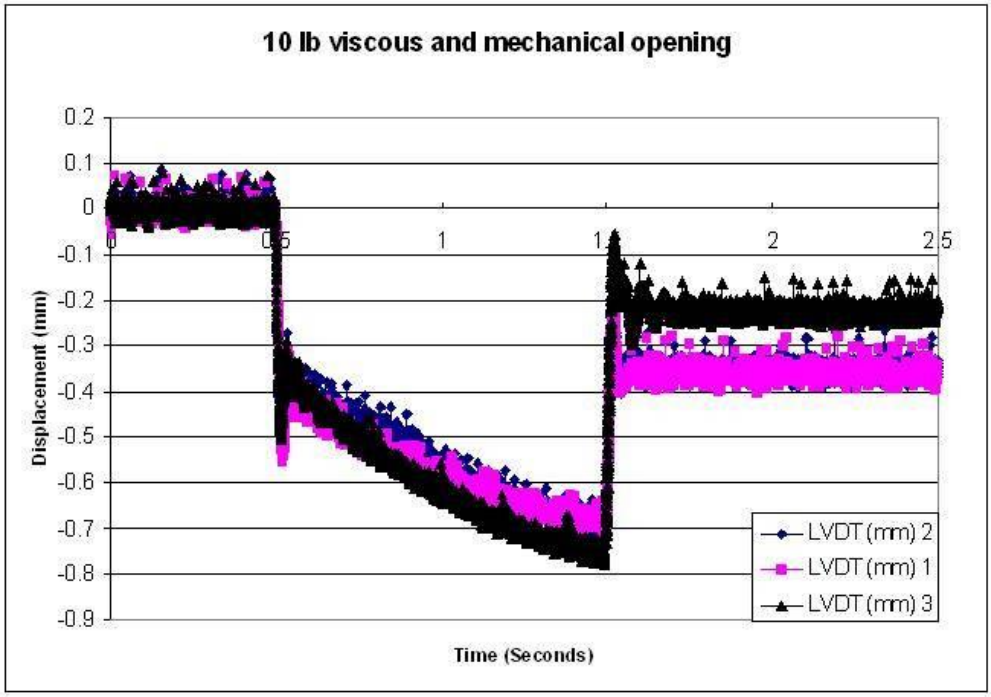

Figure 4-27: 10 lb Dual Latch LVDT

Looking at forces larger than 10 lbs applied to the door in this setup, as shown in Figures 4-28 through 4-31 the behavior is less repeatable. The door either barely moves a millimeter, or it opens completely. Originally, it was expected that the mechanical latch would not significantly interfere with the operation of the viscous latch. However, the unpredictability of the opening behavior shown in Figure 4-29 and Figure 4-31 suggests that the two latches are fighting each other. In any case, more analysis is needed to understand how they interact. Based on these results more consistent results appear to be achievable without the use of the mechanical latch.

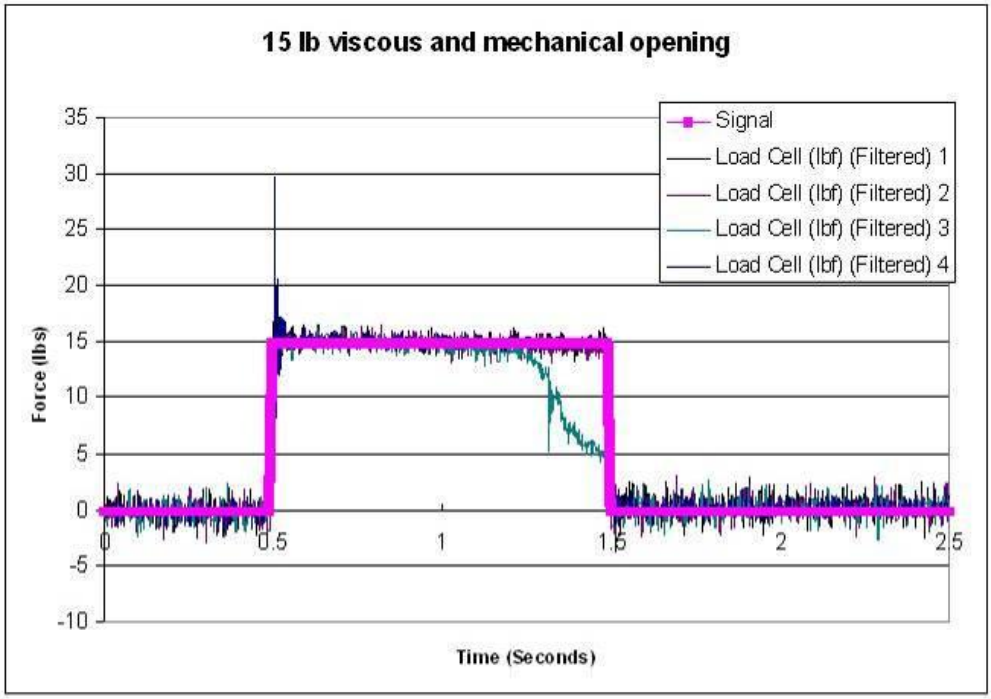

Figure 4-28: 15 lb Dual Latch Load Cell

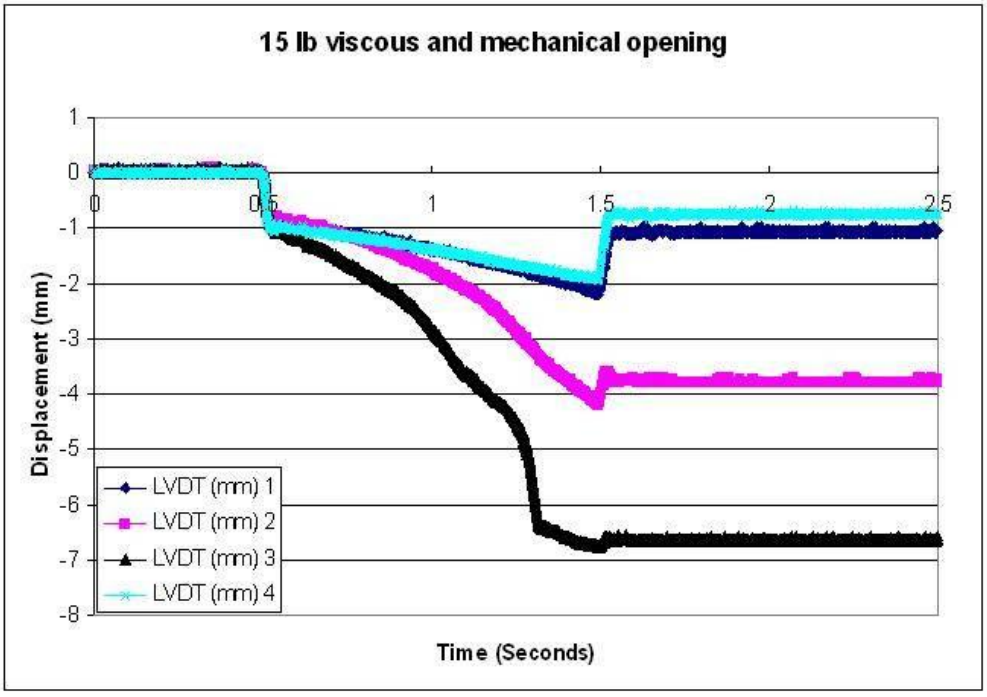

Figure 4-29: 15 lb Dual Latch LVDT

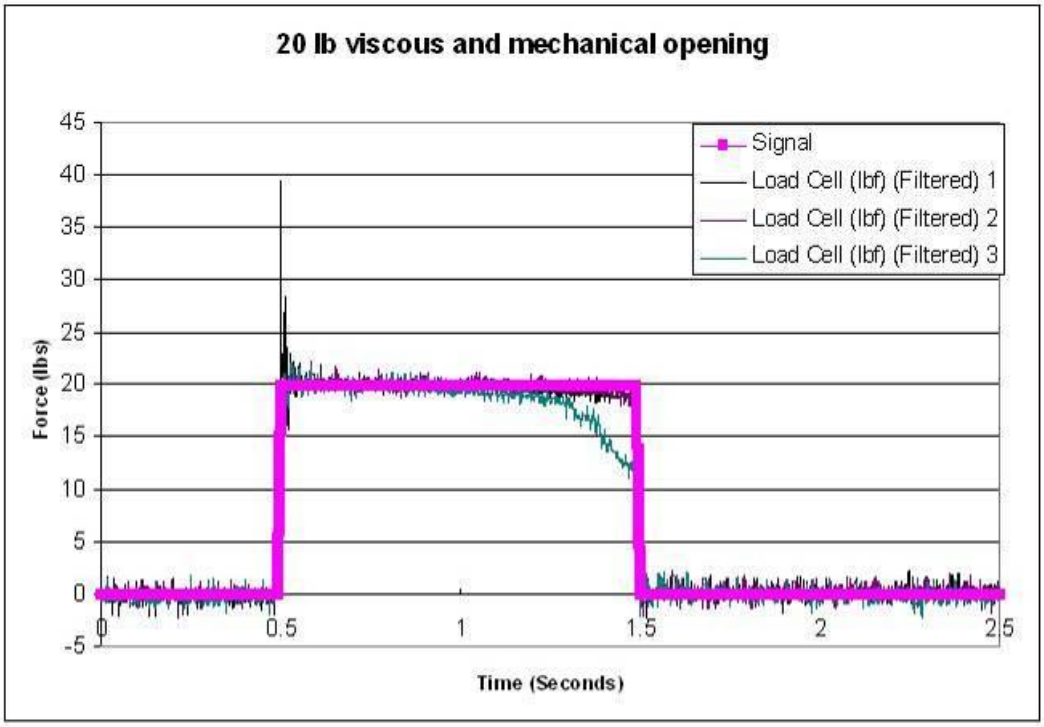

Figure 4-30: 20 lb Dual Latch Load Cell

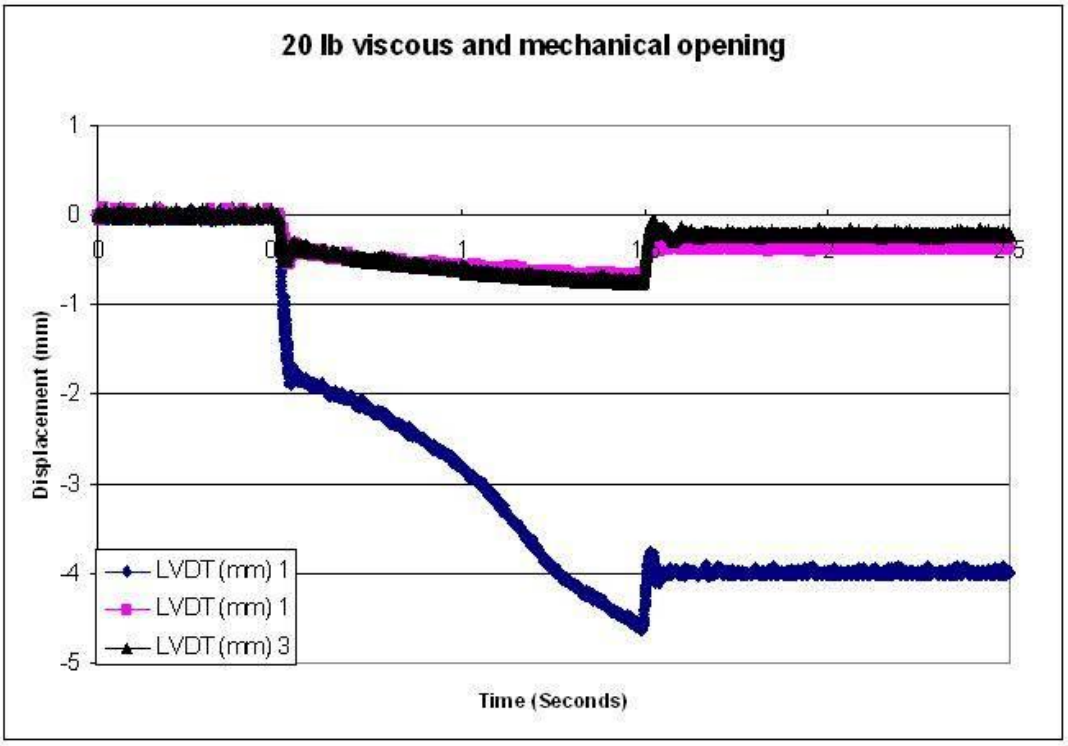

Figure 4-31: 20 lb Dual Latch LVDT

Extreme Case

The extreme loading scenario was repeated for the dual latch configuration, with 40 lbs applied to the handle for a 0.5 second duration. The results for this test are presented in Figures 4-32 and 4-33. The results in this case were similar to the viscous only results. The mechanical latch failed almost instantly allowing the door to pivot (or twist) a significant amount, but the viscous latch itself shifted less than a millimeter.

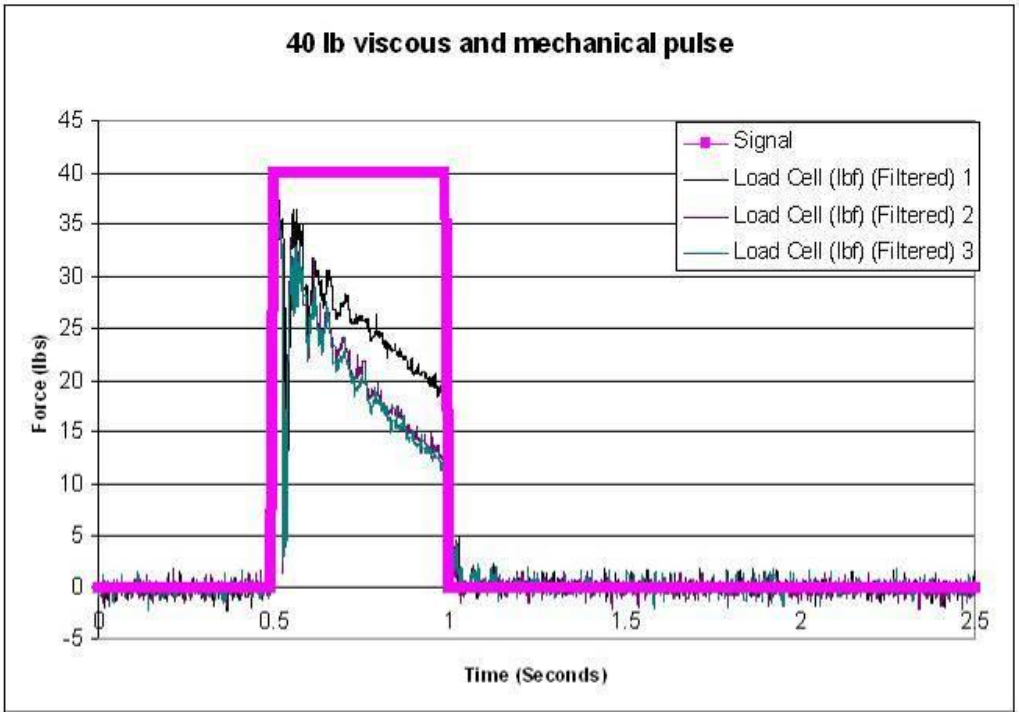

Figure 4-32: 40 lb Dual Latch Load Cell

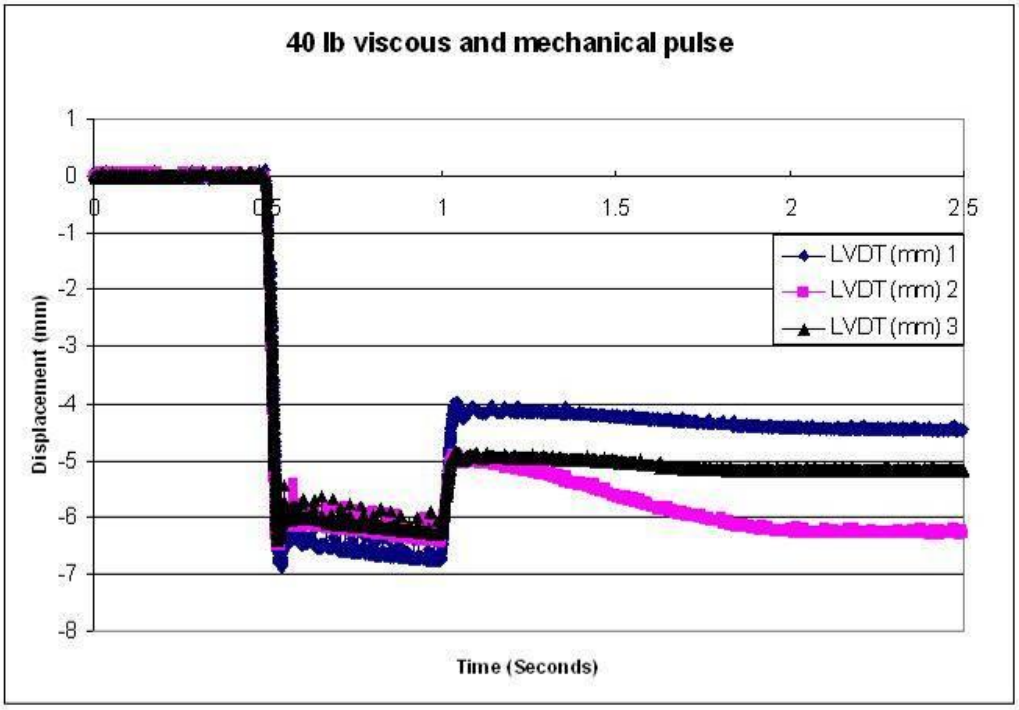

Figure 4-33: 40 lb Dual Latch LVDT

Latch Closing

In order to test the closing action of the both latches, an opening force of 20 lbs was applied to the door followed by a 0.5 second duration closing force. Some of the results of these tests are shown below in Figures 4-34 through 4-37.

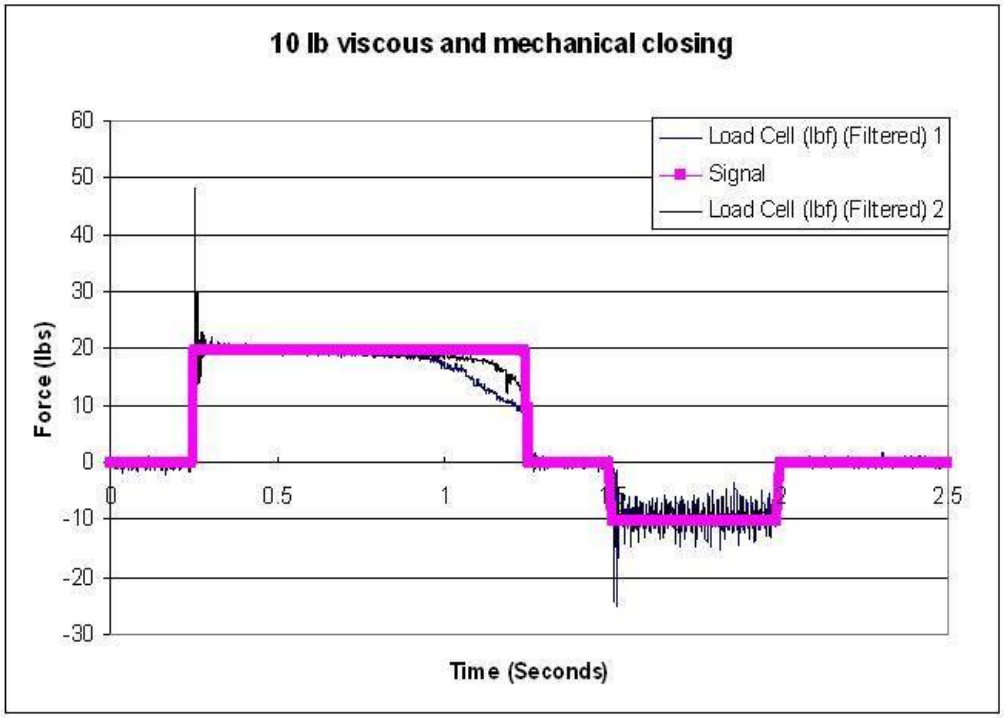

Figure 4-34: 10 lb Closing Test (Load Cell)

Figure 4-34 shows a loading similar to that used for the viscous latch only tests, from 0.25 sec to 1.25 sec a 20 lbs opening force is applied to the door followed by a -10 lbs closing force from 1.5 sec to 2 sec. The result of this loading is shown in Figure 4-35. Due to the addition of the mechanical latch the opening rate from 0.25 to 1.25 seconds is no longer controlled and constant. From 1.5 to 2 seconds during the application of the closing force, -10 lbs was not enough to engage the mechanical latch keeping the door from closing. Figure 4-37 shows that increasing the closing force to -15 lbs was sufficient the close the door.

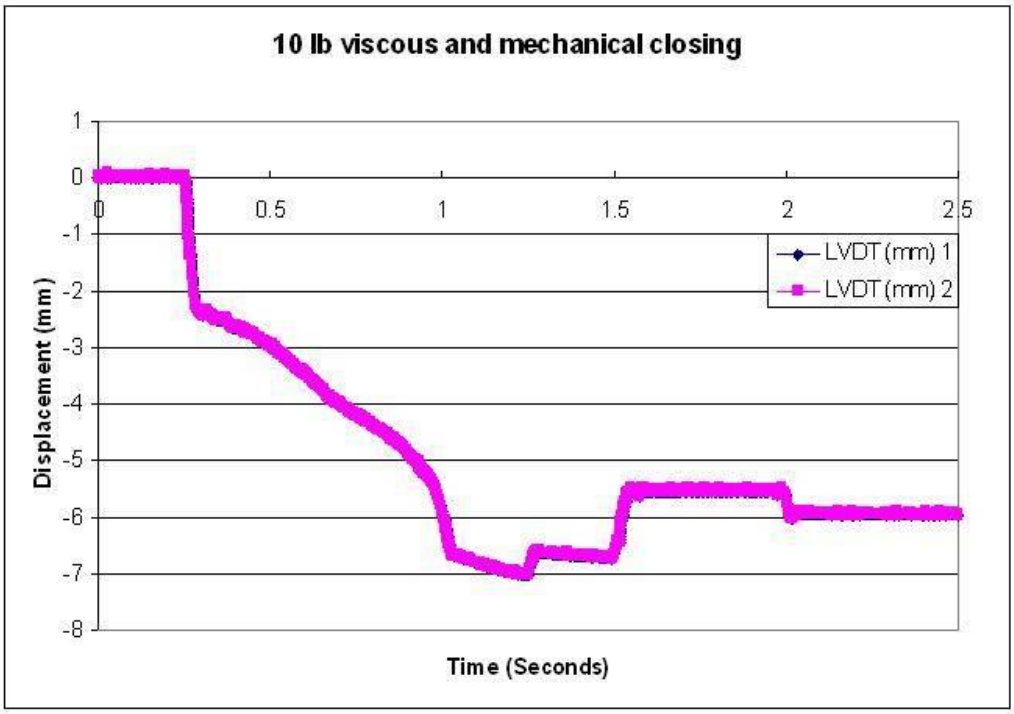

Figure 4-35: 10 lb Closing Test (LVDT)

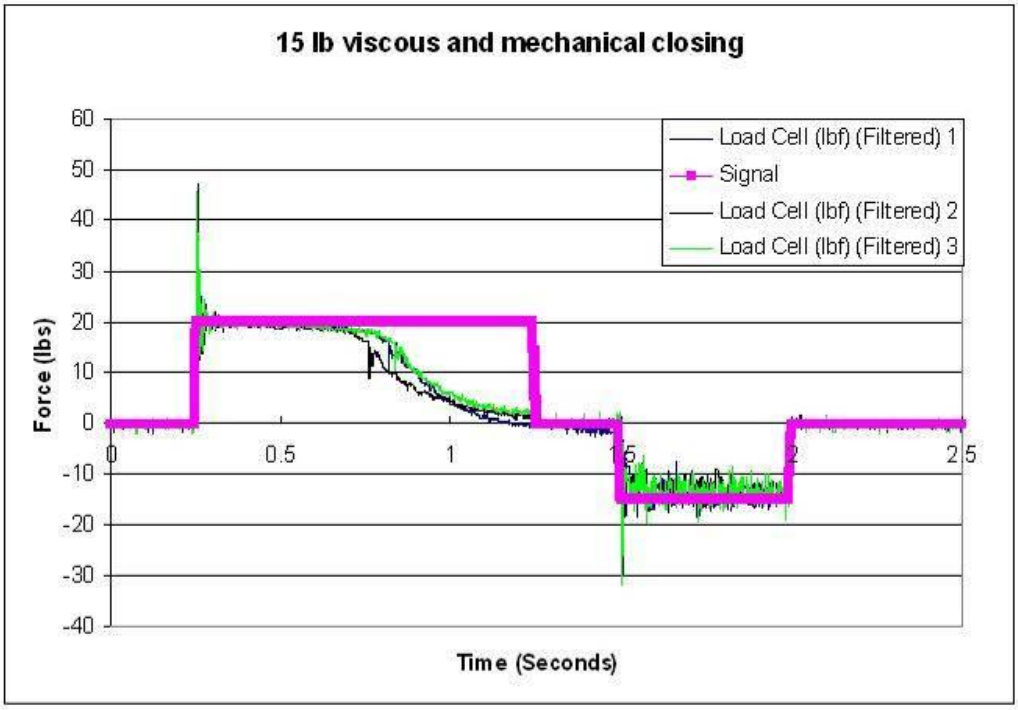

Figure 4-36: 15 lb Closing Test (Load Cell)

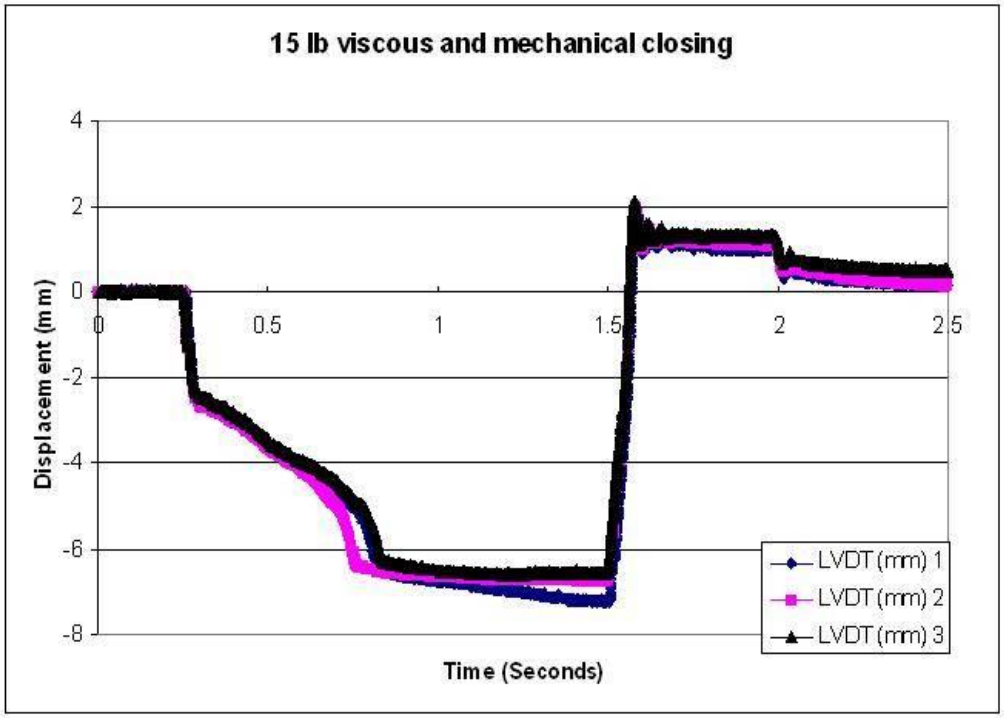

Figure 4-37: 15 lb Closing Test (LVDT)

Testing Obstacles

During the course of the testing there were some problems and possible concerns that had to be addressed. These included being sure that the rotational element was not grinding on the casing, the avoidance of binding in the catch element, and the need to prevent drying of the fluid in the damper.

Self-Centering Effect

Due to the way the spindle is supported within the damper, there was originally some concern that a side load on the shaft would cause the rotary element to grind against the walls. From observations during testing, and from inspection of the pieces for damage after testing, it appears the fluid actually helps prevent misalignment and grinding.

Catch Binding

During the first test there were issues with the catch mechanism binding. This was due to the fact that the extremely short moment arm, in addition to the odd orientation of the latch in the door, made it very easy for the pin to bind in the clasp. In order to address this problem, two

actions were taken. First, the sleeve shown in Figure 4-38 was added to the clasp piece so the moment arm could be extended 0.25 inch (6.35 mm) to 0.5 inch (12.7 mm).

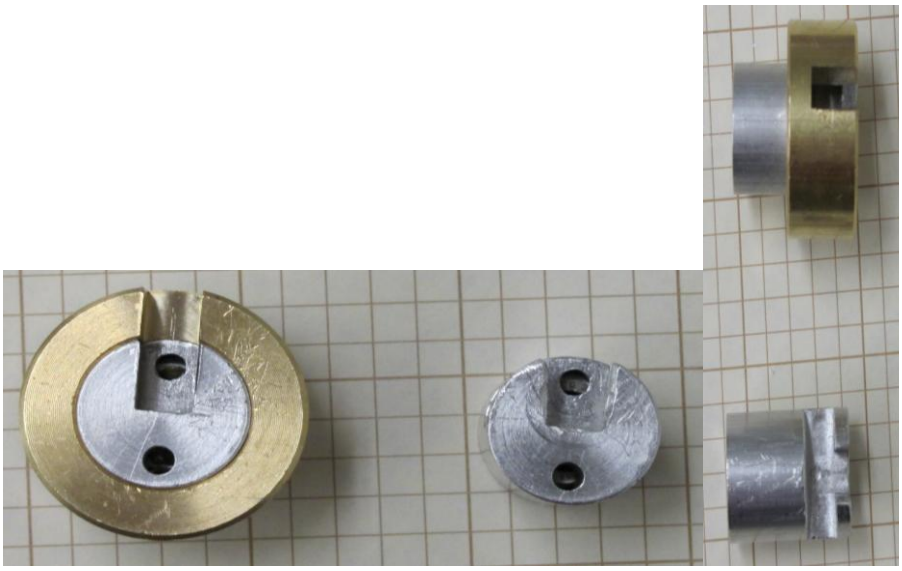

Figure 4-38: Clasp Extension Sleeve

Secondly, the length of the pin that extended into the door was shortened so that, when the door was completely closed, the angle of the slot to the horizontal axis of the door was never more than 90 degrees, as suggested from Figure 4-39.

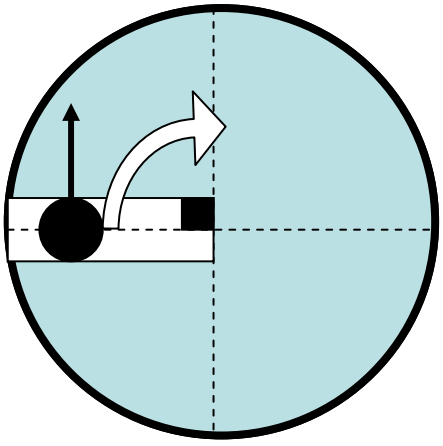

Figure 4-39: Pin and Clasp Starting Orientation

Drying:

For all its benefits noted above, the water-based fluid had the drawback of drying out easily. If properly sealed this should not be a problem inside the damper. However, the current

damper lid seal is not quite adequate, and this is allowing the layer of fluid between the top of the spindle head and the inside of the lid to dry out. This causes the damper to effectively "freeze up". Evidence for this drying out is shown in Figure 4-40.

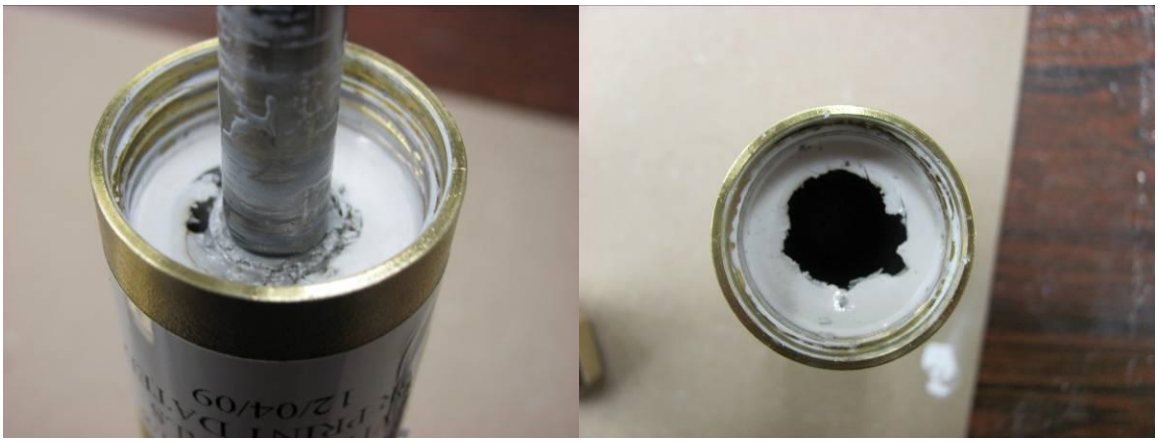

Figure 4-40: Fluid Drying

4.3 Phase III Summary

In conclusion, the second prototype has proved to be a significant improvement over the original large-scale device. By successfully reducing the size and implementing it within an existing door, it was successfully demonstrated that a viscous damper mechanism can be incorporated into a commercial dryer design and function properly. The large amount of damping force exhibited by the unit during testing also suggests that there may even be room for further size reduction.

Other successfully demonstrated improvements in the second prototype device include the addition of a ratcheting device onto the shaft of the damper, which allows for unrestricted closing of the door, and the use of a water-based shear thickening fluid that allows for an almost force-independent opening rate.

CHAPTER 5 - Summary and Future Work

5.1 Summary

The objective of this project was to develop a concept for a Non-Newtonian viscously damped latch, and to evaluate its feasibility. Research was performed to identify existing damping devices using Newtonian fluids as well as different types of Non-Newtonian fluids and their desired properties. Based on this preliminary research, several concepts were developed that involved creating a resistance force from a shear thickening fluid in (STF) Couette flow. From the STF research, a suspension of precipitated calcium carbonate (PCC) particles in a medium of polyethylene glycol (PEG) was selected as the best candidate for proof of concept testing. Preliminary testing was performed using rheometer equipment in order to gain a better understanding of how the fluid behaved. Using the results of these tests, a Matlab program was developed to estimate how a viscous latch would perform under different loadings. The program also evaluated whether any of the design concepts could provide enough resistance force to meet the requirements of the project. Based on these analyses, a rotating cylinder type design determined to be effective.

The focus for the second phase of the project was to demonstrate a proof of concept for the viscous damper design in the form of a working model prototype. This prototype did not need to be of identical shape and proportions as the finalized design, instead it was developed to facilitate experimental testing and evaluation of performance under the desired operating conditions. This prototype was a simple cylinder mounted on a rotating shaft surrounded by a thin layer of fluid. The fluid layer was 0.02 inch thick and the shearing of fluid between the rotor and the housing provided the resistance force. The fluid used was a dispersion of calcium carbonate (CaCO3) in polyethylene glycol (PEG) with a volume fraction of 48.6% CaCO3. It was necessary to design and construct the test setup for the dynamic testing of a dryer door using the viscous latch. The test setup consisted of a LVDT, a load cell, and a voice coil linear actuator. All instruments were linked using LabView, which allowed for the measurement of the linear door opening position and the force applied as a function time. These tests verified that the viscous latch had the desired damping behavior, and they provided some initial verification of the mathematical models for the prediction of the door and latch behavior. These tests also

illustrated the behavior and possible problems arising from flexing of the door and panel. But overall they seem to clearly provide a proof of concept for the basic desired viscous damper behavior in resisting large abrupt forces applied to the dryer door.

The objective of the final phase was to produce a second prototype that improved upon the original. The intent was to prove the validity of a viscous latch beyond the proof of concept phase, in a form closer to what is desired for the commercial product. The main target improvements for the commercial prototype were to (1) reduce size and design the latch to fit within a particular unit provided, (2) incorporate a one-way ratcheting device into the latch to allow unrestricted closing of the door, and finally (3) to have an operational temperature range from 70-120 degrees Fahrenheit. In order to reduce the size of this prototype from the original, two actions were taken. First, in order to maximize the surface area of the sheared fluid layer for the smaller volume, the rotating element was changed from a solid cylinder to a thin walled tube. This provided two layers of fluid resisting shear force instead of just one. Secondly, the thicknesses of the fluid layers were reduced in order to produce a more dramatic thickening effect. For unrestricted closing of the door, a simple one-way needle bearing was used as the ratcheting mechanism. Finally, in an attempt to meet the temperature requirements it was decided to use a suspension of PCC (Precipitated Calcium Carbonate) in water. While this fluid had the drawback of drying out rapidly when exposed to air, compared to the polyethylene glycol based fluids used previously, the water based fluid greatly reduced temperature sensitivity as well as extremely rapid and distinct thickening at all temperatures. Due to these changes the second prototype proved to be a significant improvement over the original large-scale device. By successfully reducing the size and implementing it within an existing door, it was successfully demonstrated that a viscous damper mechanism could be incorporated into a commercial dryer design and function properly. The addition of a ratcheting device onto the shaft of the damper allowed for unrestricted closing of the door as desired. The use of a water-based shear thickening fluid also provided for an almost force-independent opening rate. While there was not enough time to perform ample testing to determine the temperature range of the improved prototype, limited rheometer testing of water-based fluids have shown them to be temperature resilient.

5.2 Future Work

The testing performance of the improved prototype has shown that there is a great deal of potential for the continued development of the Non-Newtonian latch design. More specifically, the testing and correlation to the numerical simulations have shown that the mechanical design and physical sizing of the dampers are well understood. Furthermore, as long as the behavior of the shear thickening fluid is known, the internal geometry can be designed so that the door opening and closure will have the desired behavior. Based on current findings, the project's future efforts should be focused on selecting the fluid. While the water based calcium carbonate suspension has shown acceptable temperature properties and excellent shear thickening characteristics, it is also unstable and prone to drying if not sealed properly. Other dilatant fluid options such as ionomer solutions might be a better choice.

References

Berret, J. F., Gamez-Corralez, R., Oberdisse, J., Walker, L. M., & Linder, P. (1998). Flow-structure relationship of shear-thickening surfactant solutions. *Europhysics Letters, 41*(6), 677-82.

Boersma, W. H., Laven, J., & Stein, H. N. (1990). Shear thickening (dilatancy) in concentrated dispersions. *American Institute of Chemical Engineers Journal, 36*(3), 321-32.

Drew, D., & Davis, J. (2010). *The viscous coupling.* Retrieved 4/5/2010, 2010, from http://syncro.org/VCTest.html

Egres, R. G., Netteshein, F., & Wagner, N. J. (2006). Rheo-SANS investigation of acicular-precipitated calcium carbonate colloidal suspensions through the shear thickening transition. *Journal of Rheology, 50*(5), 685-709.

Lee, Y. S., & Wagner, N. J. (2006). Rheological properties and small-angle neutron scattering of a shear thickening, nanoparticle dispersion at high shear rates. *Industrial Engineering Chemistry Research, 45*(21), 7015-7024.

Lundberg, R. D., & Makowski, H. S. (1980). SOLUTION BEHAVIOR OF IONOMERS - 1. METAL SULFONATE IONOMERS IN MIXED SOLVENTS. *Journal of Polymer Science.Part A-2, Polymer Physics, 18*(8), 1821-1836.

Lundberg, R. D. (1982). SOLUTION BEHAVIOR OF IONOMERS - 3. SULFO-EPDM-MODIFIED HYDROCARBON SOLUTIONS. *Journal of Applied Polymer Science, 27*(12), 4623-4635.

Lundberg, R. D., & Duvdevani, I. (1989). Shear thickening of ionomers and their complexes. *Polymeric Materials, 61*, 259-264.

McFarland, R. W. (2000). In ADAC Plastics Inc. (Ed.), *Fluid-damped automotive door latch actuator*

Özışık, M. N. (1993). *Heat conduction*. New York, N.Y.: Wiley.

Raghavan, S. R., & Khan, S. A. (1997). Shear-thickening response of fumed silica suspensions under steady and oscillatory shear. *Journal of Colloid and Interface Science, 185*(1), 57-67.

Rude, E. T., & Brokowski, W. (2006). In TorqMaster Inc. (Ed.), *Friction hinge with viscous damping* (16/342 ed.)

Shenoy, S. S., & Wagner, N. J. (2005). Influence of medium viscosity and adsorbed polymer on the reversible shear thickening transition in concentrated colloidal dispersions. *Rheologica Acta, 44*(4), 360-370.

Sigma-Aldrich. (2010). *BioUltra reagents detergents & surfactants.* Retrieved 4/6/2010, 2010, from http://www.sigmaaldrich.com/life-science/metabolomics/bioultra-reagents/detergents-surfactants.html

Wetzel, E. D., Lee, Y. S., Egres, R. G., Kirkwood, K. M., Kirkwood, J. E., & Wagner, N. J. (2004). The effect of rheological parameters on the ballistic properties of shear thickening fluid (STF)-kevlar composites. *AIP Conference Proceedings, 712*(1), 288-293.

Appendix A - Simulation Programs

As described in sections 2.5 and 2.6, in order to determine if it was feasible to move forward to the next phase of the project simulations were performed to see if the requirements could be met.

A.1 Dynamic Door Opening Model

Using the formulas detailed in section 2.5, an iterative simulation was programmed in MatLab to predict door opening rates under various loading conditions

MatLab Code

Dynamic Opening Model

```
% Program for commercial prototype simulation (2 fluid layers)
clear;
duration= 1.5; %seconds
dt= 0.000001; %seconds
iterate= duration/dt;

%Inputs and initial conditions
y1= 0.3308;      %thickness of fluid layer 1(mm)
Li= 80.5; % length of inner surface (mm)
Lo= 93.8; % length of outer surface (mm)
z= (7/16)*25.4; %arm (mm)
rm1= 12.37;%outer radius of tube (mm)
thick= 0.86;%tube wall thickness (mm)
rm2= rm1-thick;%inner radius of tube (mm)
y2= 0.31      %thickness of fluid layer 2(mm)
ro= rm1+y1; %outer radius (mm)
ri= rm2-y2; %inner radius (mm)
D1 = 254; %mm to door center from hinge
D2 = 469.9; %mm from door handle to hinge
D3 = 460; % Damper to hinge (mm)
area = 148387; %mm^2
time = zeros(1, iterate);
time(1)= 0; %seconds
mass= 29.56*0.45359237; %kg mass of door
Fu= 15/0.22481; %N opening force applied to door handle
Fm= zeros(1, iterate); % Resistance Force from Mechanical Latch
Fm(1)= 0; %N
v = zeros(1, iterate);
v(1)= 0; %mm/s
w = zeros(1, iterate);
w(1)=0; %rad/s
w2 = zeros(1, iterate);
w2(1)=0; %rad/s
pos = zeros(1, iterate);
```

```
pos(1)=0; %mm
dampos = zeros(1, iterate);
dampos(1) = 0; %mm
rate1 = zeros(1, iterate);
rate1(1)=0; %1/s
rate2 = zeros(1, iterate);
rate2(1)=0; %1/s
kik = zeros(1, iterate);
kik(1)=0;
vis1 = zeros(1, iterate);
vis1(1)= (52.05); %Pa-s, initial viscosity
vis2 = zeros(1, iterate);
vis2(1)= (52.05); %Pa-s
pmax=0/0.0040147; %Pa 1.6 ave, 5.2 max
prate=pmax/0.1; %Pa/s
I = (1/12)*mass*D2^2+mass*D1^2; %Mass moment of inertia kg-mm^2
thet = zeros(1, iterate);
thet(1)=0;
stress1 = zeros(1, iterate);
stress1(1)=0;
stress2 = zeros(1, iterate);
stress2(1)=0;
Friction= 0/0.22481;%N
axlerad= 3; %mm
FR = zeros(1, iterate);
FR(1)= Friction*(axlerad/z); %N
FR1 = zeros(1, iterate);
FR2 = zeros(1, iterate);
FR1(1) = 0;
FR2(1) = 0;
P = zeros(1,iterate);
F = zeros(1,iterate);
cuttoff = 5; %mm
tcut= duration;

for x = 1:iterate
    if time(x) < 0.1
        P(x)=prate*time(x); %Pa
    elseif time(x) >= 0.1 && time(x) < 0.4
        P(x)=pmax; %Pa
    elseif time(x) >= 0.4
        P(x)=pmax-prate*(time(x)-0.4); %Pa
    end
    if P(x) <= 0
        P(x) = 0;
    end

    F(x)=P(x)*area*10^-6; %N
    w(x+1)=(((D1*F(x)-D3*FR(x)+D2*Fu-Fm(x)*D2))/(I/1000))*dt+w(x); %rad/s
    v(x+1)=w(x+1)*D3;%mm/s
    dpos=v(x+1)*dt;%mm
    pos(x+1)=dpos+pos(x);
    dampos(x+1)=dpos+dampos(x);
    % Displacement dependant mechanical resistance not used
    %if pos(x+1) <= 0.34
    %    Fm(x+1)=0; %N
```

```
    %elseif pos(x+1) > 0.34 && pos(x+1) <= 5
    %    Fm(x+1)=-0.1868*(pos(x+1)^3)-0.3333*(pos(x+1)^2)+11.513*pos(x+1)-
3.8142; %N
    %elseif pos(x+1) > 5
        Fm(x+1)=0;
    %end
    w2(x+1)=((atan(dampos(x+1)/z)-(atan(dampos(x)/z)))/dt);
    rate1(x+1)=(w2(x+1)*rm1)/y1;
    rate2(x+1)=(w2(x+1)*rm2)/y2;
    kik(x+1)=w2(x+1);
    thet(x+1)=w2(x+1)*dt+thet(x);
    %vis(x+1)=(2299.6)/(47.9*1000); %lbf*s/ft^2
    %Approximation of Viscosity vs Shear rate Curve
    if abs(rate1(x+1)) <= 1
        vis1(x+1) = 54.042;
    elseif abs(rate1(x+1)) > 1 && abs(rate1(x+1)) <= 14
        vis1(x+1) = (54.042*abs(rate1(x+1))^(-0.6973)); %Pa-s
    elseif abs(rate1(x+1)) > 14
        vis1(x+1) = 5.89+(abs(rate1(x+1))-14)*(165); %Pa-s
    end

    if abs(rate2(x+1)) <= 1
        vis2(x+1) = 54.042;
    elseif abs(rate2(x+1)) > 1 && abs(rate2(x+1)) <= 14
        vis2(x+1) = (54.042*abs(rate2(x+1))^(-0.6973)); %Pa-s
    elseif abs(rate2(x+1)) > 14
        vis2(x+1) = 5.89+(abs(rate2(x+1))-14)*(165); %Pa-s
    end

    stress1(x+1)=2*vis1(x+1)*rate1(x+1)*((ro^2)/(rm1*(ro+rm1))); %Pa
    stress2(x+1)=2*vis2(x+1)*rate2(x+1)*((ri^2)/(rm2*(rm2+ri))); %Pa
    FR1(x+1)=stress1(x+1)*(2*pi()*rm1*Lo)*(1/1000^2)*(rm1/z);
    FR2(x+1)=stress2(x+1)*(2*pi()*rm2*Li)*(1/1000^2)*(rm2/z);

FR(x+1)=stress1(x+1)*(2*pi()*rm1*Lo)*(1/1000^2)*(rm1/z)+stress2(x+1)*(2*pi()*
rm2*Li)*(1/1000^2)*(rm2/z)+FR(1); %N
    time(x+1)= time(x)+dt; %seconds
    if dampos(x+1) >= cuttoff && dampos(x+1) < (cuttoff+1), tcut = time(x+1);
end


end

if x == iterate
    F(x+1)=0;
end

%Plotting Results
figure(1)
plot(time,F,time,FR,time,FR1,time,FR2,time,Fm);
xlim([0 tcut])
xlabel('time (second)')
ylabel('Force (N)')
title ('Reaction Force During Opening (70F)')
figure(2)
```

```
plot(time,pos);
xlim([0 tcut])
xlabel('time (second)')
ylabel('displacement (mm)')
title ('Door Position (70F)')
figure(3)
plot(time,rate1,time,rate2);
xlim([0 tcut])
xlabel('time (second)')
ylabel('Shear Rate (1/s)')
title ('Shear Rate of Fluid (70F)')
figure(4)
plot(time,v);
xlim([0 tcut])
xlabel('time (second)')
ylabel('velocity (mm/s)')
title ('Opening Speed of Door (70F)')
figure(5)
plot(time,vis1,time,vis2); %Pa-s
xlim([0 tcut])
xlabel('time (second)')
ylabel('Viscosity (Pa-s)')
title ('Viscosity of Fluid (70F)')
figure (6)
plot(time,stress1,time,stress2);
xlim([0 tcut])
xlabel('time (second)')
ylabel('Shear Stress (Pa)')
title ('Shear Stress of Fluid (70F)')
figure(7)
plot(time,kik);
xlim([0 tcut])
```

Dynamic Opening Model Results

A version of the above program was used to simulate the latch geometry described in Figure 2-20. This program used the approximate viscosity curve displayed in Figure A-1 in order to prove the project's feasibility.

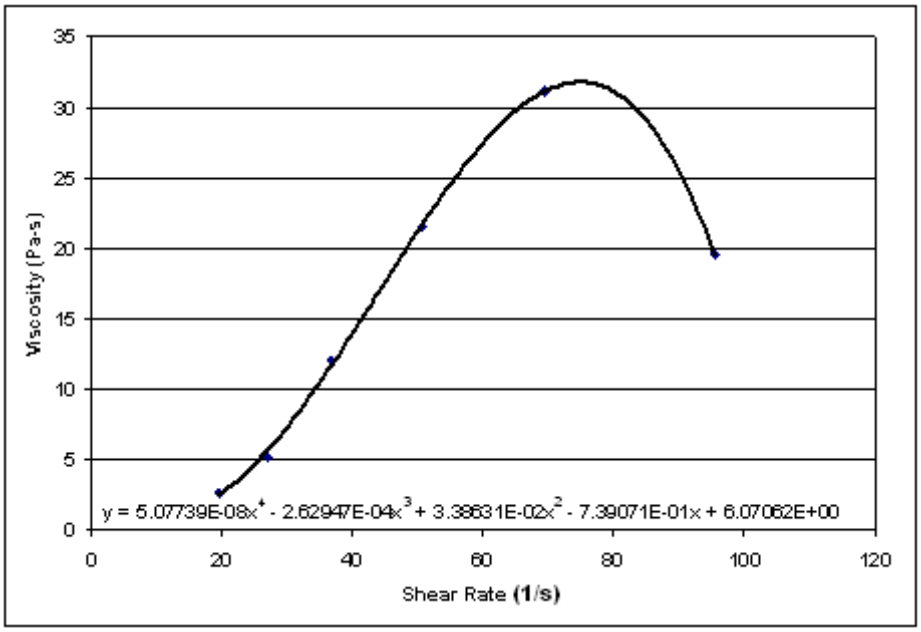

Figure A-1: Viscosity Curve 48.6% PCC in PEG

Figures A-2 through A-7 show some selected inputs and corresponding results from the program. Figures A-2, A-4, and A-6 are the force loadings that were input to the program to test how the theoretical damper would perform under different conditions. Figures A-3, A-5, and A-7 are the corresponding outputs from the program showing the displacement of the door in respect to time as a result of the force applied.

Worst Case Pressure Pulse: 5.2 in. of H20 for 0.5 seconds

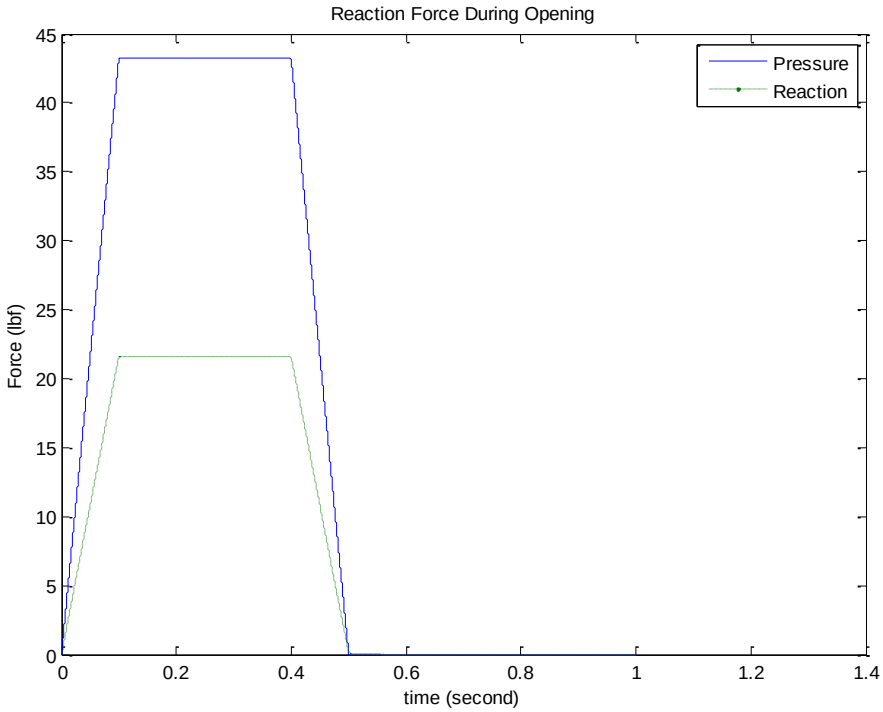

Figure A-2: Force Applied at Center of Pressure

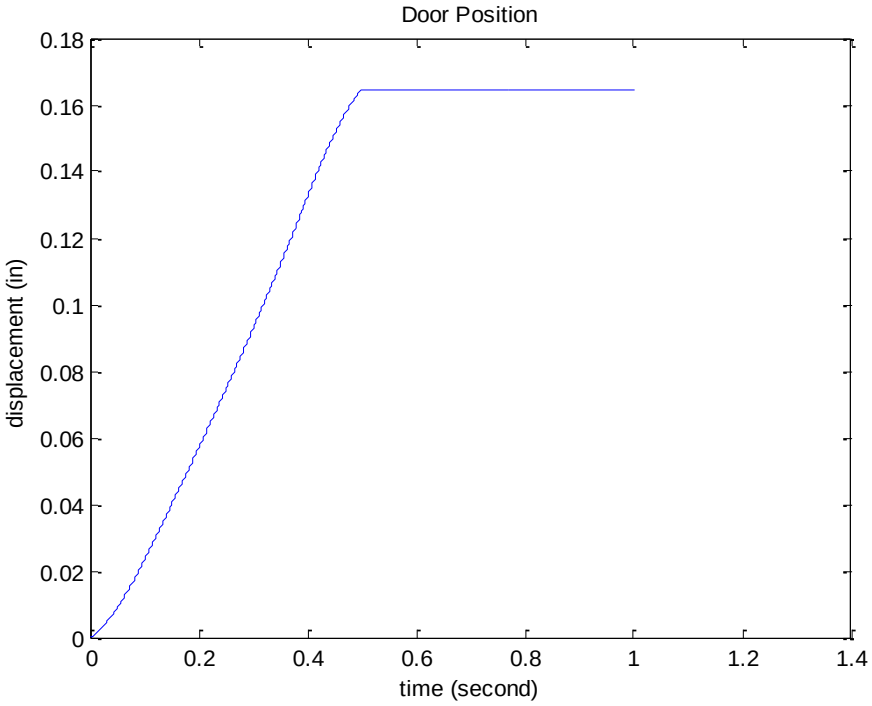

Figure A-3: Simulated Door Displacement

Maximum Opening Force: 15 lbf on handle

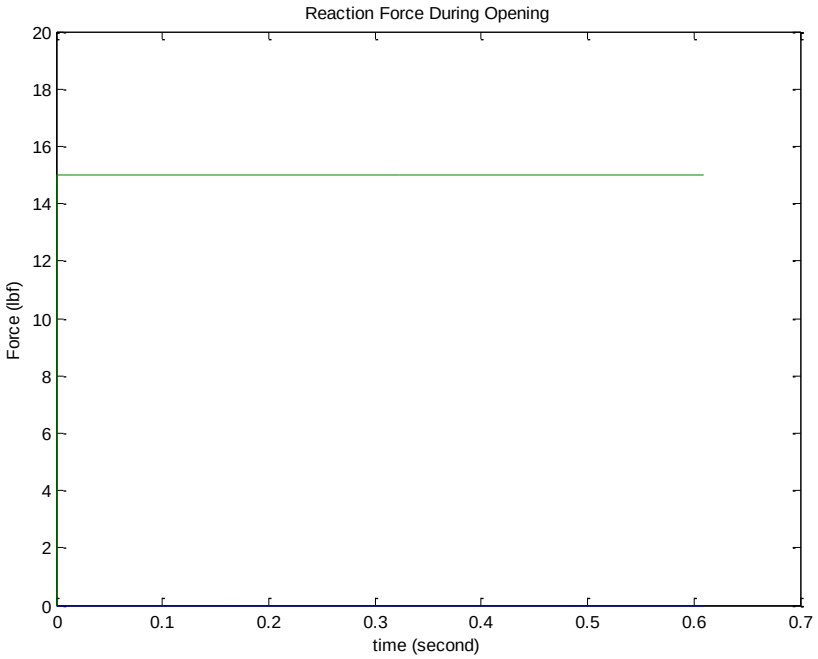

Figure A-4: Force Applied at Handle

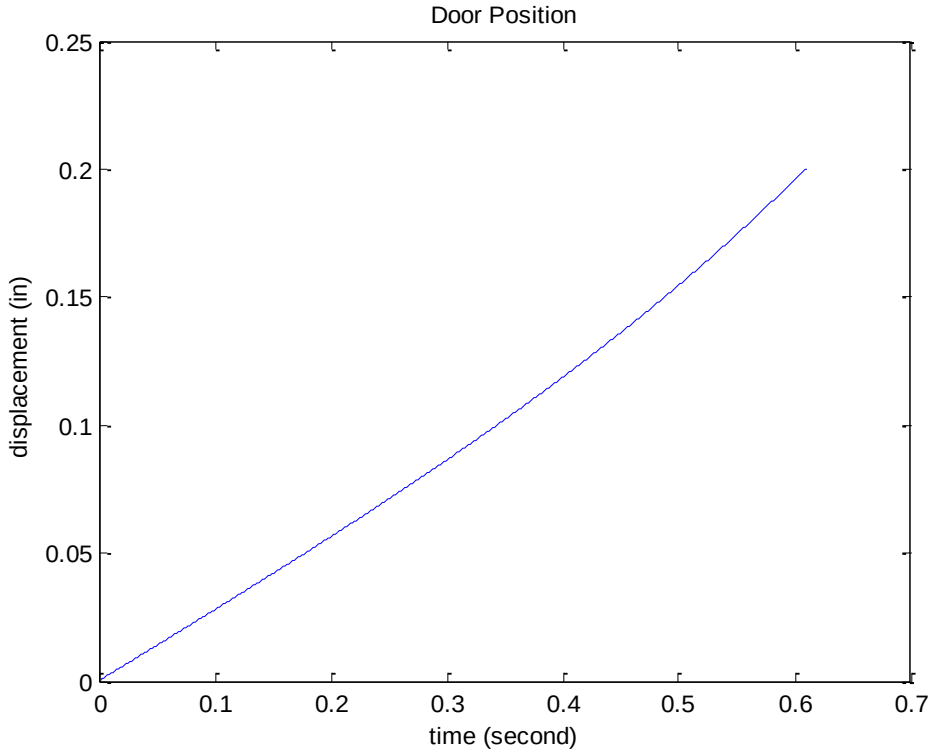

Figure A-5: Simulated Door Displacement

Minimum Opening Force: 6 lbf on handle

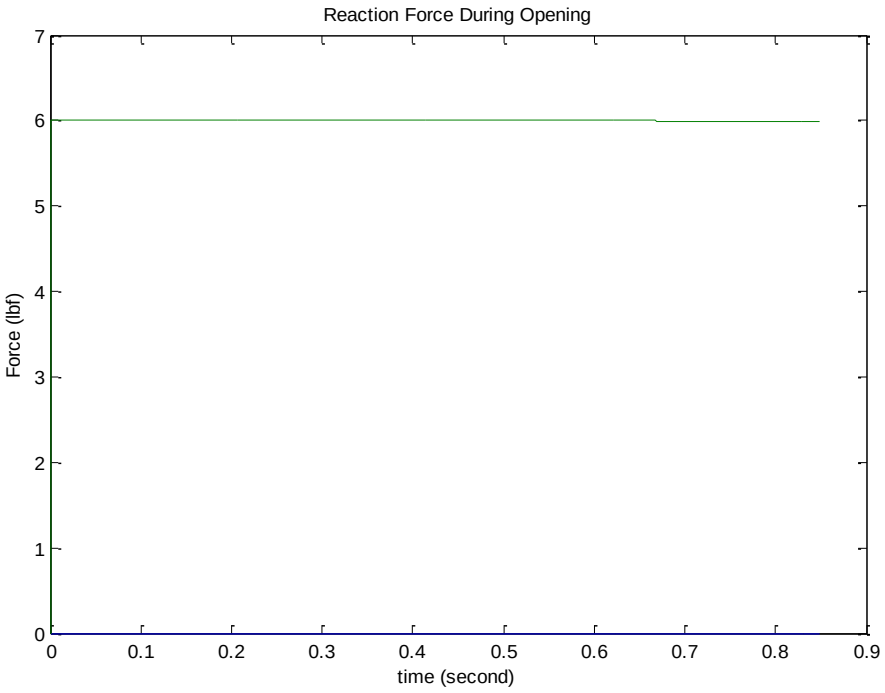

Figure A-6: Force Applied at Handle

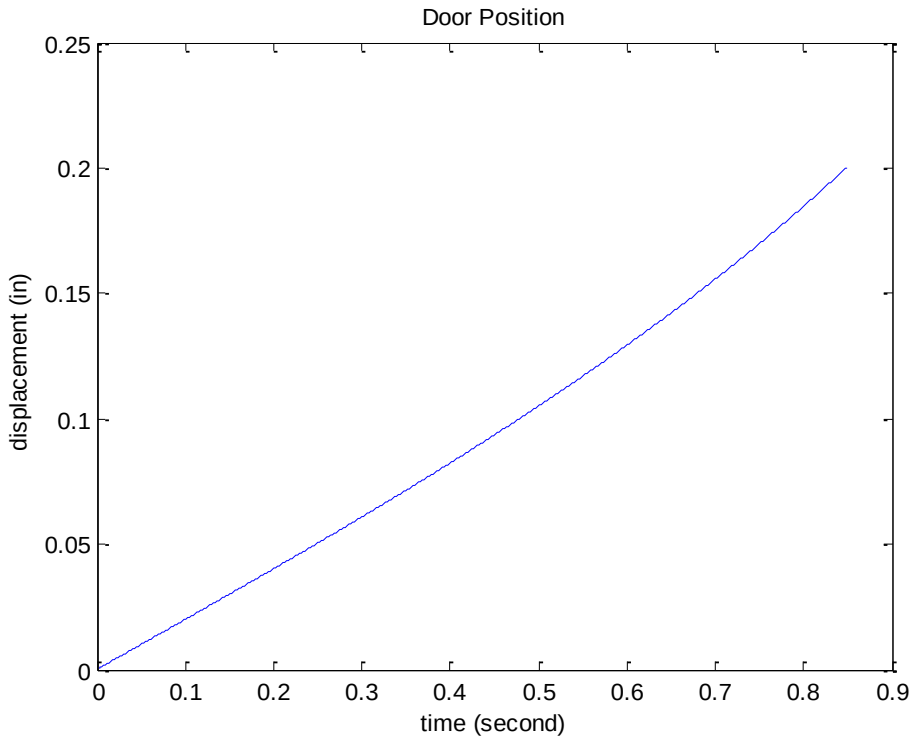

Figure A-7: Simulated Door Displacement

A.2 Temperature Pulse Analysis

In order to simulate the temperature change that the hinge could possibly see, the following conditions were used. It is assumed that the latch is shielded from the interior of the dryer by 1/4 inch of glass fiber blanket insulation with a thermal resistance per unit area of 0.18 m^2K/W, and a $1/32^{nd}$ inch layer of steel simulating the door's construction. Ti is treated as the steady state operating temperature of the dryer at (150 F), and Ta is treated as the maximum air temperature inside the dryer during a temperature pulse, (1000 F).

Step 1: Steel Plate

The plate is modeled as a lumped capacitance, and the "outside" is considered to be adiabatic as a worst case. The transient temperature change for a constant Ta was found from this analysis. The plate was taken to have the same thickness as the walls of the current door, which also helped delay the temperature increase.

Figure A-8 represents the boundary conditions and temperature response of the steel plate from the described conditions.

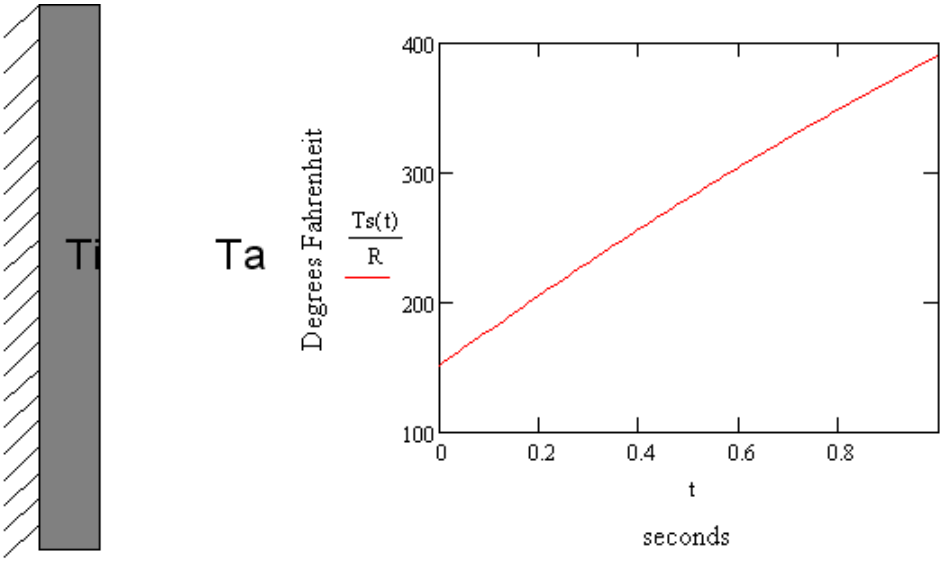

Figure A-8: Steel Plate

In order to account for the transient internal dryer temperature, Du Hamel's theory (Özışık, 1993) is used:

F1(t) represents the dimensionless internal ambient temperature change as a function of time.

$$F1(t) = \frac{T(t) - Ti}{Ta - Ti} \tag{A-1}$$

Figure A-9 shows the simplified dimensionless impulse input that was used to evaluate the model.

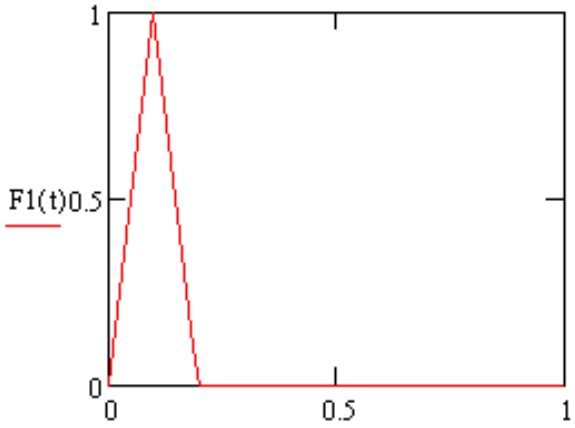

Figure A-9: Internal Temperature Change

θ(t) is the dimensionless response of the lumped capacitance analysis given by.

$$\theta(t) = \frac{Ts(t) - Ti}{Ta - Ti} \tag{A-2}$$

In the next step Du Hamel's theorem is applied, yielding

$$\theta p(t) = \int_{0s}^{1s} \frac{d\theta}{dt} \cdot F1(\tau) \cdot d\tau \tag{A-3}$$

Therefore, the temperature response of the plate to the transient internal temperature is give by.

$$Temp(t) = \theta p(t) \cdot (Ta - Ti) + Ti \tag{A-4}$$

Figure A-10 shows the predicted temperature rise.

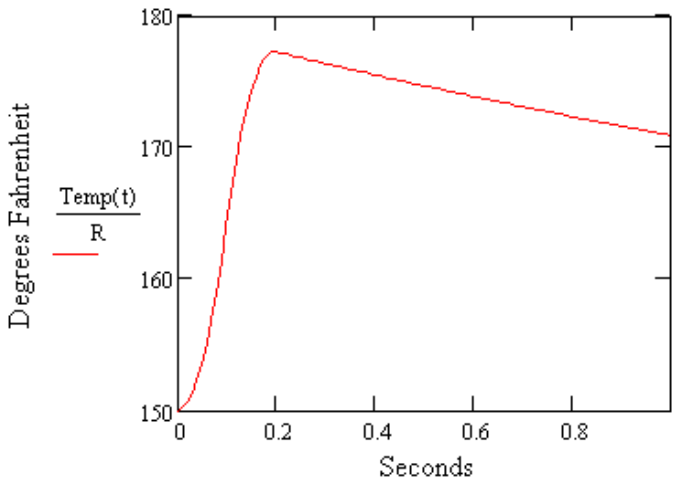

Figure A-10: Temperature Response of Plate

Step 2: Insulation

Step 2 focuses on evaluating the Insulation used to shield the damper using the same boundary conditions as those applied to the steel plate in step 1. However, the insulation is not treated as a lumped capacitance. Instead, the temperature distribution throughout the thickness of the insulation layer is found. Figure A-11 displays the boundary conditions applied to the system as well as the temperature response with respect to time of the adiabatic side of the insulation layer. The scenario assumes the ambient temperature (Ta) is held at a constant 150 F.

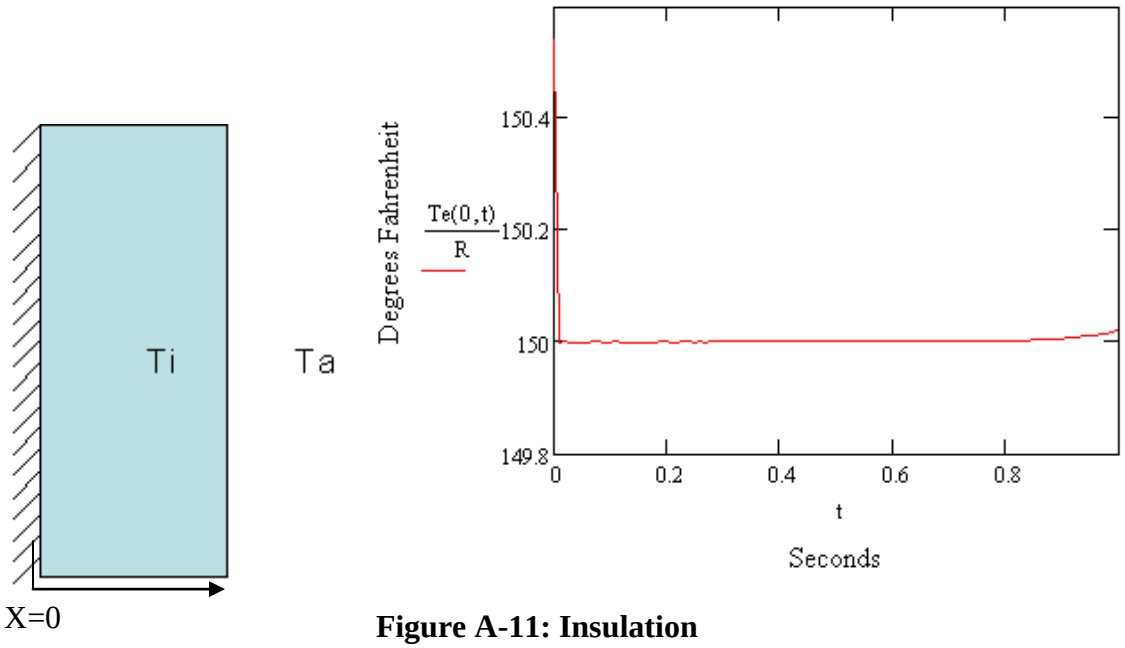

Figure A-11: Insulation

Assuming a worst case scenario of the insulation and the plate being perfectly bonded, Du Hamel's theorem was utilized, this time with the transient temperature response of the plate $\theta p(t)$ as the temperature input, yielding.

$$\theta e(t) = \frac{Te(t) - Ti}{Ta - Ti} \tag{A-5}$$

and

$$\theta f(t) = \int_{0s}^{1s} \frac{d\theta e}{dt} \cdot \theta p(\tau) \cdot d\tau \tag{A-6}$$

Where the resulting temperature response at x=0 is given by.

$$Temperature(0,t) = \theta f(t) \cdot (Ta - Ti) + Ti \tag{A-7}$$

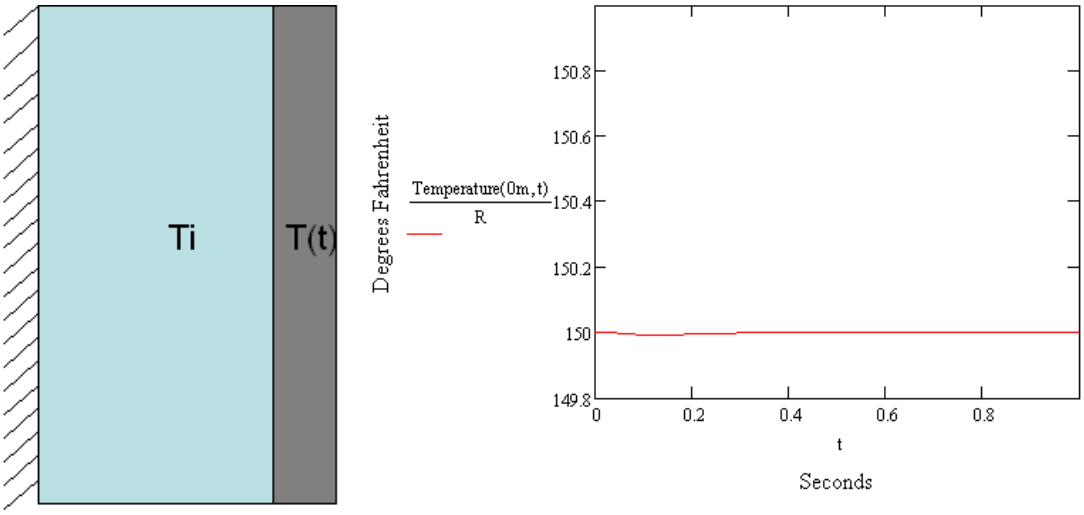

Figure A-12: Complete Scenario

Figure A-12 shows the resulting worst case temperature response. These results show that it is very feasible to shield the latch from a temperature pulse for at least long enough for it to withstand the associated impulse pressure force.

Mathcad Worksheet

The Mathcad program used to evaluate the above simplified model for the door temperature response is given below in Figures A-13 through A-17.

Estimate of Warmup Transient for Insulated Viscous Hinge:

Input of Insulation Parameters and Physical Properties:

$ORIGIN := 1$ $W := 1 \cdot watt$ $TOL := 0.0001$ $CTOL := 0.0001$

$T_i := 150 \cdot R$ $T_a := 1000 \cdot R$ $h := 100 \cdot \frac{W}{m^2 \cdot K}$ $k := 0.035 \cdot \frac{W}{m \cdot K}$ $L := 6.35 \cdot mm$

$tmax := 5s$ $tp := 0.5s$ $x := 0mm, 0.1mm .. L$

$t := 0s, 0.01s .. tmax$ $tp2 := 2 \cdot tp$

Rough properties of blanket insulation:

$\rho := 40 \cdot \frac{kg}{m^3}$ $C_p := 835 \cdot \frac{joule}{kg \cdot K}$ $\alpha := \frac{k}{\rho \cdot C_p}$ $\alpha = 1.048 \times 10^{-6} \frac{m^2}{s}$

$Bi := \frac{h \cdot L}{k}$ $Bi = 18.14286$ $f(n, Z) := root[Z \cdot tan[Z + (n - 1) \cdot \pi] - Bi, Z]$

$n := 1 .. 550$

$\lambda L_1 := \frac{\pi}{2}$

$\lambda L_{n+1} := (2 \cdot n + 1) \cdot \left(\frac{\pi}{2}\right)$ $\lambda_n := \frac{\lambda L_n}{L}$

$\lambda L =$

	1
1	1.571
2	4.712
3	7.854
4	10.996
5	14.137
6	17.279
7	20.42
8	23.562
9	26.704
10	29.845
11	32.987
12	36.128
13	39.27
14	42.412
15	45.553
16	48.695

Figure A-13: Mathcad Worksheet Page 1

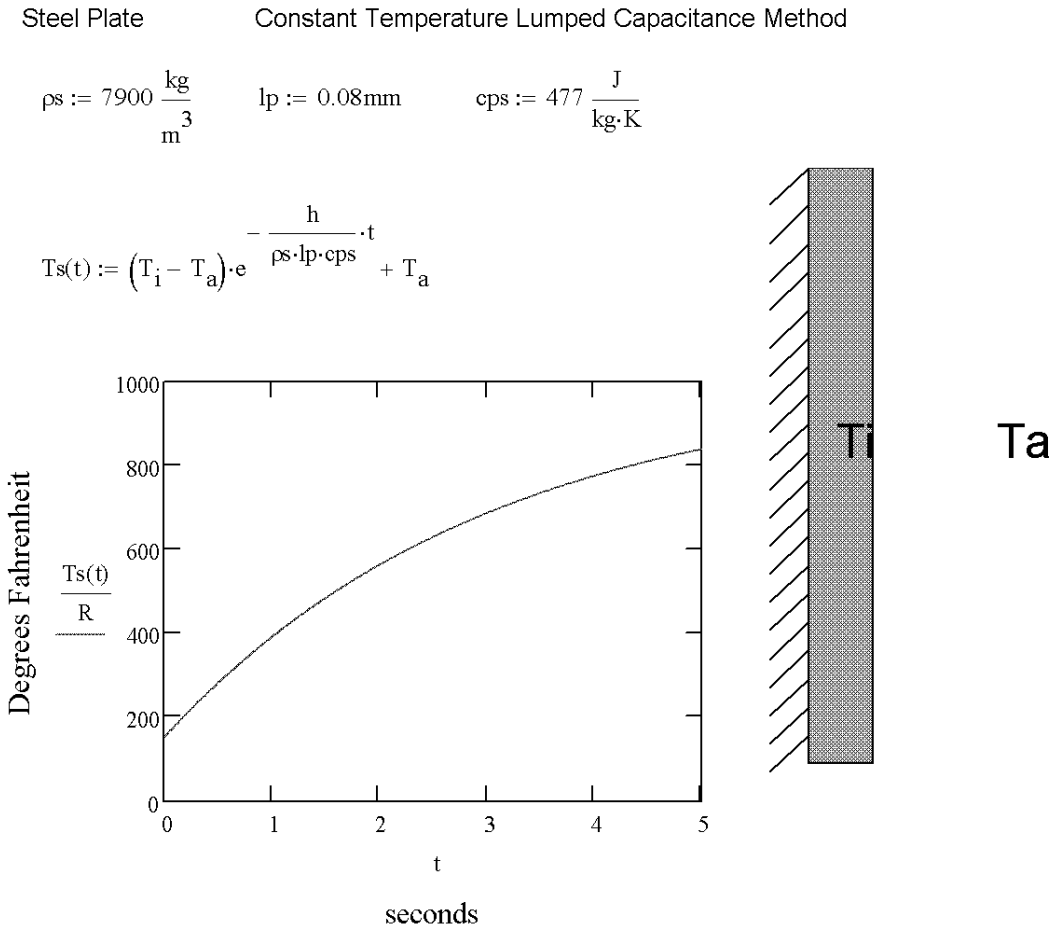

Figure A-14: Mathcad Worksheet Page 2

Transient Temperature: Du Hamel's Theorem

$$F1(t) := \begin{cases} \frac{t}{tp} & \text{if } t \le tp \\ 1 - \frac{t - tp}{tp} & \text{if } tp < t \le (tp2) \\ 0 & \text{otherwise} \end{cases} \qquad F2(t) := \begin{cases} 1 & \text{if } t \le (tp2) \\ 0 & \text{otherwise} \end{cases}$$

$$d\theta 1dt(t,\tau) := (T_i - T_a)\cdot\left(-\frac{h}{\rho s\cdot lp\cdot cps}\right)\cdot e^{\left(-\frac{h}{\rho s\cdot lp\cdot cps}\cdot t\right)+\left(\frac{h}{\rho s\cdot lp\cdot cps}\cdot\tau\right)}$$

$$dS1dt(t,\tau) := \frac{d\theta 1dt(t,\tau)}{T_a - T_i}$$

$$\theta p(t) := \int_{0s}^{t} dS1dt(t,\tau)\cdot F1(\tau)\,d\tau$$

$$\theta p2(t) := \int_{0s}^{t} dS1dt(t,\tau)\cdot F2(\tau)\,d\tau$$

$$Temp(t) := \theta p(t)\cdot(T_a - T_i) + T_i$$

$$Temp2(t) := \theta p2(t)\cdot(T_a - T_i) + T_i$$

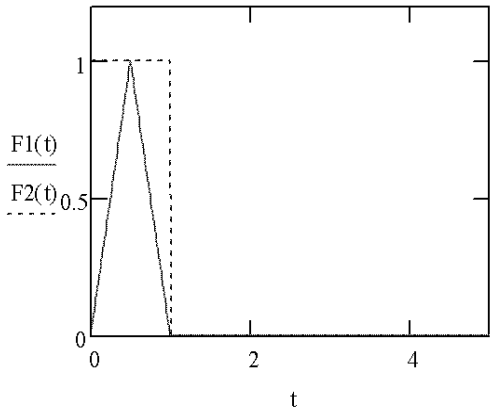

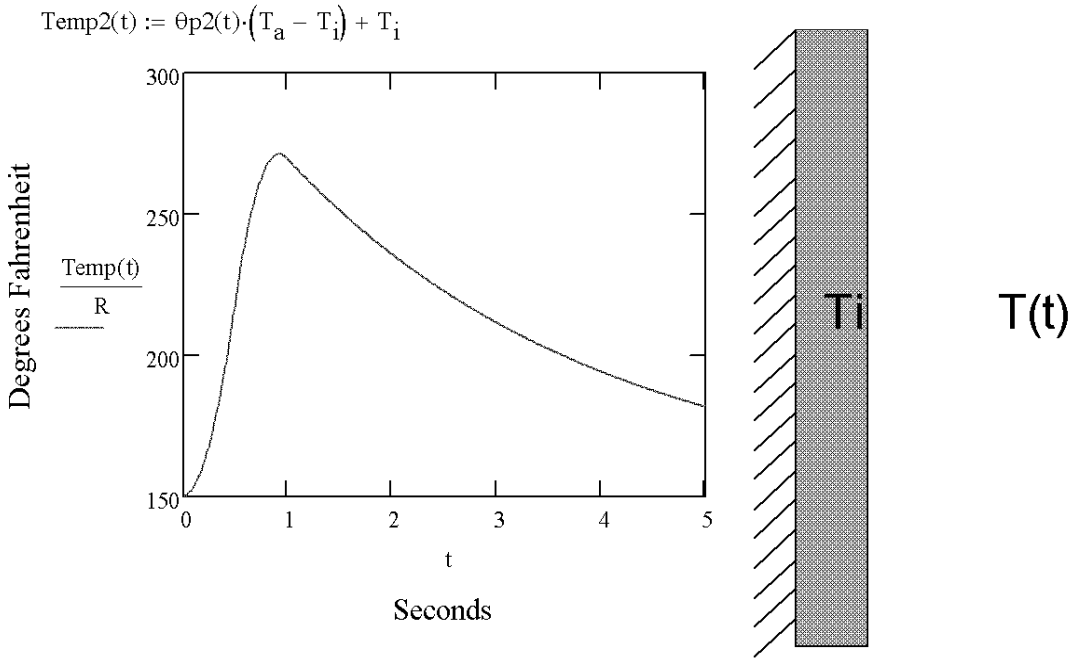

Figure A-15: Mathcad Worksheet Page 3

Insulation: Constant Temperature

$$\theta(x,t) := 2\cdot \sum_{n=1}^{500} \left[\left[\frac{(-1)^{n-1}}{\lambda L_n} \right] \cdot \left[e^{-\alpha\cdot(\lambda_n)^2\cdot t} \right] \cdot \left(\cos\left(\lambda_n \cdot x\right) \right) \right]$$

$$S(x,t) := 1 - \theta(x,t$$

$$Te(x,t) := -S(x,t)\cdot\left(T_i - T_a\right) + T_i$$

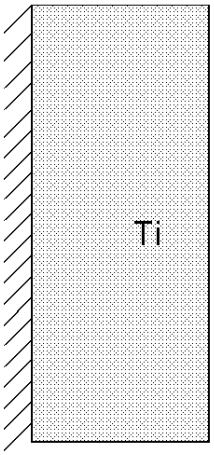

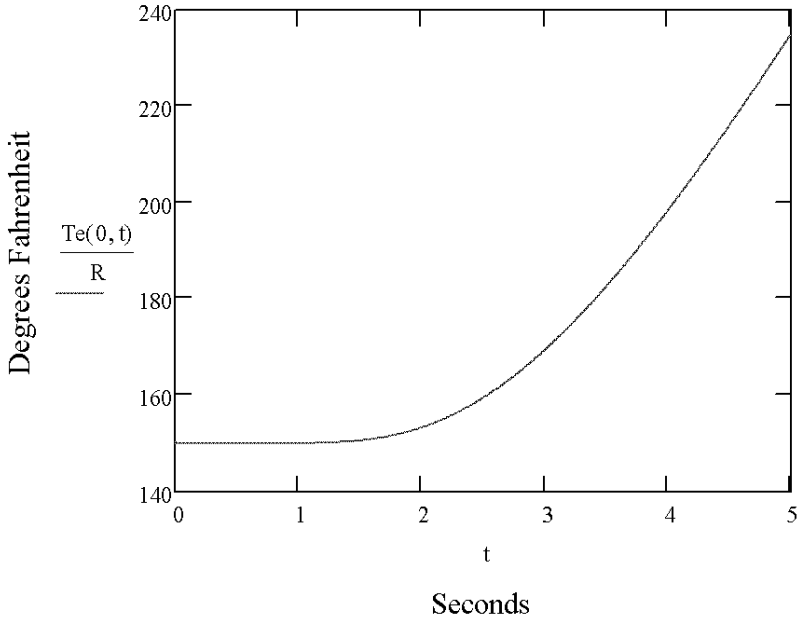

Figure A-16: Mathcad Worksheet Page 4

Insulation: Transient steel temperature, Du Hamel's theorem

$$dsds(x,t,\tau) := -\sum_{n=1}^{250}\left[\left[\frac{(-1)^{n-1}}{\lambda L_n}\right]\cdot\left[-\alpha\cdot(\lambda_n)^2\right]\cdot\left[e^{-\alpha\cdot(\lambda_n)^2\cdot t+\alpha\cdot(\lambda_n)^2\cdot\tau}\right]\cdot\left(\cos(\lambda_n\cdot x)\right)\right]$$

$$ge(x,t) := \left[\int_{0s}^{t}\left(\theta p(\tau)\right)\cdot\left(dsds(x,t,\tau)\right)d\tau\right]$$

$$ge2(x,t) := \left[\int_{0s}^{t}\left(\theta p2(\tau)\right)\cdot\left(dsds(x,t,\tau)\right)d\tau\right]$$

$$Temperature(x,t) := -\left[ge(x,t)\cdot\left(T_i - T_a\right) - T_i\right]$$

$$Temperature2(x,t) := -\left[ge2(x,t)\cdot\left(T_i - T_a\right) - T_i\right]$$

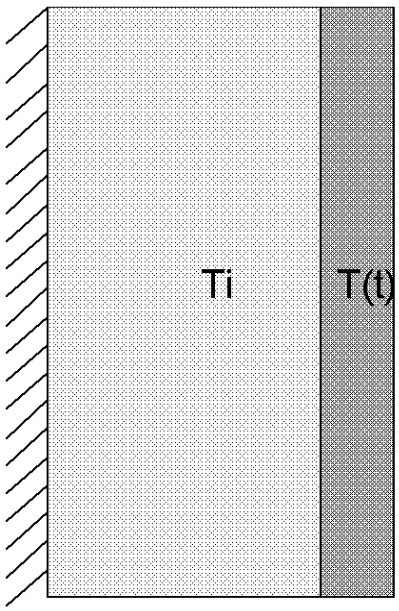

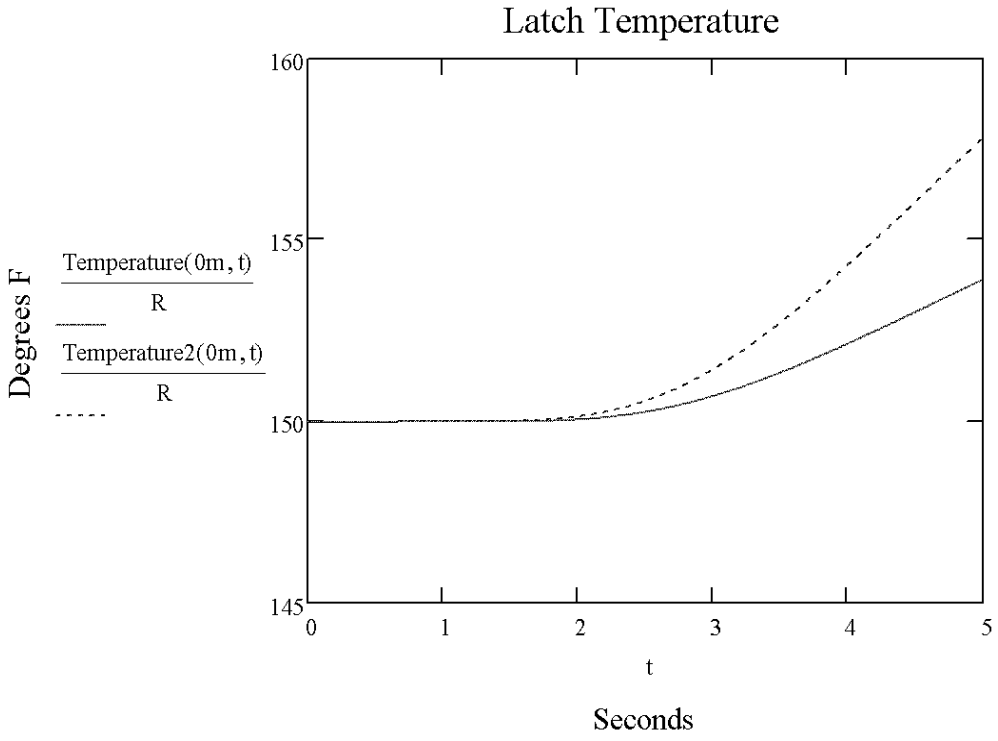

Figure A-17: Mathcad Worksheet Page 5

Appendix B - Viscosity Testing

B.1 Testing Equipment

The initial fluid testing for the project was performed by the Kansas State University Bio-Materials & Technology Lab. Two different pieces of testing equipment were used during this phase. The first is shown below in Figure B-1, which is the equipment used at the KSU Bio-Materials & Technologies Lab.

Brookfield Engineering DV-III Rheometer with SC4-28 Spindle

Figure B-1: Brookfield Engineering DV-III Rheometer

This rheometer measured fluid properties by rotating a spindle freely suspended in sample of fluid. Temperature was controlled by the water jacket surrounding the test sample. Figure B-2 (A) shows the spindle use for testing, Figure B-2 (B) is the water jacket used to control the temperature of the sample.

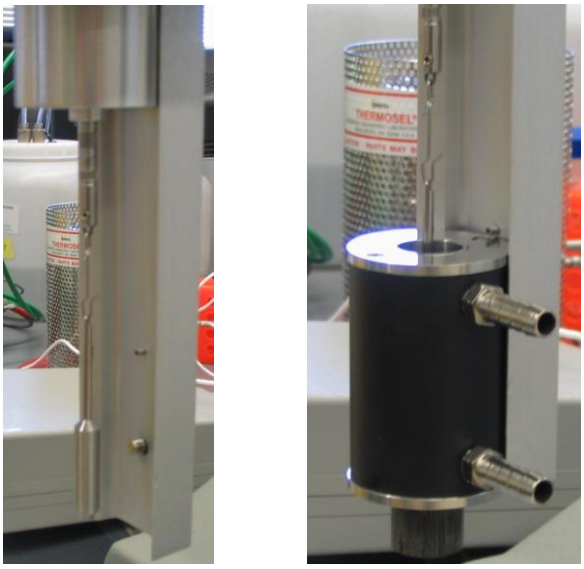

(A) SC4-28 Spindle (B) Temperature Control

Figure B-2: DV-III Rheometer Accessories

This type of rheometer has the advantage of applying constant shear rate to the entire sample. Unfortunately, the maximum torque it is capable of applying to the sample is limited.

Malvern Instruments: C-VOR Digital Rheometer

In order to test thicker fluids at shear rates above the Brookfield's test range, the Malvern C-VOR rheometer was utilized. A close-up photograph of this rheometer is shown in Figure B-3.

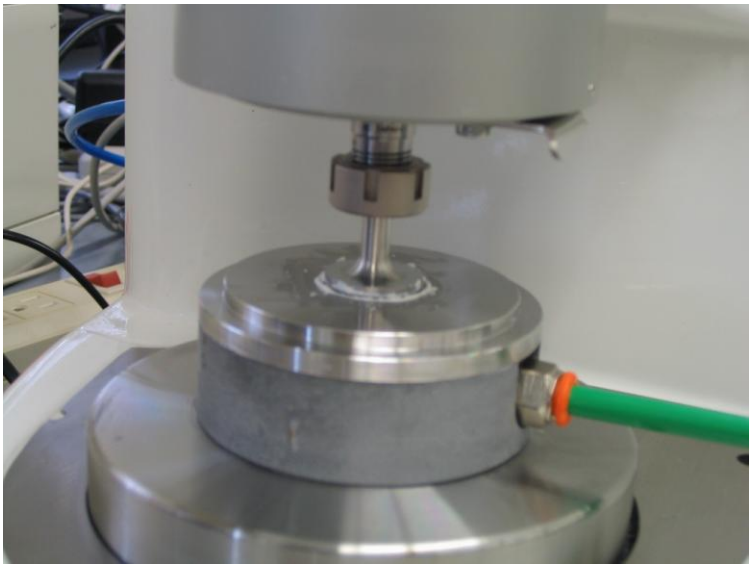

Figure B-3: Rheometer Test Section

The C-VOR rheometer uses a paddle and plate type configuration as shown in Figure B-3. A 150 micrometer thick layer of fluid is sandwiched between two plates. The upper plate is a 10 mm radius disk which rotates to provide the torque. This instrument had the advantage of being able to test at higher shear rates; however, the shear rate changes along the radius of the plate leading to more uncertainty in the testing. This is because the gap thickness is constant along the radius.

Brookfield R/S-CPS Rheometer

After initial testing had been performed it was discovered that a rheometer was available for use within the department. Since this option was more economical and convenient, viscosity tests were performed using this machine for the remainder of the project.

Figure B-4: Brookfield R/S-CPS Rheometer

The R/S rheometer uses a cone and plate type configuration, meaning that the upper plate is a truncated cone allowing for a constant shear rate of the sample over the entire surface of the rheometer. A simplified schematic of the cone and plate configuration is shown in Figure B-5.

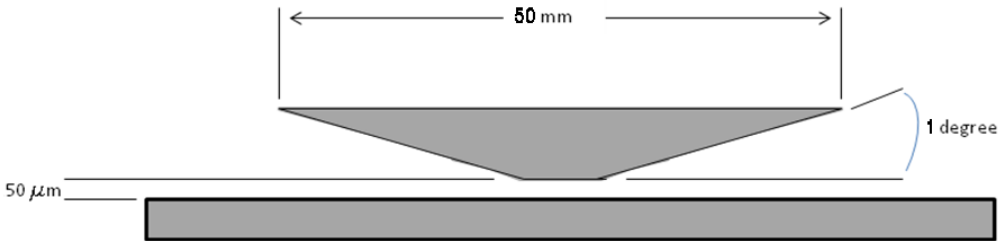

Figure B-5: Cone and Plate Configuration

Temperature was regulated during testing with a Peltier Thermo Regulator, as shown in Figure B-6. Both a 25 mm and a 50 mm cone were used over the course of the testing, as shown in Figure B-7. The technical specifications are given in Figures B-8 through B-12.

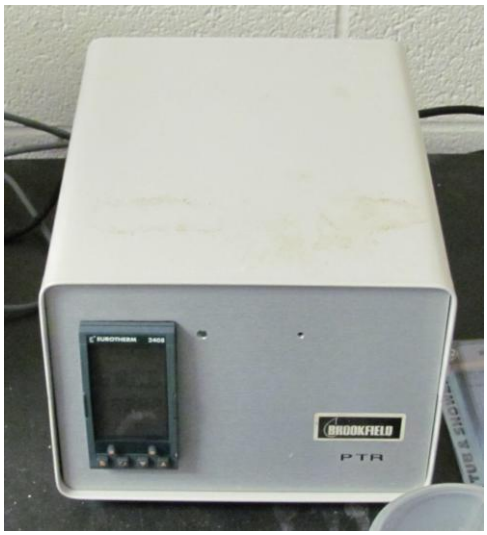

Figure B-6: Peltier Thermal Regulator PTR-1

Figure B-7: C25-1 and C50-1 spindles

VIII. Technical data

R/S-CPS Rheometer	
Dimensions	480 mm x 300 mm x 290 mm
Weight	12 kg
Nominal operating voltage **Power consumption (average)** **Power consumption (maximum)**	+/- 15 V, 5 V 12 W 22 W
Ambience conditions **Temperature** in operation out of operation **Relative humidity (not condensable)** in operation out of operation	 10° to 40°C 10° to 45°C 20% to 80% 10% to 90%
Accuracy	± 1.0 % of maximum range value ± 1 digit
Torque range	0.05 to 50 mNm
Torque resolution	0.01 mNm
Speed range	0.7 to 800 min^{-1}
Angle resolution	0.8 mrad
Temperature range	Depending on the thermostatting device used -20° to +250°C
Range of shear rate	Depending on the measuring system used 0 to 4,800 s^{-1}
Range of shear stress	Depending on the measuring system used 0 to 16,000 Pa
Viscosity range The given range is a standard value (not maximum value)	Depending on the measuring system used 0.009 to 10,000 Pas

AC-Adaptor	
Dimensions	160 mm x 85 mm x 35 mm
Weight	0.5 kg
Power supply **operating voltage** **output voltage** **output current** **output power**	 **100 to 240 V AC** **5V, +/- 15 V DC** **2 A, 0.9 / -0.2 A** **20 W**
Frequency	**50 to 60 Hz**
Ambience conditions **Temperature** **in operation** **out of operation** **Relative humidity (not condensable)** **in operation** **out of operation**	 **+10° to +40°C** **+10° to +45°C** **20% to 80%** **10% to 90%**

Figure B-8: Brookfield R/S-CPS Rheometer technical data from operating instructions

5. Technical data

Power supply	:	230 V AC / 50 Hz, +10/-15 %
Output	:	ca. 85 VA
Dimensions (width x depth x height)	:	205 x 260 x 165 mm
Protective system	:	IP 40
Protection class	:	I
Weight	:	6 kg
Permissible ambience temperature	:	+10°C ... +35°C
Storing temperature	:	-10°C ... +65°C
Range of adjustable temperatures	:	0 ... +135°C
Temperature display	:	4-digit LED 7-segment
Temperature resolution	:	0.1 K
Temperature stability	:	± 0.1 K
Working temperature sensor	:	Pt100 DIN IEC 751 class A, three-wire system
Heat exchanger sensor	:	NTC 100 kOhm

Figure B-9: Peltier Thermo Regulator PTR-1 technical data from operation manual

BROOKFIELD

Meauring System Data

Cone/Plate Systems according to DIN 53018

Shear Rate = Ky.n
Shear Stress = t% .M

Ky = Shear Rate factor (-sec/rpm) = K_gamma
n = rotational speed (RPM)
t% = Shear Stress factor (Pa/%) = Tau_Prom
M = torque (%)

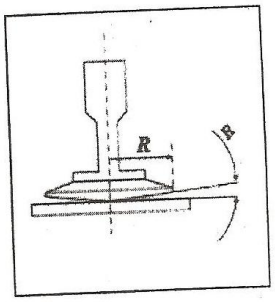

Cone Number:		467				
Measuring System	C25-1	C25-2	C50-1	C50-2	C75-1	C75-2
Shear Rate Factor (K_gamma)			5.8861			
Shear Stress Factor (Tau_Prom)	12.223	12.223	1.528	1.528	0.4527	0.453
Sample Volume (mL)	0.08	0.15	0.6	1.2	2	3.9
Radius R (mm)	12.5	12.5	25	25	37.5	37.5
Cone Angle a (.)			1.0194			
Cone Truncation (mm)			0.05			
Date:		02/06/2002				

Figure B-10: 50 mm cone specifications from measuring system data

BROOKFIELD

Measuring System Data

Cone/Plate Systems according to DIN 53018

Shear Rate = $K\gamma.n$

Shear Stress = τ_{prom} .M

$K\gamma$ (K_gamma) = Shear Rate factor (s^{-1}/rpm)
n = rotational speed (RPM)
τ_{prom} (Tau_Prom) = Shear Stress factor (Pa/%)
M = torque (%)

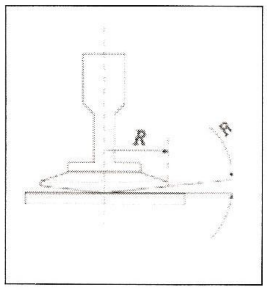

Cone Number:	1273					
Measuring System	**C25-1**	C25-2	C50-1	C50-2	C75-1	C75-2
Shear Rate Factor (K_gamma)	**6.2315**					
Shear Stress Factor (Tau_Prom)	**12.223**	12.223	1.528	1.528	0.4527	0.4527
Sample Volume (mL)	**0.08**	0.15	0.6	1.2	2	3.9
Radius R (mm)	**12.5**	12.5	25	25	37.5	37.5
Cone Angle a (.)	**0.9629**					
Cone Truncation (mm)	**0.045**					

Figure B-11: 25 mm cone specifications from measuring system data

Appendix C - Dryer Door Test Setup

This section gives the specifications for all the instrumentation used in conducting the experimental tests associated with this thesis. The test setup is explained in detail in Section 3.2 of the text.

C.1 Component Specifications

Load Cell

SPECIFICATIONS

Excitation: 10 Vdc, 15 Vdc max
Output: 3 mV/V ±0.0075 mV/V
Linearity: ±0.03% FSO (0.1% 40 K)
Hysteresis: ±0.02% FSO (0.1% 40 K)
Repeatability: ±0.01% FSO (0.05% 40 K)
Zero Balance: ±1% FSO
Agency Approval: FM Intrinsically Safe IS/I.II.III/1/CDEFG (standard)
Operating Temp Range: -40 to 93°C (-40 to 200°F)
Compensated Temp Range: 17 to 71°C (60 to 160°F)
Thermal Effects:
Zero: 0.002% FSO/°C
Span: 0.002% FSO/°C
Safe Overload: 150% of capacity
Ultimate Overload: 300% of capacity
Input Resistance: 350 ±10 Ω
Output Resistance: 350 ±10 Ω
Full Scale Deflection: 0.010 to 0.020"
Construction: 17-4 PH stainless steel

Electrical (LC101/LCM101) (4-Conductor Shielded Cable):
≤100 kgf/250 lb: 9 m (30') 24 AWG
250 to 1000 kgf/250 to 2000 lb: 9 m (30') 20 AWG
≥1500 kgf/3000 lb: 4.5 m (15') 20 AWG

Mating Connector (LC111/LCM111):
≤100 kgf/200 lb: PT06F8-4S, sold separately
≥250 kgf/250 lb: PT06F10-6S, sold separately

Dimensions: mm (in)

CAPACITY	A	B	C	D	E	WEIGHT kg (lb)
lb						
25 to 200	¼-28	19 (0.75)	13 (0.50)	38 (1.5)	64 (2.5)	0.45 (1.0)
250 to 2.5K	½-20	32 (1.25)	25 (1.0)	51 (2.0)	76 (3.0)	1.1 (2.5)
3K to 5K	⅝-18	32 (1.25)	25 (1.0)	51 (2.5)	89 (3.5)	1.6 (3.5)
10K to 20K	1-14	44 (1.75)	38 (1.5)	76 (3.0)	108 (4.3)	2.0 (4.5)
25K to 30K	1-14	57 (2.25)	51 (2.0)	102 (4.0)	108 (4.3)	4 (9)
40K	1¼-12	83 (3.25)	76 (3.0)	102 (4.0)	140 (5.5)	6 (13)
kgf						
10 to 100	M6 x 1.00	19 (0.75)	13 (0.50)	38 (1.5)	64 (2.5)	0.45 (1.0)
250 to 1000	M12 x 1.75	32 (1.25)	25 (1.0)	51 (2.0)	76 (3.0)	1.1 (2.5)
1500 to 2000	M16 x 2.0	32 (1.25)	25 (1.0)	51 (2.5)	89 (3.5)	1.6 (3.5)
5K to 10K	M24 x 2.00	44 (1.75)	38 (1.5)	76 (3.0)	108 (4.3)	2.0 (4.5)

Figure C-1 Omega LC111-100 load cell specifications from information sheet

LVDT

the range. This makes installation easier and helps prevent misalignment.

SPECIFICATIONS

Linearity: <0.2% FSO
Excitation Voltage: 10 to 30 Vdc @ 100 mA
Output: LD620, ±5 Vdc; LD621, 0 to 10 Vdc
Output Ripple: 0.02% FSO
Bandwidth: 500 Hz (-3 dB)
Storage Temp: -20 to 85°C (-4 to 185°F)
Operating Temp: 0 to 65°C (32 to 149°F)
Sealing: IP67
Vibration (Sinusoidal Frequency):
10 to 50 Hz: 1 to 10 g rms linear amplitude
50 Hz to 1 kHz: 10 g rms amplitude
Shock:
Drop Testing: 1 m (3') onto hard surface
Topple Testing: 10 times each end onto hard surface
Case Material: 300 SS
Cable: PFA, 2 m (6') long
Core Material: Nickel-iron

MODEL NO. ±5 Vdc	RANGE mm (in)
LD620-2.5	±2.5 (±0.1)
LD620-5	±5 (±0.2)
LD620-7.5	±7.5 (±0.3)
LD620-10	±10 (±0.4)
LD620-15	±15 (±0.6)
LD620-25	±25 (±1.0)
LD620-50	±50 (±2.0)
LD620-75	±75 (±3.0)
LD620-100	±100 (±3.9)
LD620-150	±150 (±5.9)

Ordering Example: LD62(
with ±5 Vdc output, ***$400.***

ACCESSORIES

MODEL NO.	PF
LD-TIP	
LD-UJOINT-KIT	

J-15

Figure C-2: Omega LD620-25 LVDT specifications from information sheet

Voice Coil Linear Actuator

SPECIFICATIONS	
Motor P/N	NCM05-28-180-2LB
Stroke	0.50"
Bearing Type	Linear Bushing
Moving Mass	1.0 LBS
Total Mass	5.5 LBS
Resistance	9.75 ohms
Force Constant	2.95 LBS/(Watt)^1/2
Continuous Force	18.0 LBS
Peak Force	54.0 LBS
Power In @ 100% Duty	40 WATTS

Figure C-3: H2W NCM05-28-180-2LB voice coil specification from H2W Technologies

Servo Amplifier

	MODELS	
POWER STAGE SPECIFICATIONS	**30A20AC**	**16A20AC**
SINGLE PHASE AC SUPPLY VOLTAGE *	30 – 125 VAC @ 50 - 60 Hz	
PEAK CURRENT (2 sec. Max., internally limited)	± 30 A	± 16 A
MAXIMUM CONTINUOUS CURRENT (internally limited)	± 15 A	± 8 A
MINIMUM LOAD INDUCTANCE**	250 µH	250 µH
SWITCHING FREQUENCY	22 kHz ± 15%	
HEATSINK (BASE) TEMPERATURE RANGE	0° to +65° C, disables if > 65° C	
POWER DISSIPATION AT CONTINUOUS CURRENT	150 W	80 W
OVER-VOLTAGE SHUT-DOWN (self-reset)	195 VDC	
BANDWIDTH (load dependent)	2.5 kHz	
SHUNT RESISTOR (30A20AC)	10 Ω @ 50 W	N/A
SHUNT REGULATOR TRIP VOLTAGE (30A20AC)	185 V = On,180 V = Off	N/A
BUS CAPACITANCE	3600 µF	
SHUNT FUSE (d = .25 inches, L = 1.25 inches)	3 A, 250 VAC Motor Delay	N/A
BUS FUSE (5 X 20 mm)	15 A slow-blow rated @ 250 VAC	

MECHANICAL SPECIFICATIONS	
POWER CONNECTOR	Screw terminals
SIGNAL CONNECTOR	Molex connector
SIZE	7.35 x 4.23 x 2.45 inches 186.7 x 107.4 x 62.2 mm
WEIGHT	2.5 lb. 1.14 kg

Figure C-4: Advanced Motion Controls 16A20AC PWM Brush-type servo amplifier specifications from manual

Data Acquisition Card

Analog Input

Number of channels
- NI 6220/6221 ..... 8 differential or 16 single ended
- NI 6224/6229 ..... 16 differential or 32 single ended
- NI 6225 ..... 40 differential or 80 single ended

ADC resolution ..... 16 bits

DNL ..... No missing codes guaranteed

INL ..... Refer to the *AI Absolute Accuracy Table*

Sampling rate
- Maximum ..... 250 kS/s single channel, 250 kS/s multi-channel (aggregate)
- Minimum ..... No minimum
- Timing accuracy ..... 50 ppm of sample rate
- Timing resolution ..... 50 ns

Input coupling ..... DC

Input range ..... ±10 V, ±5 V, ±1 V, ±0.2 V

Maximum working voltage for analog inputs (signal + common mode) ..... ±11 V of AI GND

CMRR (DC to 60 Hz) ..... 92 dB

Input impedance
- Device on
  - AI+ to AI GND ..... >10 GΩ in parallel with 100 pF
  - AI– to AI GND ..... >10 GΩ in parallel with 100 pF
- Device off
  - AI+ to AI GND ..... 820 Ω
  - AI– to AI GND ..... 820 Ω

Input bias current ..... ±100 pA

Crosstalk (at 100 kHz)
- Adjacent channels ..... –75 dB
- Non-adjacent channels ..... –90 dB[1]

Small signal bandwidth (–3 dB) ..... 700 kHz

Input FIFO size ..... 4,095 samples

Scan list memory ..... 4,095 entries

Data transfers
- PCI/PXI devices ..... DMA (scatter-gather), interrupts, programmed I/O
- USB devices ..... USB Signal Stream, programmed I/O

Figure C-5: National Instruments PCI 6221 Multi-Function DAQ analog input specifications from NI 622X specifications sheet

Overvoltage protection (AI <0..79>, AI SENSE, AI SENSE 2)

Device on ..... ±25 V for up to two AI pins

Device off ..... ±15 V for up to two AI pins

Input current during overvoltage condition ..... ±20 mA max/AI pin

Settling Time for Multichannel Measurements

Accuracy, full scale step, all ranges

±90 ppm of step (±6 LSB) .....4 µs convert interval

±30 ppm of step (±2 LSB) .....5 µs convert interval

±15 ppm of step (±1 LSB) .....7 µs convert interval

Typical Performance Graphs

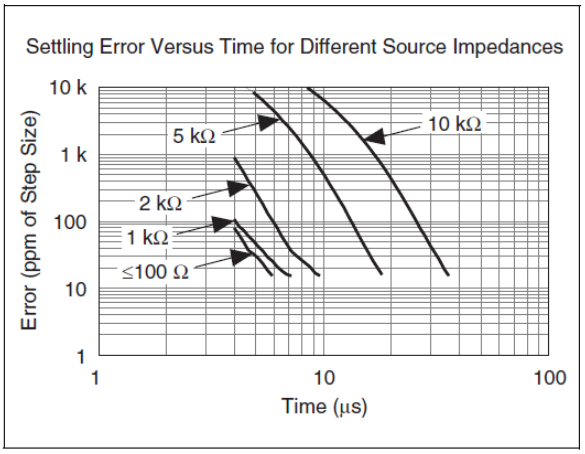

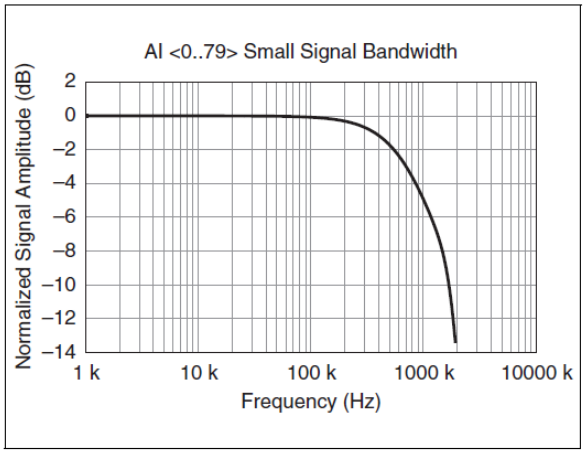

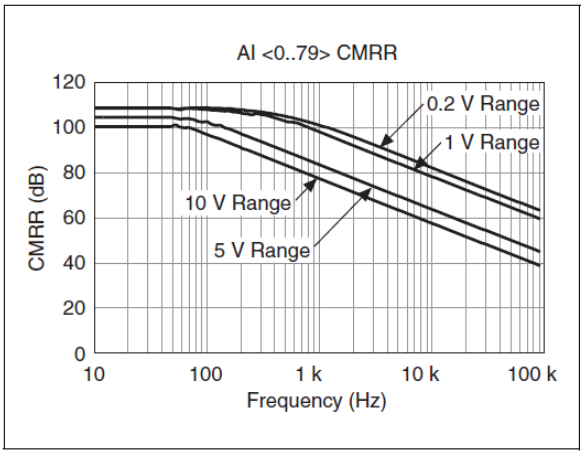

Figure C-6: National Instruments PCI 6221 Multi-Function DAQ analog input specifications from NI 622X specifications sheet (cont.)

Analog Output

Number of channels
- NI 6220/6224 0
- NI 6221/6225 2
- NI 6229 4

DAC resolution ..... 16 bits

DNL ..... ±1 LSB

Monotonicity ..... 16 bit guaranteed

Maximum update rate
- 1 channel ..... 833 kS/s
- 2 channels ..... 740 kS/s per channel
- 3 channels ..... 666 kS/s per channel
- 4 channels ..... 625 kS/s per channel

Timing accuracy ..... 50 ppm of sample rate

Timing resolution ..... 50 ns

Output range ..... ±10 V

Output coupling ..... DC

Output impedance ..... 0.2 Ω

Output current drive ..... ±5 mA

Overdrive protection ..... ±25 V

Overdrive current ..... 10 mA

Power-on state ..... ±20 mV[1]

Power-off glitch ..... 400 mV for 200 ms

Output FIFO size ..... 8,191 samples shared among channels used

Data transfers
- PCI/PXI devices ..... DMA (scatter-gather), interrupts, programmed I/O
- USB devices ..... USB Signal Stream, programmed I/O

AO waveform modes:
- Non-periodic waveform
- Periodic waveform regeneration mode from onboard FIFO
- Periodic waveform regeneration from host buffer including dynamic update

Settling time, full scale step
15 ppm (1 LSB) ..... 6 µs

Slew rate ..... 15 V/µs

Glitch energy
- Magnitude ..... 100 mV
- Duration ..... 2.6 µs

Calibration (AI and AO)

Recommended warm-up time ..... 15 minutes

Calibration interval ..... 1 year

Figure C-7: National Instruments PCI 6221 Multi-Function DAQ analog output specifications from NI 622X specifications sheet

C.2 LabVIEW Code

A National Instrument's LabView program was used to control the linear actuator and process the signals from the load cell and LVDT. The block diagram developed to perform these tasks is shown in Figure C-8. A brief description of its operation is as follows:

(1) Is where the magnitude and shape of the force pulse is defined. The pulse lasts 2.5 seconds, consists of 12,500 samples output at 5000 Hz.

(2) Scales the force pulse signal, which is in lbf, to the proper voltage level for (3).

(3) Takes the signal from (2) and sends it to the servo amplifier as an analog output. The output signal controls the force output of the voice coil through the servo amplifier.

(4) Scales the signal back into the original input value for comparison purposes.

(5) Reads the input signals from the load cell and LVDT and scales them, using the devices calibrations formulas, into the force and displacement readings

(6) Due to electronic noise from the servo amplifier the force data is filtered through a 3^{rd} order Butterworth filter with a 250 Hz cutoff. The LVDT was located far enough away from the amplifier to avoid the noise.

(7) Writes all 12.5 k samples of the input signal, filtered and unfiltered load cell readings, and LVDT displacement readings to a text file.

(8) Displays the readings on waveform graphs in the front panel shown in figure C-9

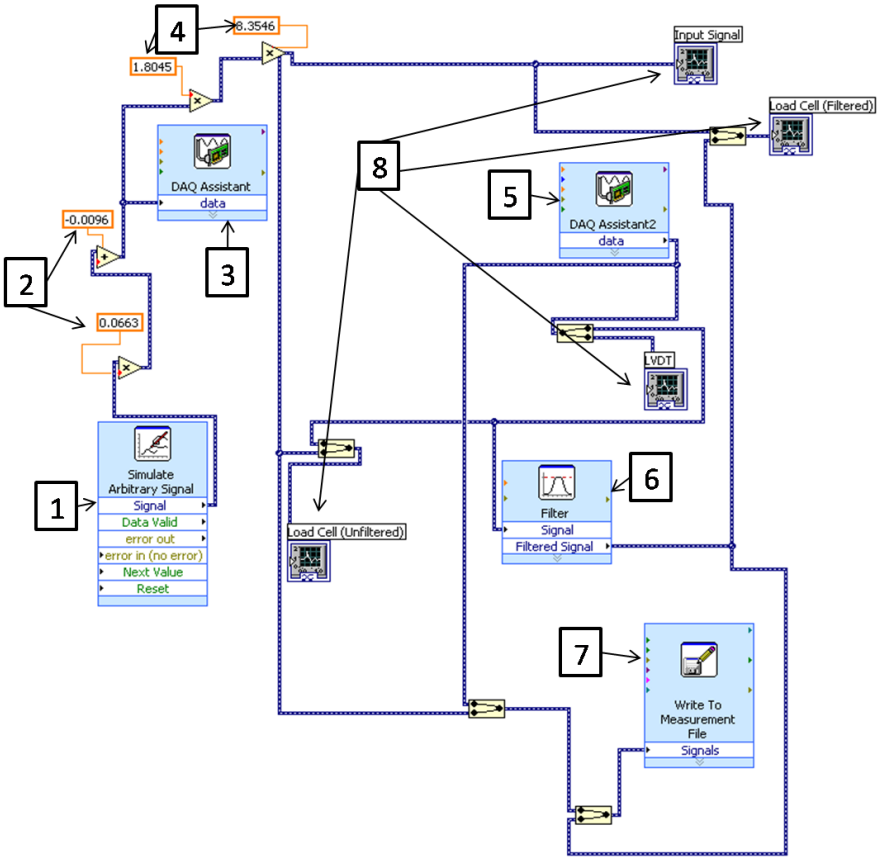

Figure C-8: LabVIEW block diagram

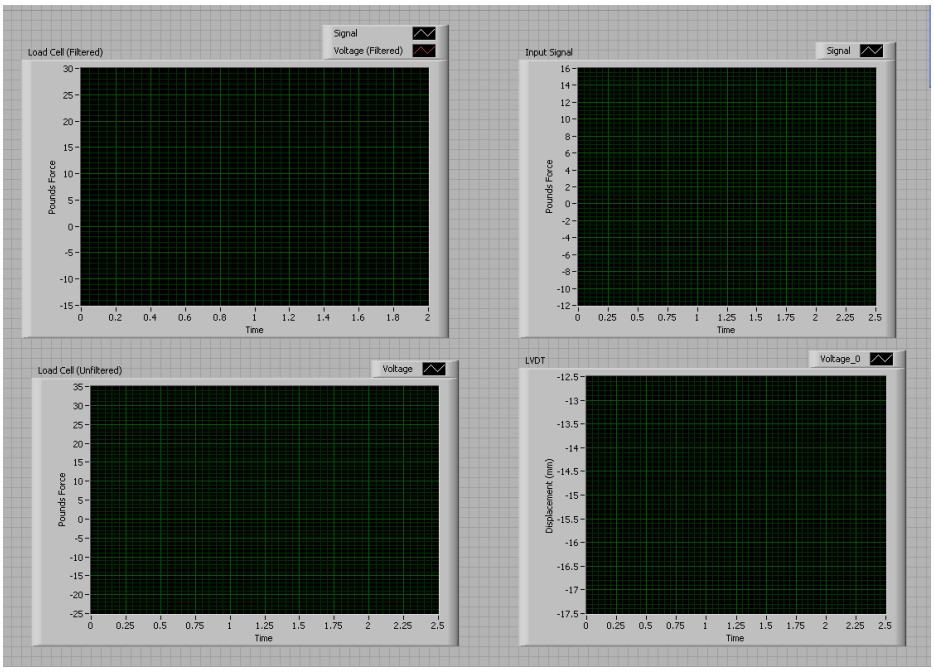

Figure C-9: LabVIEW front panel

C.3 Reading Test Cell Data

LabVIEW saves data in text files with the format shown below in Figure C-10.

- First column labeled X_Value , time count, seconds
- Second column labeled Voltage, unfiltered load cell reading , pounds-force
- Third column labeled Voltage_0, LVDT reading, millimeters
- Fourth column labeled Signal, control signal sent to voice actuator, pounds-force
- Fifth column labeled Voltage (Filtered), filtered load cell reading, pounds-force

LabVIEW Measurement				
Writer_Version	0.92			
Reader_Version	1			
Separator	Tab			
Multi_Headings	Yes			
X_Columns	One			
Time_Pref	Absolute			
Operator	Administrator			
Date	2/11/2010			
Time	21:52.0			
End_of_Header				
Notes	X values guaranteed valid only for Signal			
Channels	4			
Samples	12500	12500	12501	12500
Date	2/11/2010	2/11/2010	2/11/2010	2/11/2010
Time	21:56.5	21:56.5	21:52.0	21:56.5
X_Dimension	Time	Time	Time	Time
X0	0.00E+00	0.00E+00	0.00E+00	0.00E+00
Delta_X	0.0002	0.0002	0.0002	0.0002
End_of_Header				
X_Value	Voltage	Voltage_0	Signal	Voltage (Filtered)
0	-0.259129	8.188795	-0.144728	-0.000751
0.0002	-0.193857	8.194398	-0.144728	-0.004598
0.0004	-0.259129	8.204804	-0.144728	-0.014156
0.0006	-0.193857	8.224016	-0.144728	-0.030388
0.0008	0.067232	8.217612	-0.144728	-0.051584
0.001	-0.237372	8.221614	-0.144728	-0.073908
0.0012	-0.1721	8.239225	-0.144728	-0.094649
0.0014	-0.215614	8.24803	-0.144728	-0.113548
0.0016	-0.346159	8.251232	-0.144728	-0.131349

Figure C-10: Test Cell Output File

C.4 Calibration

Load Cell

O M E G A D Y N E I N C.

LOAD CELL
FINAL CALIBRATION

0.00 - 100.00 LBS
Excitation 10.000 Vdc

Job: MLS5215 Serial: 233785
Model: LC111-100 Tested By: ED
Date: 5/28/2008 Temperature Range: 60 to 160 F
Calibrated: 0.00 - 100.00 LBS Specfile: LC111 0-500 LBS

Force LBS	Unit Data mVdc
0.00	0.0000
50.00	15.0219
100.00	30.0216
50.00	15.0248
0.00	0.0007

Balance - 0.0697 mVdc
Sensitivity 30.0216 mVdc
In Resist 350.20 Ohms
Out Resist 350.10 Ohms

ELECTRICAL LEAKAGE: PASS

ELECTRICAL WIRING/CONNECTOR: Pin A: + Output
Pin B: - Output
Pin C: - Input
Pin D: + Input

This Calibration was performed using Instruments and Standards that are traceable to the United States National Institute of Standards Technology.

S/N	Description	Range	Reference	Cal Cert
SN15	1000lb Dead-Weights	0 - 1000 LBS	C-2690	
US36037840	HP34401A DMM UUT	Unit Under Test	C-2452	C-2452

Q.A. Representative : Ed Suchman Jr Date: 5/28/2008
This transducer is tested to & meets published specifications. After final calibration our products are stored in a controlled stock room & considered in bonded storage. Depending on environment & severity of use factory calibration is recommended every one to three years after initial service installation date.
COMMENTS: FINAL TEST

Omegadyne, Inc., 149 Stelzer Court, Sunbury, OH 43074 (740) 965-9340
http://www.omegadyne.com email: info@omegadyne.com (800) USA-DYNE

Figure C-11: Load Cell Factory Calibration

Figure C-11 above is the load cell calibration data from the manufacturer. In order to verify it, a calibration test using the setup shown in Figure C-12 was performed. This involved

simply hooking up the load cell into the DAQ and loading it with different known weights. The calibrated output characteristics are shown in Figure C-13.

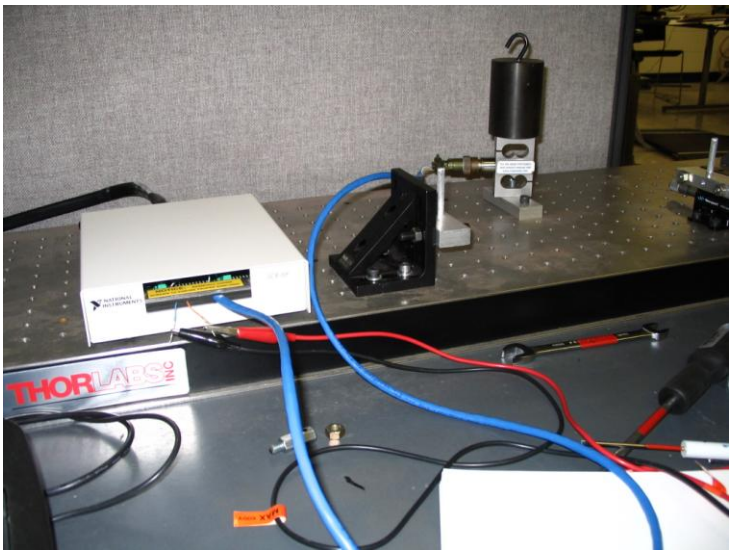

Figure C-12: Load Cell Calibration Test

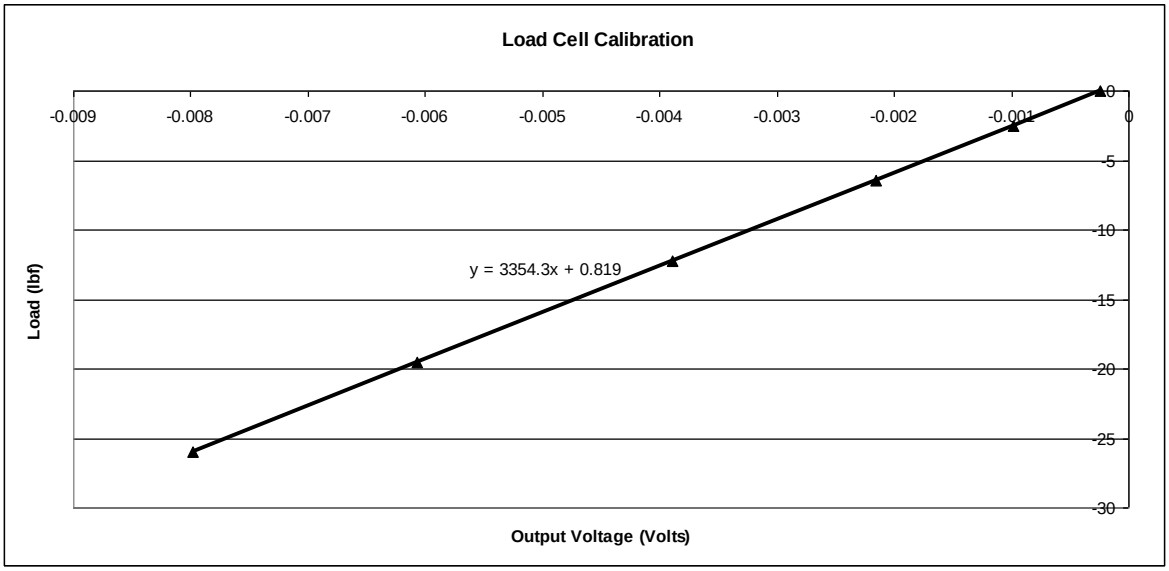

Figure C-13: Load Cell Calibration Results

LVDT (Linear Variable Differential Transformer)

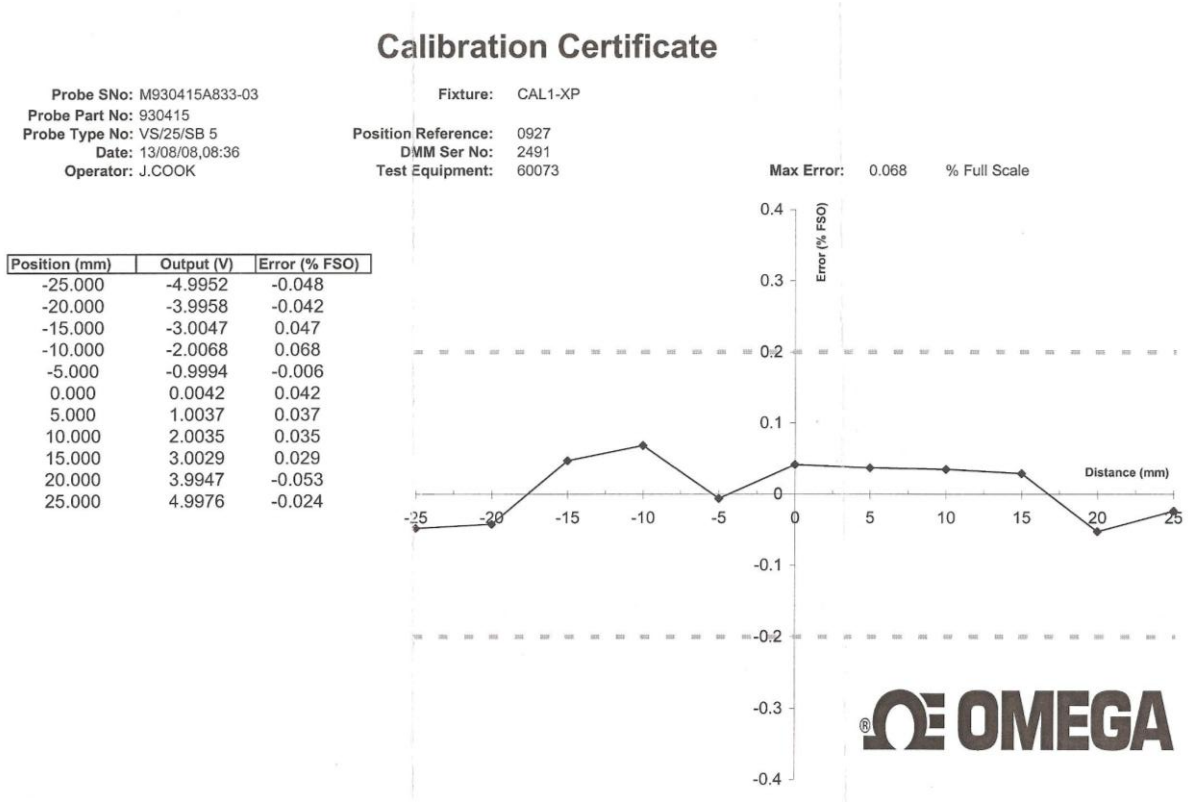

Calibration Certificate

Probe SNo: M930415A833-03
Probe Part No: 930415
Probe Type No: VS/25/SB 5
Date: 13/08/08,08:36
Operator: J.COOK

Fixture: CAL1-XP
Position Reference: 0927
DMM Ser No: 2491
Test Equipment: 60073

Max Error: 0.068 % Full Scale

Position (mm)	Output (V)	Error (% FSO)
-25.000	-4.9952	-0.048
-20.000	-3.9958	-0.042
-15.000	-3.0047	0.047
-10.000	-2.0068	0.068
-5.000	-0.9994	-0.006
0.000	0.0042	0.042
5.000	1.0037	0.037
10.000	2.0035	0.035
15.000	3.0029	0.029
20.000	3.9947	-0.053
25.000	4.9976	-0.024

Figure C-14: Manufacturer LVDT Calibration

In order to test the calibration of the LVDT, it was attached to an optics stand with a micrometer so that the displacement could be carefully monitored. This setup is shown in Figure C-15.

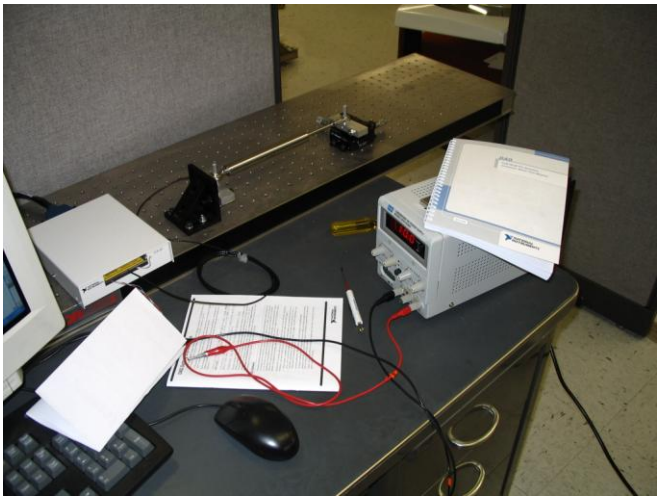

Figure C-15: LVDT Calibration Test

The calibration curve for the LVDT is shown in Figure C-16.

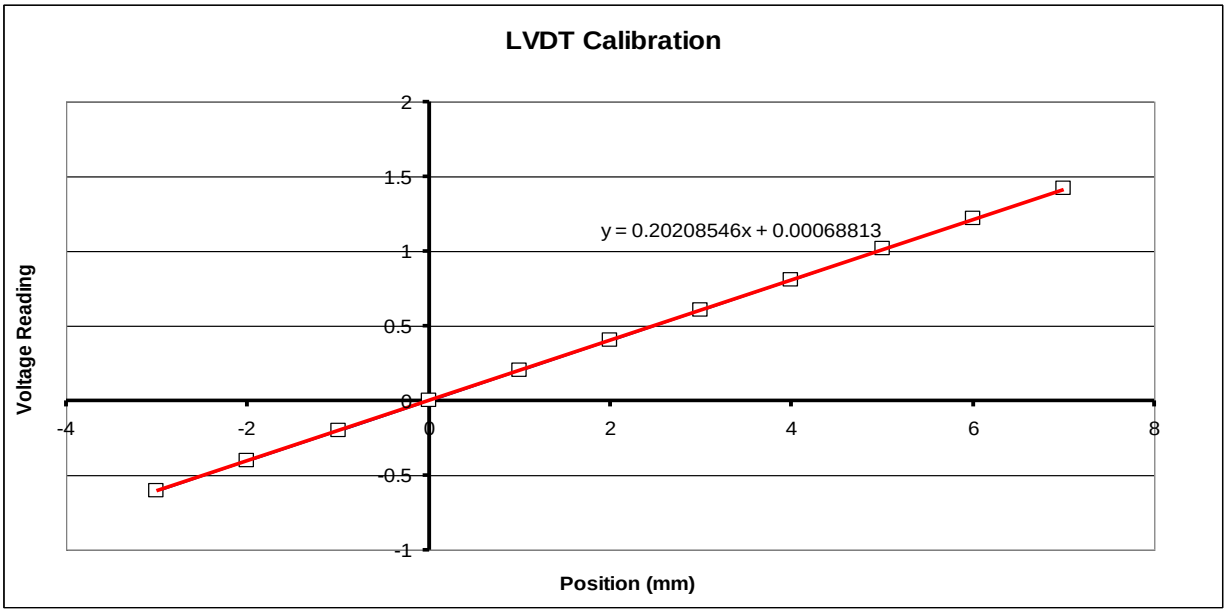

Figure C-16: LVDT Calibration Test Results

Voice Coil and Amplifier

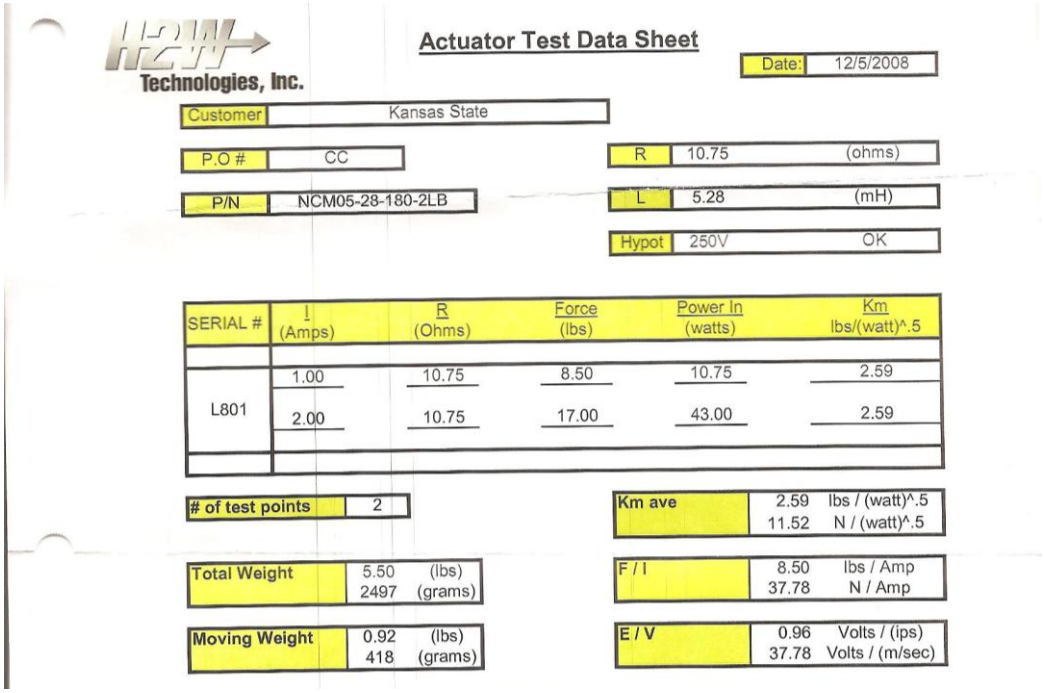

Actuator Test Data Sheet

Technologies, Inc.

Date: 12/5/2008

Customer: Kansas State

P.O #: CC

P/N: NCM05-28-180-2LB

R: 10.75 (ohms)

L: 5.28 (mH)

Hypot: 250V OK

SERIAL #	I (Amps)	R (Ohms)	Force (lbs)	Power In (watts)	Km lbs/(watt)^.5
L801	1.00	10.75	8.50	10.75	2.59
	2.00	10.75	17.00	43.00	2.59

# of test points: 2

Km ave: 2.59 lbs / (watt)^.5; 11.52 N / (watt)^.5

Total Weight: 5.50 (lbs); 2497 (grams)

F / I: 8.50 lbs / Amp; 37.78 N / Amp

Moving Weight: 0.92 (lbs); 418 (grams)

E / V: 0.96 Volts / (ips); 37.78 Volts / (m/sec)

Figure C-17: Voice Coil Test Data Sheet

Figure C-17 shows the specification sheet for the voice coil which was used to provide the dynamic force loading.

Calibrating the voice coil and amplifier together was a more involved process. The voice coil is current driven and has a fairly straight forward conversion of 8.5 lbf per amp. This current is applied through a servo amplifier and the current output is a ratio to the ±10 V dc control signal from the DAQ. The gain is adjustable through a potentiometer in the amplifier. In order to find the Voltage-to-Force ratio, the load cell was attached to the voice coil as shown below in Figure C-18.

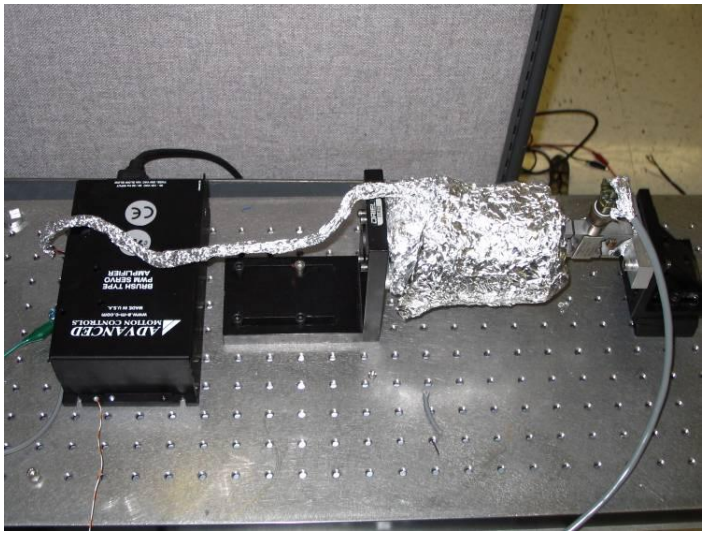

Figure C-18: Actuator Calibration

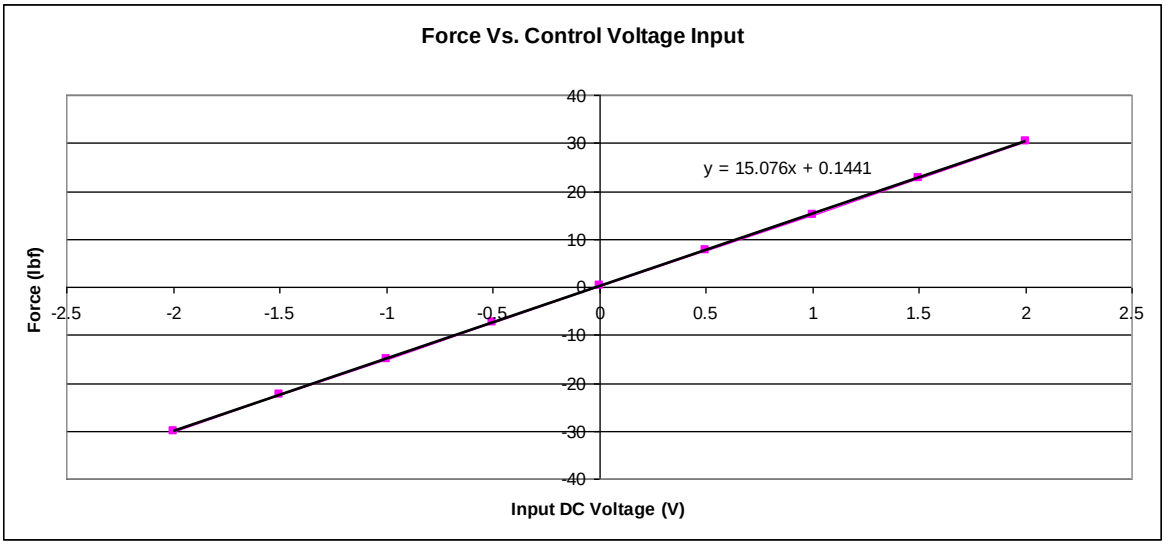

Figure C-19: Voice Coil Calibration

The calibration curve for the voice cool is shown in Figure C-19.

C.4 Uncertainty

This section provides basic uncertainty information for the instruments used in all experimental tests

Load Cell

The load cell has uncertainties of ±0.03% FSO for linearity, ±0.02% FSO Hysteresis, and ±0.01% FSO for repeatability. The full scale output for the load cell is ±30 mV at ±100 lbs making the uncertainties ±0.03 lb, ±0.02 lb, and ±0.01 lb for a total absolute force measurement uncertainty of about ±0.037 lbs for just the load cell.

LVDT

For the LVDT, the most significant uncertainty is ±0.2% FSO for linearity. The full scale output for the LVDT is ±5 volts at ±25 mm making the displacement uncertainty about ±0.05 mm.

DAQ

The DAQ card used had a resolution of 16 bits. Therefore, for the ±10 V range, this yields a relative uncertainty of about:

$$u_{DAQ} = \frac{10V}{2^{16}} = \pm 0.000153V$$

For the ±1 V range that the load cell uses, the complex relative uncertainty was about.

$$u_{DAQ} = \frac{1V}{2^{16}} = \pm 0.0000153V$$

At 5 mm per V sensitivity, this translates into an absolute uncertainty of ±0.000763 mm for the LVDT, and for the load cell's 3.33 lb per mV sensitivity it yields ±5e-5 lbs for the absolute sensitivity. The DAQ uncertainty contribution is thus quite small.

Appendix D - Prototype Drawings

Figures D-1 thru D-5 are drawings of the damper prototypes.

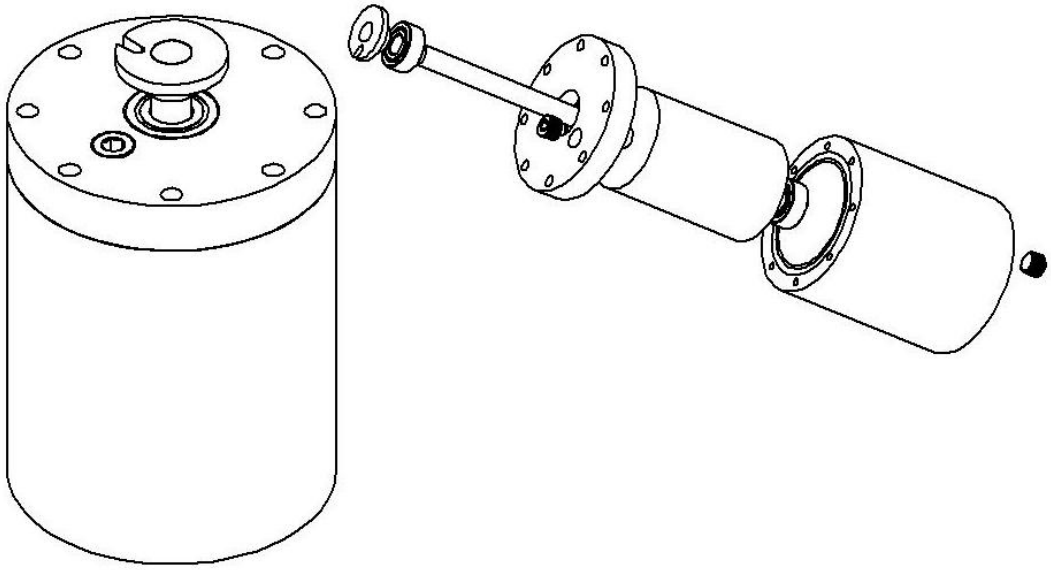

Figure D-1: Proof of Concept Prototype

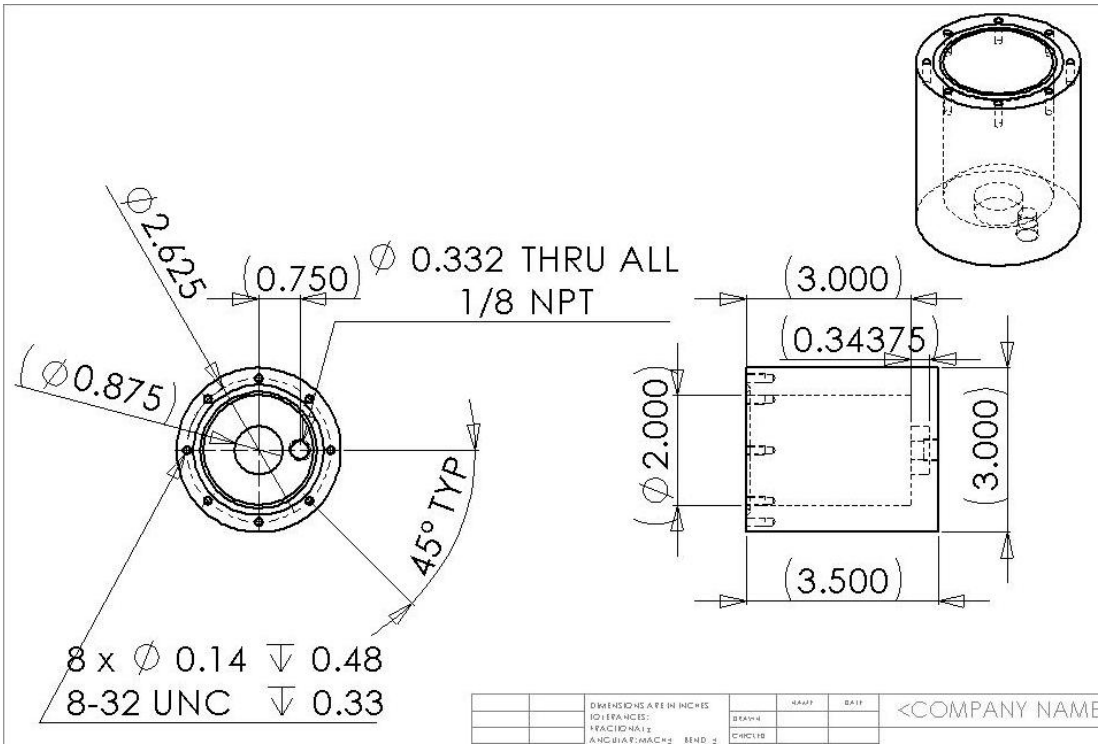

Figure D-2: Proof of Concept Outer Cylinder

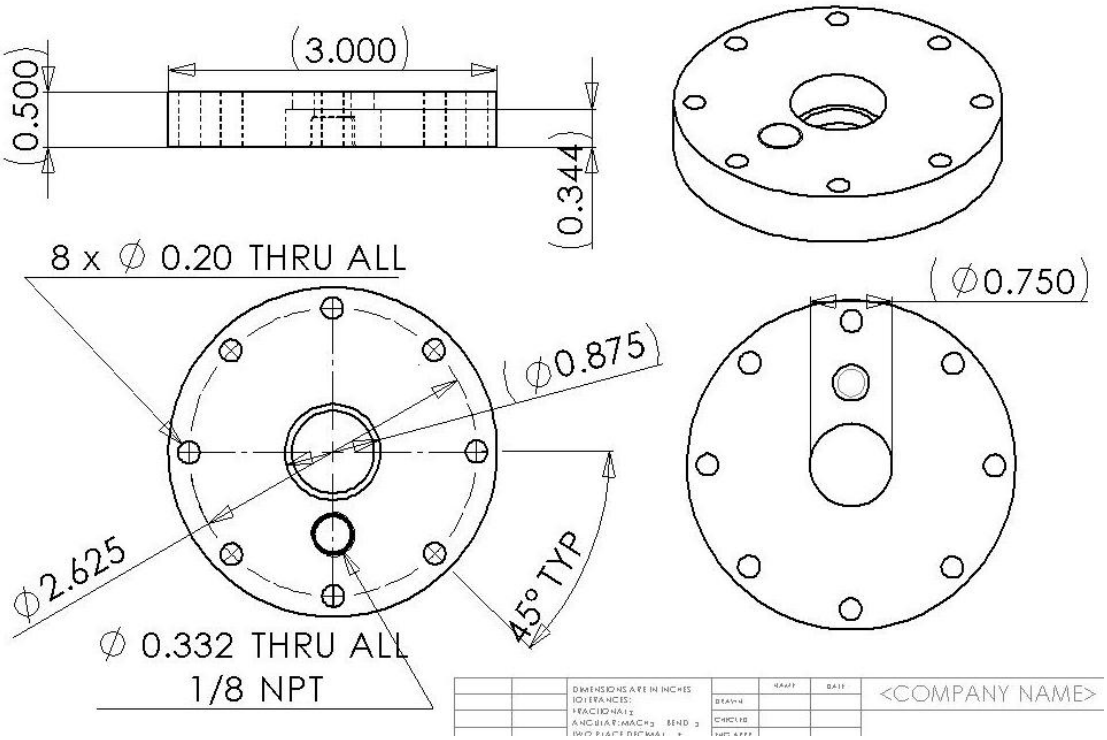

Figure D-3: Proof of Concept Lid

Figure D-4: Disassembled Commercial Prototype

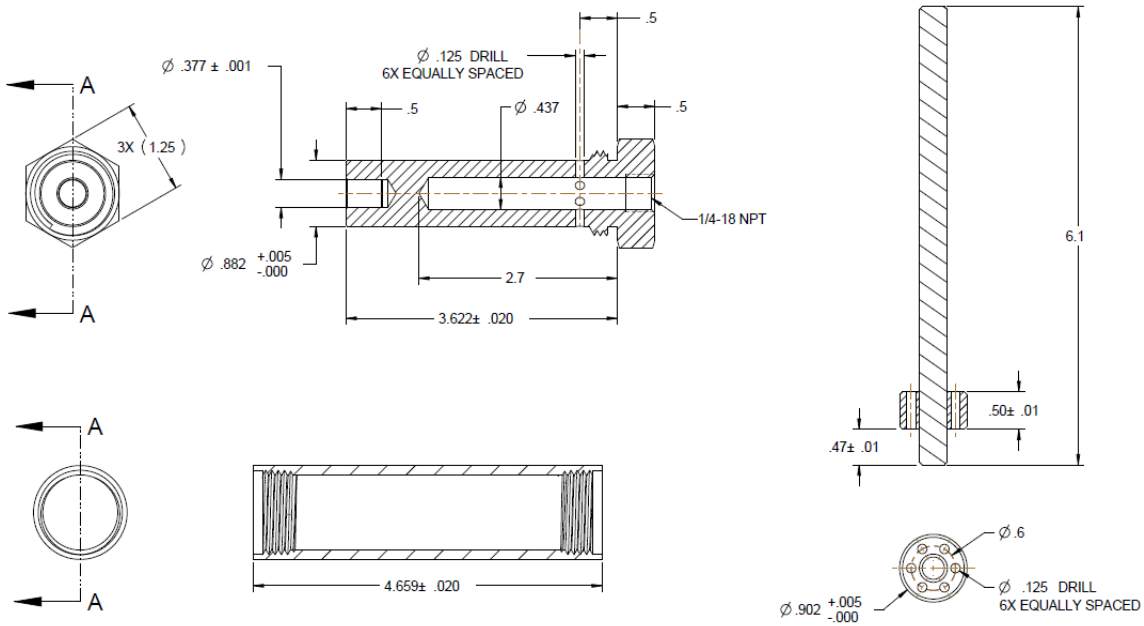

Figure D-5: Commercial Prototype Components